STUDENT BRANCH

JOURNAL OF THE AERONAUTICAL SCIENCES

VOLUME 20 AUGUST, 1953 NUMBER 8

CONTENTS

Supersonic Flow About Slender Bodies of Elliptic Cross Section.....A. KAHANE AND A. SOLARSKI 513

Three-Dimensional Laminar Boundary-Layer Flow.....FRANKLIN K. MOORE 525

Critical Bending Stress for Flat Rectangular Plates Supported Along All Edges and Elastically Restrained Against Rotation Along the Unloaded Compression Edge.....JAMES H. JOHNSON, JR., AND ROBERT G. NOEL 535

The Aerodynamic Characteristics of Low Aspect Ratio Wing-Body Combinations in Steady Subsonic Flow.....H. R. LAWRENCE 541

A Constant-Area, Constant-Temperature Combustor.....PHILIP ROSEN AND R. W. HART 549

Studies of Some Effects of Airplane Configuration on the Response to Longitudinal Control in Landing Approaches..RALPH W. STONE, JR., AND WILLIAM BIHRLE, JR. 555

Supersonic Flow over Conical Bodies Without Axial Symmetry.....ANTONIO FERRI, NATHAN NESS, AND THADDEUS T. KAPLITA 563

Readers' Forum: "On the Nonexistence of a Finite Critical Time for Linear Viscoelastic Columns," by Joseph Kempner and Frederick V. Pohle; "The Minimum Weight Design of Wings for Flutter Conditions," by E. P. MacDonough; "Gap Effect on Slender Wing-Body Interference," by H. Mirels; "The Propulsive Efficiency and Best Division of Power in an Augmented Jet Engine," by John Mitchell Stephenson; "On the Role of Three-Dimensional Disturbances in the Stability of Supersonic Boundary Layers," by D. W. Dunn and C. C. Lin; "Apparent Recovery Factors on the Leading Edge of a Flat Plate in Supersonic Laminar Flow," by Irving Korobkin; "Effect of Gas Radiation in the Boundary Layer on Aerodynamic Heat Transfer," by John W. Smith; "On the Flow at the Rear of a Two-Dimensional Supersonic Airfoil with Thickness," by Ronald F. Probstein; "Interaction of a Plane Flame Front with a Plane Sinusoidal Shear Wave," by George H. Markstein; "Errata—'An Experimental Study of Natural Vibrations of Cantilevered Triangular Plates,'" by P. N. Gustafson, W. F. Stokey, and C. F. Zorowski; "Transformation Between Compressible and Incompressible Boundary-Layer Equations," by Nguyen Van Le.....572–584

Published by the

INSTITUTE OF THE AERONAUTICAL SCIENCES, INC.

JOURNAL OF THE AERONAUTICAL SCIENCES

Editor: HUGH L. DRYDEN, *Director, NACA*

Associate Editor: ROBERT R. DEXTER *Managing Editor:* BERNEICE H. JARCK

Editorial Committee

Aerodynamics

Francis Clauser
Howard Emmons
Antonio Ferri
Alexander Flax
R. Paul Harrington
R. T. Jones
Carl Kaplan
H. W. Liepmann
C. C. Lin
H. F. Ludloff
Harold Luskin
John R. Markham
Clark B. Millikan
Shatswell Ober
W. Bailey Oswald
Allen E. Puckett
Elliott G. Reid
H. J. E. Reid
Russell Robinson
G. B. Schubauer
W. R. Sears
John Stack
Theodore von Kármán
Richard von Mises

Air Transport

Charles Froesch
J. A. Herlihy
R. D. Kelly
Otto E. Kirchner
Jerome Lederer
John C. Leslie
R. Dixon Speas

Flight Testing

W. K. Ebel
R. R. Gilruth
Melvin N. Gough
E. G. Stout

Structures and Materials

W. B. Bleakney
E. W. Conlon
L. H. Donnell
E. C. Hartmann
N. J. Hoff
Samuel Levy
E. E. Lundquist
Alfred S. Niles
W. Ramberg
E. Reissner
F. R. Shanley
H. W. Sibert
C. R. Strang
S. Timoshenko
H. S. Tsien
Chi-Teh Wang

Rotating Wing Aircraft

F. B. Gustafson
K. H. Hohenemser
Bartram Kelley
R. B. Maloy
Ralph McClarren
R. H. Miller
R. H. Prewitt
Igor I. Sikorsky

Vibration and Flutter

Lee Arnold
M. A. Biot
R. L. Bisplinghoff
William Bollay
Chieh-Chien Chang
I. E. Garrick
Martin Goland
J. P. Den Hartog

Aircraft Design

W. E. Beall
W. K. Ebel
Hall L. Hibbard
Richard Hutton
C. L. Johnson
A. A. Kartveli
C. J. McCarthy
Fred E. Weick
Robert J. Woods

Electronics in Aviation

K. C. Black
E. F. Herzog
David S. Little
D. K. Martin
George Rappaport
Paul Rosenberg
L. M. Sherer

Physiologic Problems

H. G. Armstrong
Louis H. Bauer
Robert J. Benford
Eugene Du Bois
W. Randolph Lovelace, II
Ross A. MacFarland

Fuels and Oils

D. P. Barnard
J. H. Doolittle
Graham Edgar
R. T. Goodwin
S. D. Heron
A. M. Rothrock

Flight Propulsion

George W. Brady
Frank W. Caldwell
L. S. Hobbs
E. E. Johnson
Joseph Keenan
R. P. Kroon
Hans Reissner
Abe Silverstein
C. Fayette Taylor
E. S. Taylor
P. Taylor
E. S. Thompson
H. S. Tsien

Instruments

Allan G. Binnie
J. R. Bradburn
Charles H. Colvin
C. S. Draper
S. G. Eskin
O. E. Esval
H. W. Holzapfel
W. L. Howland
George H. Purcell
C. F. Savage
O. Hugo Schuck
C. L. Seward, Jr.
L. D. Statham
R. C. Sylvander
D. K. Warner

Meteorology

C. F. Brooks
D. M. Little
E. J. Minser
F. W. Reichelderfer
H. C. Willett

SUBSCRIPTION RATES

JOURNAL OF THE AERONAUTICAL SCIENCES, Published Monthly.—United States and Possessions: 1 Year, $12.00; Single Copies, $1.50. Foreign Countries Including Canada (American Currency Rates): 1 Year, $13.00; Single Copies, $1.50.

AERONAUTICAL ENGINEERING REVIEW, Published Monthly.—United States and Possessions: 1 Year, $3.00; Single Copies, $0.50. Foreign Countries Including Canada (American Currency Rates): 1 Year, $3.50; Single Copies, $0.50.

Notices of change of address should be sent to the Institute at least 30 days prior to actual change of address.

Manuscripts for publication, proofs, and all correspondence should be addressed to the Editorial Office of the JOURNAL.

Correspondence regarding subscriptions may be addressed to Publication Office, 20th and Northampton Sts., Easton, Pa., or to the Editorial Office of the JOURNAL OF THE AERONAUTICAL SCIENCES, 2 East 64th Street, New York 21, New York.

Copyright, 1953, by the Institute of the Aeronautical Sciences, Inc.

Entered as Second Class Matter at the Post Office, Easton, Pa., May 1, 1937. Acceptance for mailing at a special rate of Postage provided for in the Act of August 24, 1912. Authorized April 29, 1937.

JOURNAL OF THE AERONAUTICAL SCIENCES

VOLUME 20 AUGUST, 1953 NUMBER 8

Supersonic Flow About Slender Bodies of Elliptic Cross Section

A. KAHANE* AND A. SOLARSKI†

Republic Aviation Corporation

SUMMARY

A theory for slender bodies of elliptic cross section in supersonic flow, based on the generalized cross-section slender body theory of Ward,[7] is presented. The theory is applied to the zero angle of attack pressure distribution on elliptic cones and parabolic arc bodies of elliptic cross section; results of several example computations are presented. Comparison is made with the nonlinear elliptic cone calculations and experimental results of Ferri;[6] good agreement is obtained. The wave drag of bodies with elliptic bases is also treated. Application of the theory to bodies at angle of attack is indicated.

INTRODUCTION

THE BODY OF REVOLUTION in supersonic flow has been treated extensively in the literature (see Van Dyke[1] for bibliography), since the appearance of the initial paper on the subject by von Kármán and Moore.[2] Bodies of noncircular cross section, on the other hand, have received but brief attention.

Maslen[3] has presented a linearized solution method for cones of arbitrary cross section in which a finite number of oblique supersonic line sources extending downstream from the cone vertex are positioned so as to satisfy the boundary conditions for the body. A linearized conical flow treatment of the elliptic cone, which yields an infinite series solution, was given by Laporte and Bartels.[4] Graham[5] has treated with linear theory, using a continuous distribution of quadripoles along the body axis, a body that undergoes a transition from a circular cross section to a two-lobed cross section. A nonlinear method, (the so-called linearized method of characteristics) was originated by Ferri[6] for treatment of bodies of arbitrary shape and cross section. This method should yield more accurate results than any of the linearized methods but, on the other hand, requires the lengthiest calculations. The method entails, first, a calculation by the nonlinear method of characteristics of the flow field about the equivalent body of revolution (same area distribution as given body); a new solution is then obtained by perturbing the boundary conditions. Finally, Ward[7] has presented a general first-order linear solution for slender bodies of arbitrary cross section, the application of which involves the determination of the two-dimensional incompressible potential for the expanding cross-sectional boundary of the body.‡

This paper treats the slender body of elliptic cross section, moving at supersonic velocity, according to the method of Ward. The theory is applicable to bodies with either pointed noses or infinite cylindrical forebodies and of arbitrary shape except as subject to restrictions on slope and curvature as detailed in the footnote on page 514. Solutions of particular cases are given in relatively simple analytical closed forms, which are more amenable to computation than those of any of the existing methods. The theory is applied to cones, and comparisons are made with the experimental and linearized characteristics method results of Ferri.[6] A further example calculated is that of a parabolic arc body, and the resulting pressure distribution is compared with that for the equivalent parabolic body of revolution. The wave drag of bodies having elliptic bases is considered, and wave drag coefficients for elliptic cones are calculated. Application of the method to bodies at angle of attack is also indicated.

Presented at the Aerodynamics Session, Twenty-First Annual Meeting, IAS, New York, January 26–29, 1953.

* Principal Aerodynamicist, Development Division.

† Senior Aerodynamicist, Development Division; now with Cook Research Laboratories.

‡ Consider a plane fixed in space normal to the flight direction. The trace of a body passing through the plane comprises a boundary, which, in general, expands (or contracts) and translates.

A comparison of the results of several theories for cones and parabolic bodies of revolution is given in Appendix (B) to indicate the order of accuracy of the slender theory.

Symbols

a	= ellipse semimajor axis
b	= ellipse semiminor axis
B	= Mach Number function, $B^2 = M_1^2 - 1$
c	= one-half distance between foci of ellipses, $c^2 = a^2 - b^2$
$a_n,\ b_n,\ c_n$ $d_n,\ A_n,\ B_n$ $C_n,\ D_n$	= series coefficients, $n = 0, 1, 2, \ldots$
C_D	= drag coefficient based on base area
C_p	= static pressure coefficients, $C_p = (p - p_1)/q_1$
d	= effective thickness ratio (thickness ratio of equivalent body of revolution)
d^*	= maximum thickness of body of unit length
D	= drag force
$F(c/r, \theta)$	= function defined by Eq. (28)
$G(c/r, \theta)$	= function defined by Eq. (A-1)
M	= Mach Number
p	= static pressure
q	= dynamic pressure
r, θ, s	= polar coordinates
R	= radius of circular body boundary
s	= axial coordinate
S	= cross-sectional area
t	= time
$u_x,\ u_y,\ u_s$	= perturbation velocity components
U	= free-stream velocity
$\delta(\ )$	= differential of ( ) along outward normal to boundary
ϵ	= ratio of ellipse minor and major axes, $\epsilon = b/a$
γ	= ratio of specific heats
μ	= circular cone semivertex angle
ξ, η	= elliptic coordinates
ρ	= air mass density
σ	= dummy variable for s
τ	= tangent to boundary
ν	= outward normal to boundary
φ	= potential function

Subscripts

c	= circular cross section
e	= elliptic cross section
0	= boundary value
1	= free-stream value

Primes denote differentiation with respect to s.

The Ward Slender Body Theory

Consider a body in supersonic flight at velocity U and fix a cartesian (x, y, s) system of coordinates, with origin on the body nose, so that the s-axis is in the stream direction and increasing toward the rear of the body. On assumption of vanishing fluid viscosity and heat conductivity, a potential φ exists, and a second-order nonlinear hyperbolic equation for φ as dependent variable can be deduced from the equations of motion. The perturbation velocity components u_x, u_y, u_s are expressible in terms of the potential by

$$u_x = U\frac{\partial \varphi}{\partial x}, \quad u_y = U\frac{\partial \varphi}{\partial y}, \quad u_s = U\frac{\partial \varphi}{\partial s} \tag{1}$$

The nonlinear potential equation is linearized by neglecting squares and products of the velocity perturbations, giving[8]

$$B^2\varphi_{ss} - \varphi_{xx} - \varphi_{yy} = 0 \tag{2}$$

where $B^2 = M_1^2 - 1$ and M_1 is the flight Mach Number. Ward,[7] using operational methods, obtains a general series solution of Eq. (2) in polar coordinates and, after further approximation of this solution in the neighborhood of the surface of the body, obtains the so-called slender approximation† to φ,

$$\varphi = \frac{S'(s)}{2\pi}\ln r + b_0 + \sum_1^\infty a_n r^{-n}\cos(n\theta + \beta_n) \tag{3}$$

where the coefficients a_n and b_0 are functions of s; b_0 is given by

$$b_0(s) = \frac{1}{2\pi}\left[S'(s)\ln\frac{B}{2} - \int_0^s \ln(s-\sigma)S''(\sigma)\,d\sigma\right] \tag{4}$$

It will be noted from Eq. (3) that, in any plane s = constant, φ is a harmonic function—i.e., a solution of the two-dimensional Laplace equation,

$$\varphi_{xx} + \varphi_{yy} = 0 \tag{5}$$

which governs the two-dimensional flow of an inviscid incompressible fluid. It is apparent that Eq. (5) also can be obtained directly from Eq. (2) by assuming that the flight Mach Number is close to unity or φ_{ss} is small compared with φ_{xx} and φ_{yy}. The latter assumption is equivalent to the assumption that the body is slender, since it has been shown[7] that near the body φ_{ss} is $0(d^{*2}\ln d^*)$, whereas φ_{xx} and φ_{yy} are $0(1)$. From Eq. (5) the solution for the flow about such a body may be obtained by treatment of the relevant two-dimensional incompressible flow problem. This approach was used in 1924 by Munk[9] to obtain the lift and moment of slender airship hulls, by Jones[10] with regard to the lift of thin pointed low aspect-ratio wings, and more recently by many other investigators. The solution of Ward is an improvement over the method of Munk and Jones (whose "cross flow" approach is applicable only to systems at angle of attack), since it furnishes the relation for b_0, which is required for zero angle of attack problems—i.e., thickness problems.

† The following restrictions apply to the Ward[7] slender body theory. If the body is of unit length and has a maximum thickness of d^*, then, since body is assumed slender, d^* must be small compared to unity. The angle that any tangent plane to the boundary makes with the free-stream direction must be small and $0(d^*)$; the rate of change of this angle must be small and $0(d^*)$. If d^{**} is the maximum thickness of any section, then the radius of curvature of the body in any plane normal to the free-stream direction must be $0(1/d^{**})$ for all points where the section is convex outward, with no restriction if the curve is convex inwards. With these restrictions, the error in Eq. (3) is a factor $1 + 0(d^*)$. This error term and the error terms given in the remainder of the text are from Ward.[7]

Potential for Expanding Two-Dimensional Elliptic Boundary

Consider a slender body of elliptic cross section at zero angle of attack moving at supersonic speed. As the body passes through a plane fixed in space normal to the flight direction, the locus of the intersection of the body boundary and the plane comprises an expanding (or contracting) elliptic curve (see Fig. 1). Since the partial differential equation of the flow is the two-dimensional Laplace equation, Eq. (5), which governs inviscid, incompressible, and steady or unsteady flows, the problem is reduced to the determination of the potential of an elliptic curve (which may be considered the boundary of a two-dimensional elastic body) which expands in a fixed plane. Since the fluid surrounding the elliptic boundary is considered incompressible, lateral disturbances in the plane are propagated at infinite velocity, and the flow pattern at any instant is dependent, therefore, only on the boundary conditions (the normal velocity distribution on the boundary) at that instant. This classical type of boundary value problem is known in the mathematical literature as the Neumann problem or the second boundary value problem of potential theory. The problem may be stated as follows: Let the closed elliptic boundary be denoted by C and the region of fluid exterior to the boundary by R. The partial differential equation and boundary conditions are

$$\varphi_{xx} + \varphi_{yy} = 0, \text{ in } R$$

$$\varphi_\nu = \varphi_{\nu_0}(x, y), \text{ on } C$$

where $\varphi_{\nu_0}(x, y)$ is the prescribed normal velocity on points on the boundary. [The particular functional form of $\varphi_{\nu_0}(x, y)$ is dependent on the manner of expansion of the boundary.] Since elliptic bodies are treated herein, a restriction on the manner of expansion of the boundary is that the new boundary be an ellipse. The center of the ellipses are assumed to lie at $x = y = 0$; translation of the boundary, therefore, need not be considered.

Inasmuch as the boundary conditions are to be satisfied on an ellipse, the appropriate coordinate system for this problem is elliptic coordinates (see, for example, Milne-Thompson[11]). If

$$\left.\begin{aligned} x &= c \cosh \xi \cos \eta \\ y &= c \sinh \xi \sin \eta \end{aligned}\right\} \tag{6}$$

it can be shown that the curves ξ = constant are confocal ellipses and that the curves η = constant are confocal hyperbolae orthogonal to the ellipses, the foci of the ellipses and hyperbolae being at $x = \pm c$, $y = 0$. (see Fig. 2). The semimajor axis, a, and semiminor axis, b, of each ellipse are related by

$$c^2 = a^2 - b^2 \tag{7}$$

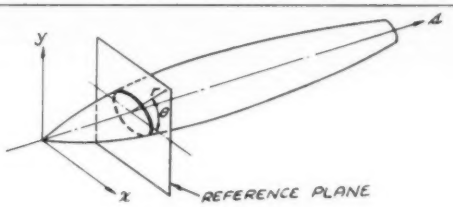

FIG 1a ELLIPTICAL BODY PIERCING REFERENCE PLANE.

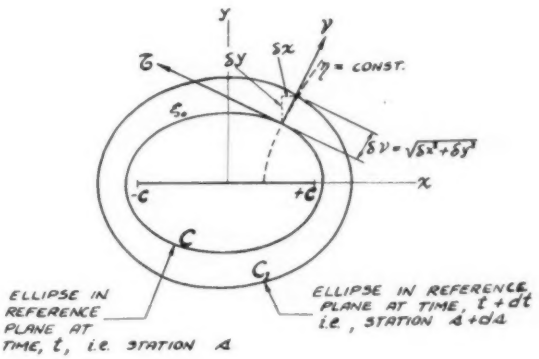

FIG. 1b CROSS-SECTION OF BODY

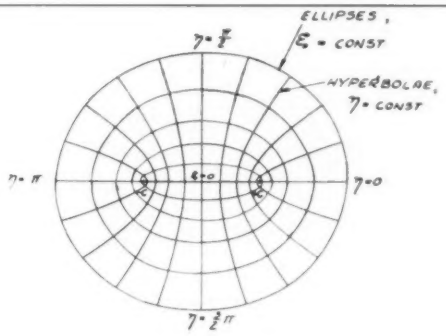

FIG 2 ELLIPTIC COORDINATE SYSTEM

The Laplace equation, Eq. (5), in elliptic coordinates transforms to (see, for example, Bateman[12])

$$\varphi_{\xi\xi} + \varphi_{\eta\eta} = 0 \tag{8}$$

and the boundary conditions become

$$\frac{\partial \varphi}{\partial \xi} = \left[\frac{\partial \varphi}{\partial \xi}(\eta)\right]_0 \quad \text{on} \quad \xi = \xi_0 \tag{9}$$

where ξ_0 is the boundary ellipse. Eq. (8) is solved by separation of variables (see, for example, Pipes[13]), yielding

$$\varphi = a_0\xi + c_0 + \sum_{n=1}^{\infty} (A_n e^{n\xi} + B_n e^{-n\xi}) \times (C_n \cos n\eta + D_n \sin n\eta) \quad (10)$$

Since the velocity is zero at $\xi = \infty$, the A_n's are zero and Eq. (10) becomes

$$\varphi = a_0\xi + c_0 + \sum_{n=1}^{\infty} e^{-n\xi}(a_n \cos n\eta + b_n \sin n\eta) \quad (11)$$

On the elliptic boundary, $\xi = \xi_0$,

$$\left(\frac{\partial\varphi}{\partial\xi}\right)_0 = a_0 - \sum_{n=1}^{\infty} n e^{-n\xi_0}(a_n \cos n\eta + b_n \sin n\eta) \quad (12)$$

and the coefficients a_n and b_n in the Fourier series are found in the usual manner (by multiplying either by $\sin n\eta$ or $\cos n\eta$ and integrating between the limits 0 and 2π) as

$$\left.\begin{aligned} a_0 &= \frac{1}{2\pi}\int_0^{2\pi}\left(\frac{\partial\varphi}{\partial\xi}\right)_0 d\eta \\ a_n &= -\frac{e^{n\xi_0}}{n\pi}\int_0^{2\pi}\left(\frac{\partial\varphi}{\partial\xi}\right)_0 \cos n\eta\, d\eta \\ b_n &= -\frac{e^{n\xi_0}}{n\pi}\int_0^{2\pi}\left(\frac{\partial\varphi}{\partial\xi}\right)_0 \sin n\eta\, d\eta \end{aligned}\right\} \quad (13)$$

The coefficient c_0 is evaluated in Appendix (A).

Consider now the boundary conditions of the problem. Since the boundary, which is at station s and intersects the fixed plane at time t, is denoted by C, let the boundary at $s + ds$, which intersects the plane at time $t + dt$, be denoted by C_1 (see Fig. 1b). The equation of C is

$$(x^2/a^2) + (y^2/b^2) = 1 \quad (14)$$

If ν is a normal to C directed outward and if $\delta\nu$† is the distance along this normal between C and C_1, then

$$(\partial\varphi/\partial\nu)_0 = (1/U)(\partial\nu/dt) \quad (15)$$

Thus,

$$\left.\begin{aligned} (\partial\varphi/\partial\xi)_0 &= (\partial\varphi/\partial\nu)_0(\delta\nu/\partial\xi)_0 \\ &= \frac{1}{U}\frac{\delta\nu}{dt}\left(\frac{\partial\nu}{\partial\xi}\right)_0 \\ &= \frac{1}{U}\left(\frac{\delta\nu}{\delta\xi}\right)_0^2\left(\frac{\delta\xi}{dt}\right)_0 \end{aligned}\right\} \quad (16)$$

where the subscript 0 indicates the value of the derivative on the boundary. From Fig. 1b it is evident that

$$(\delta\nu)^2 = (\delta x)^2 + (\delta y)^2$$

and since‡

$$\left.\begin{aligned} \delta x &= \left(\frac{\partial x}{\partial\xi}\right)_0 = \delta\xi\, b \cos\eta\, \delta\xi \\ \delta y &= \left(\frac{\partial y}{\partial\xi}\right)_0 \delta\xi = a \sin\eta\, \delta\xi \\ &(\delta\eta \text{ being zero}) \end{aligned}\right\} \quad (17)$$

then,

$$(\delta\nu/\delta\xi)_0^2 = a^2 \sin^2\eta + b^2 \cos^2\eta \quad (18)$$

Differentiation of Eq. (14), considering a and b variable, yields

$$b^2x\, dx + a^2y\, dy = a(b^2 - y^2)\, da + b(a^2 - x^2)db$$

This equation relates dx and dy from C to C_1 given (x, y) on C and da and db. Along the normal ν [using Eq. (17)],

$$\begin{aligned} dx &= \delta x = b \cos\eta\, \delta\xi \\ dy &= \delta y = a \sin\eta\, \delta\xi \end{aligned}$$

or

$$\frac{\delta\xi}{dt} = \frac{b\dfrac{da}{dt}\cos^2\eta + a\dfrac{db}{dt}\sin^2\eta}{a^2 \sin^2\eta + b^2 \cos^2\eta} \quad (19)$$

Substitution of Eqs. (18) and (19) into Eq. (16) yields

$$\left(\frac{\partial\varphi}{\partial\xi}\right)_0 = \frac{1}{U}\left(b\frac{da}{dt}\cos^2\eta + a\frac{db}{dt}\sin^2\eta\right) \quad (20)$$

The relation between derivatives with respect to time t and axial coordinate s may be determined by considering the boundary conditions of the body. Since the body surface is a stream surface,

$$\frac{\delta\nu}{ds} = \frac{\partial\varphi/\partial\nu}{1 + (\partial\varphi/\partial s)} = \frac{(1/U)(\delta\nu/dt)}{1 + (\partial\varphi/\varphi s)} = \frac{1}{U}\frac{\delta\nu}{dt} + 0(d^{*2} \ln d^*) \quad (21)$$

Thus Eq. (20) can be written

$$\left(\frac{\partial\varphi}{\partial\xi}\right)_0 = b\frac{da}{ds}\cos^2\eta + a\frac{db}{ds}\sin^2\eta \quad (22)$$

Eq. (22) may now be used in the evaluation of the coefficients of Eq. (13), which results in

$$\left.\begin{aligned} a_0 &= \frac{1}{2}\left(b\frac{da}{ds} + a\frac{db}{ds}\right) = \frac{S'(s)}{2\pi} \\ a_2 &= \frac{1}{4}e^{2\xi_0}a^2\frac{d}{ds}\left(\frac{b}{a}\right) \\ a_n &= 0, \qquad n = 1, 3, 4, 5\ldots \\ b_n &= 0, \qquad n = 1, 2, 3, 4\ldots \end{aligned}\right\} \quad (22a)$$

Substitution of the above relations and Eq. (A-5) in Eq. (11) gives, for the potential,

† The symbol δ preceding a quantity denotes the differential of that quantity along the normal between C_1 and C—i.e., the value at C_1 minus the value at C.

‡ From Eq. (6)

$$(\partial x/\partial\xi)_0 = c \sinh\xi_0 \cos\eta = b\cos\eta$$
$$(\partial y/\partial\xi)_0 = c \cosh\xi_0 \sin\eta = a\sin\eta$$

$$\varphi = \frac{S'(s)}{2\pi}\left(\xi + \ln\frac{c}{2}\right) + b_0 + \frac{a^2}{4}\frac{d}{ds}\left(\frac{b}{a}\right) e^{-2(\xi - \xi_0)} \cos 2\eta \quad (23)$$

Pressure Distribution on Elliptic Cone

The linearized form of the pressure equation is[7]

$$\frac{\Delta p}{q_1} = \frac{p - p_1}{q_1} = -2\frac{\partial\varphi}{\partial s} - \left(\frac{\partial\varphi}{\partial x}\right)^2 - \left(\frac{\partial\varphi}{\partial y}\right)^2 + 0(d^{*4} \ln d^*) \quad (24)$$

The potential for an elliptic cone is, from Eq. (23), since for a cone and for any other body with b/a constant $[d(b/a)/ds = 0]$,

$$\varphi = [S'(s)/2\pi][\xi + \ln (c/2)] + b_0 \quad (25)$$

The above equation indicates that, for elliptic bodies expanding so that b/a is constant, the instantaneous flow pattern is such that the ellipses confocal to the boundary (ξ = constant lines) are equipotential lines, with the set of confocal hyperbolae (η = constant lines) being the stream lines.

Clearly, the s = constant plane stream line and potential field patterns alter with time (or axial distance s), so that at each new instant of time the boundary ellipse ξ_0 is an equipotential line of a new potential field. Since the value of ξ on the boundary is constant [ξ_0 depends, as shown by Eq. (31), only on the ratio b/a], the flow pattern in each plane is identical except for scale. This conclusion is not surprising, since the flow is conical—i.e., the perturbation velocities and pressures are constant along rays extending downstream from the cone vertex.

Since the boundary is an equipotential line, the tangential velocity on the body in any plane s = constant is zero, and Eq. (24) becomes

$$C_p = \frac{\Delta p}{q_1} = -2\frac{\partial\varphi}{\partial s} - \left(\frac{\partial\varphi}{\partial\nu}\right)^2 \quad (26)$$

From Eq. (25),

$$\frac{\partial\varphi}{\partial s} = \frac{S''(s)}{2\pi}\left(\xi + \ln\frac{c}{2}\right) + \frac{S'(s)}{2\pi}\left(\frac{\partial\xi}{\partial s} + \frac{1}{c}\frac{dc}{ds}\right) + b_0'(s) \quad (27)$$

From Eq. (A-1)

$$\frac{\partial\xi}{\partial s} = -\frac{1}{c}\frac{dc}{ds}\sqrt{\frac{1 - \left(\frac{c}{r}\right)^2\cos 2\theta + \sqrt{1 + \left(\frac{c}{r}\right)^4 - 2\left(\frac{c}{r}\right)^2\cos 2\theta}}{2\left[1 + \left(\frac{c}{r}\right)^4 - 2\left(\frac{c}{r}\right)^2\cos 2\theta\right]}} = (1/c)(dc/ds)F(c/r, \theta) \quad (28)$$

where $F(c/r, \theta)$ is defined by the above equations, and c/r is found on the boundary using the equation of the ellipse. Boundary values of the quantity $F(c/r, \theta)$ are tabulated for several ellipse eccentricities in Table 1. From Eq. (4), or Ward,[7]

$$b_0'(s) = \frac{1}{2\pi}\left[S''(s) \ln\frac{B}{2} - S''(0) \ln s - \int_0^s \ln (s - \sigma)\, S'''(\sigma)\, d\sigma\right] \quad (29)$$

Table 1
Boundary Values of the Quantity $F(c/r, \theta)$ for Several Ellipse Eccentricities

Angle θ	$F(c/r, \theta)$					
	$\epsilon = 1$	$\epsilon = 2/3$	$\epsilon = 1/2$	$\epsilon = 1/3$	$\epsilon = 1/4$	$\epsilon = 1/5$
0	1.0000	1.5000	2.0000	3.0000	4.0000	5.0000
2	1.0000	1.4946	1.9690	2.7578	3.1060	2.9234
4	1.0000	1.4800	1.8916	2.2436	1.9163	1.3835
6	1.0000	1.4559	1.7747	1.7874	1.2325	0.80719
8	1.0000	1.4244	1.6401	1.3626	0.86925	0.55974
10	1.0000	1.3867	1.5005	1.0915	0.66852	0.43491
12	1.0000	1.3449	1.3745	0.90581	0.54841	0.36417
14	1.0000	1.3005	1.2524	0.77529	0.47170	0.32045
16	1.0000	1.2551	1.1478	0.68154	0.42008	0.29162
18	1.0000	1.2097	1.0906	0.61259	0.38380	0.27165
20	1.0000	1.1655	0.98082	0.56070	0.36616	0.25728
25	1.0000	1.0633	0.81649	0.47662	0.31616	0.23506
30	1.0000	0.97672	0.73685	0.42858	0.29343	0.22293
40	1.0000	0.84922	0.62229	0.38061	0.27069	0.21133
50	1.0000	0.76841	0.56323	0.35632	0.26029	0.20569
60	1.0000	0.71814	0.53061	0.34741	0.25487	0.20275
70	1.0000	0.68793	0.51232	0.33768	0.25195	0.20117
80	1.0000	0.67175	0.50292	0.33435	0.25046	0.20042
90	1.0000	0.66667	0.50000	0.33333	0.25000	0.20000

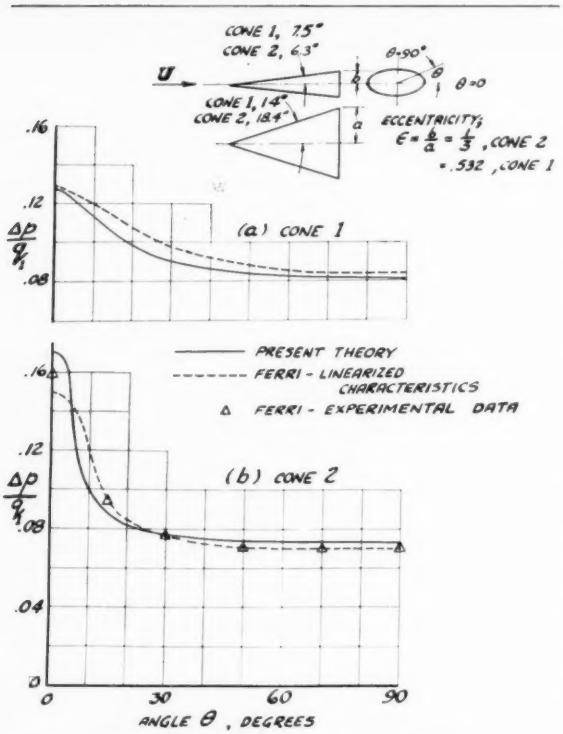

FIG. 3 PRESSURE DISTRIBUTION ON ELLIPTICAL CONES; COMPARISON OF PRESENT THEORY WITH FERRI'S LINEARIZED CHARACTERISTICS THEORY AND EXPERIMENTAL DATA. $M = 1.81$.

For a cone, $S'''(s) = 0$ and $S''(s) = S''(0)$, so that

$$b_0'(s) = [S''(s)/2\pi] \ln [B/2s]$$

If the ratio of minor to major axes of the cone is called

$$\epsilon = b/a$$

then, on the boundary,

$$\frac{dc}{ds} = \frac{c}{s} = \sqrt{1 - \epsilon^2}\,\frac{da}{ds}$$

[from Eq. (7)]

$$(1/c)(dc/ds) = (1/a)(da/ds)$$

Now, for an elliptic cone,

$$\begin{aligned} S'(s)/2\pi &= \epsilon a(da/ds) \\ S''(s)/2\pi &= \epsilon(da/ds)^2 \end{aligned} \tag{30}$$

From Eqs. (6),

$$\left.\begin{aligned} \xi = \cosh^{-1}\frac{a}{c} &= \cosh^{-1}\frac{1}{\sqrt{1-\epsilon^2}} \\ &= \ln\sqrt{(1+\epsilon)/(1-\epsilon)} \end{aligned}\right\} \tag{31}$$

The above relations when substituted into Eq. (27) yield

$$\frac{\partial\varphi}{\partial s} = \epsilon\left(\frac{da}{ds}\right)^2\left\{1 - F\left(\frac{c}{r},\theta\right) + \ln\left[\frac{B}{4}(1+\epsilon)\frac{da}{ds}\right]\right\} \tag{32}$$

On the boundary, from Eqs. (14) and (15),

$$\frac{\partial\varphi}{\partial\nu} = \epsilon\frac{da}{ds}\sqrt{\frac{\epsilon^2 + \tan^2\theta}{\epsilon^4 + \tan^2\theta}} \tag{33}$$

The pressure coefficient, Eq. (26), may now be expressed, using Eqs. (32) and (33), as

$$C_p = -\epsilon\left(\frac{da}{ds}\right)^2\left\{2\left[1 - F\left(\frac{c}{r},\theta\right) + \ln\frac{B}{4}(1+\epsilon)\frac{da}{ds}\right] + \epsilon\left(\frac{\epsilon^2 + \tan^2\theta}{\epsilon^4 + \tan^2\theta}\right)\right\}$$

where $F(c/r, \theta)$ is given by Eq. (28) or Table 1.

Pressure distributions on two elliptic cones at zero angle of attack have been calculated for $M_1 = 1.81$; the results are plotted in Fig. 3. The cones are of ratio of minor to major axes, ϵ, of 1/1.88 and 1/3. The corresponding equivalent area circular cones have semivertex angles of 10.5° and 11.0°, respectively. The geometry of the cones is given in Fig. 3. In that figure is also indicated the pressure distributions calculated by Ferri[6] with the linearized method of characteristics, as well as his experimentally obtained values. Agreement between the two theoretical methods and experimental results is good, even in the case of the $\epsilon = 1/3$ cone, whose major axis semivertex angle (18.4°) would seem to be greater than that permitted under the assumptions of the slender theory. (See footnote on page 514.)

Pressure Distribution on a Parabolic Body of Elliptic Cross Section

Consider a body of unit length of elliptic cross section whose semimajor and semiminor axes are characterized by the following parabolic arc relations:

$$\begin{aligned} a(s) &= 4\mathfrak{A}_0 s(1-s) \\ b(s) &= 4\mathfrak{B}_0 s(1-s) \end{aligned}$$

where $2\mathfrak{A}_0$ and $2\mathfrak{B}_0$ are the maximum values of the major and minor axes, respectively. The ratio, ϵ, of the elliptic sections is then constant, since

$$\epsilon = \frac{b(s)}{a(s)} = \frac{\mathfrak{B}_0}{\mathfrak{A}_0} = \text{const.}$$

so that the potential is given by Eq. (25). If an effective thickness ratio for the body is defined as

$$d = 2\sqrt{\mathfrak{A}_0\mathfrak{B}_0}$$

(i.e., the thickness ratio is the same as that for the body of revolution with equivalent area distribution); then, using Eqs. (27), (28), and (29),

$$\frac{\partial\varphi}{\partial s} = 4d^2[(1 - 6s + 6s^2)\ln Bd(1 - s) + 3s(3s - 2)] + 4d^2\left\{(1 - 6s + 6s^2)\ln\frac{1+\epsilon}{2\sqrt{\epsilon}} + (1 - 2s)^2\left[1 - F\left(\frac{c}{r}, \theta\right)\right]\right\} = \left(\frac{\partial\varphi}{\partial s}\right)_c + 4d^2\left\{(1 - 6s + 6s^2)\ln\frac{1+\epsilon}{2\sqrt{\epsilon}} + (1 - 2s)^2\left[1 - F\left(\frac{c}{r}, \theta\right)\right]\right\} \quad (34)$$

where $(\partial\varphi/\partial s)_c$ is the value of $\partial\varphi/\partial s$ for the equivalent parabolic body of revolution [see Eq. (B-5)], and $F(c/r, \theta)$ is given by Eq. (28). Using Eq. (33), the normal velocity is found to be

$$\partial\varphi/\partial\nu = 2d(1 - 2s)\sqrt{\epsilon(\epsilon^2 + \tan^2\theta)/(\epsilon^4 + \tan^2\theta)} \quad (35)$$

The pressure distribution may now be computed using Eqs. (26), (34), and (35).

The zero angle of attack pressure distribution on a parabolic arc body is shown in Fig. 4 for a Mach Number of 2. The body has an effective thickness ratio, d, of 0.10; the ratio, ϵ, of minor to major axes of the elliptic cross section is $1/3$. The dashed lines in the figure represent pressure coefficient values (these are independent of θ) of the equivalent parabolic arc body of revolution, which are obtained from Eqs. (B-8) and (B-9) of Appendix (B). The variation of pressure coefficient with angle θ at stations close to the nose and tail of the body is similar to that for the elliptic cone—i.e., the pressure peaks at $\theta = 0°$ and is fairly constant for values of θ between 30° and 90°. At the midpoint of the body ($s = 0.5$), however, C_p is independent of angle θ and varies only slightly with θ in the region close by on either side. The slight drop of C_p near $\theta = 0°$ at $s = 0.4$ and 0.6 is attributed to the predominance of the $\partial\varphi/\partial\nu$ term in this region.

Wave Drag of Bodies with Bases of Elliptic Cross Section

Ward[7] has shown that the wave drag of a body of unit length is expressed by

$$\frac{D}{(1/2)\rho_1 U^2} = \frac{1}{2\pi}\int_0^1\int_0^1 \ln\frac{1}{|s - \sigma|} S''(s)S''(\sigma)\,d\sigma\,ds - \frac{S'(1)}{2\pi}\int_0^1 \ln\frac{1}{1 - \sigma} S''(\sigma)\,d\sigma - \left(\int_{C_1}\varphi\frac{\partial\varphi}{\partial\nu}\,d\tau\right)_{s=1} + 0\,(d^{*6}\ln^2 d^*) \quad (36)$$

where the contour C_1 for the third integral is the boundary at the base of the body. Since the first two integrals are independent of the cross-sectional shape of the body, it is apparent that the wave drag of arbitrary bodies differs from the wave drag of the equivalent body of revolution by the difference of the value for both bodies of the third integral.† The third integral vanishes if the rear of the body is either pointed or cylindrical; thus, for these cases, the drag of a body of arbitrary cross section is equal to the drag of the equivalent body of revolution.

If

$$I \equiv [\textstyle\int_{C_1}\varphi(\partial\varphi/\partial\nu)\,d\tau]_{s=1}$$

then the drag difference between bodies of equivalent area distribution having elliptic and circular bases is

$$(D_e - D_c)/q = I_c - I_e$$

where the subscripts c and e denote circular and elliptic bases, respectively.

Expressions for I_c and I_e are obtained from Eqs. (B-1), (B-3), (18), (20), and (25) as

$$I_c = S'(1)\left[\frac{S'(1)}{2\pi}\ln R(1) + b_0(1)\right]$$

$$I_e = S'(1)\left\{\frac{S'(1)}{2\pi}\left[\xi_0(1) + \ln\frac{c(1)}{2}\right] + b_0(1)\right\} - \frac{\pi}{8}a^4\left(\frac{d\epsilon}{ds}\right)^2$$

† It will be noted that $-(1/2)\rho[\int_{C_1}\varphi(\partial\varphi/\partial\nu)d\tau]_{s=1}$ is the linearized value of the planar component of the kinetic energy at the station $s = 1$.

where $R(1)$ and $\xi_0(1)$ are the base radius and elliptic coordinate for the circular and elliptic body, respectively. Since the bodies are assumed equivalent [i.e., $S_c(s) = S_e(s)$], then

$$\frac{D_e - D_c}{q} = \frac{[S'(1)]^2}{2\pi}\left[\ln\frac{2R(1)}{c(1)} - \xi_0(1)\right] + \frac{\pi}{8}a^4\left(\frac{d\epsilon}{ds}\right)^2_{s=1}$$

or, using Eqs. (30) and (31),

$$C_{D_e} - C_{D_c} = \frac{[S'(1)]^2}{2\pi S(1)}\ln\frac{2\sqrt{\epsilon(1)}}{1 + \epsilon(1)} + \frac{[a(1)]^2}{8\epsilon(1)}\left(\frac{d\epsilon}{ds}\right)^2_{s=1} = \Delta C_{D_1} + \Delta C_D \quad (37)$$

The difference in drag between equivalent elliptic and circular base bodies may be considered, therefore, as the sum of two quantities, ΔC_{D_1} and ΔC_{D_2}, as given by the first and second terms, respectively, of Eqs. (37). The quantity ΔC_{D_1} arises from the rate of change of area at the base, while ΔC_{D_2} results from the rate of

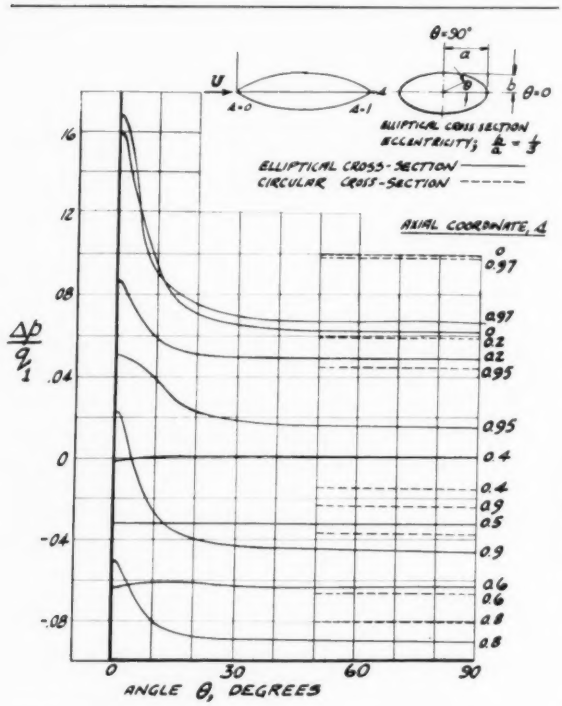

FIG 4. PRESSURE DISTRIBUTION ON PARABOLIC ARC BODIES OF ELLIPTICAL AND CIRCULAR CROSS-SECTION; MACH NUMBER 2, EFFECTIVE THICKNESS RATIO 0.10.

FIG. 5 DRAG DIFFERENCE BETWEEN EQUIVALENT ELLIPTICAL AND CIRCULAR CONES.

change of eccentricity of the base elliptic boundary. Since

$$\ln \frac{2\sqrt{\epsilon}}{1+\epsilon} \leq 0,\ 0 \leq \epsilon \leq 1$$

then $\Delta C_{D_1} \leq 0$. Then, it is also evident that

$$\Delta C_{D_2} \geq 0$$

Therefore, the wave drag of an elliptic-base body with zero rate of change of eccentricity at the base [i.e., $(d\epsilon/ds)_{s=1} = 0$] is lower than the wave drag of the equivalent body of revolution; a nonzero rate of change of eccentricity at the body base increases the drag of the body.

The drag difference between equivalent elliptic and circular cones is plotted in Fig. 5 for a range of elliptic cone eccentricities.† The limiting case of an ellipse, the flat plate ($\epsilon = 0$), has no meaning as far as Fig. 5 is concerned, since the curves give the drag difference between equivalent (in cross-sectional area) cones. The wave drag for $\epsilon = 0$ is, of course, zero.

The curves of Fig. 5 may be used to determine the difference in wave drag coefficient of two arbitrary equivalent area bodies, one having a circular base and the other having an elliptical base, with zero rate of change of eccentricity at the base. For this application, the abscissa of the figure corresponds to the angle between the meridian plane body curve at the base of the circular body and the body axis.

The wave drags of the two elliptic cones of Figs. 3a and 3b have been calculated by adding to the drags of the equivalent circular cones, Eq. (B-4), the differences given by Eq. (36). Drag coefficient values of 0.097 and 0.098, respectively, are obtained as compared to those calculated by Ferri[6] of 0.103 and 0.099 for the same cases. This good agreement is not surprising in view of the good agreement obtained between the two theories for the pressure distribution. If the percentage drag difference between equivalent elliptic and circular cones is defined by the following equation

$$\%\ \text{drag difference} = \left(\frac{C_{D\epsilon} - C_{Dc}}{C_{Dc}}\right)100$$

then for the elliptic cone of Fig. 3b, for example, the drag reduction given by the results of the slender theory is about 10 per cent, while that according to the results of Ferri's nonlinear theory is about 17 per cent. Since the elliptic cone drag given by both theories is nearly the same, the apparent wide discrepancy in percentage drag reduction is due to the difference of values of drag of the equivalent circular cone given by the nonlinear and slender theories, the nonlinear drag being about 10 per cent higher than the slender drag. Hence, the drag differences (the numerator of the above equation) are widely different, being small differences between large numbers, and account, therefore, for the lack of close agreement between the two theories. It is suggested, then, that the drag of an elliptic cross-section body be calculated directly from the slender theory [Eq. (36)], rather than by adding the drag difference between equivalent elliptic and circular cross-

† Eccentricity is defined in this paper as $1/\epsilon$; the formal definition in analytic geometry is $\sqrt{1-\epsilon^2}$.

section bodies, Eq. (37), to the drag of the equivalent circular body as calculated by more accurate methods.

Remarks on the Calculation of the Pressure Distribution on Slender Bodies of Elliptic Cross Section at Angle of Attack

In order to calculate the pressure coefficient on slender elliptic bodies at angle of attack, α, the additional pressure coefficient due to angle of attack may be superposed upon the zero angle of attack pressure coefficient as calculated from the present theory—i.e.,

$$\Delta p/q = (\Delta p/q)_{\alpha=0} + (\Delta p/q)_{\alpha}$$

The additional potential, φ_{α}, due to angle of attack (to order of the slender theory) is the two-dimensional incompressible potential of an elliptic boundary (which maintains constant area and eccentricity with time) translating in the reference plane with velocity $U\alpha$. This potential is a classical result and is given, for example, by Ward.[7]

Concluding Remarks

A theory, based on the first-order solution of Ward[7] for bodies of generalized cross section, has been presented for the supersonic flow about bodies of elliptic cross section. The theory has been applied to the calculation of zero angle of attack cones and parabolic arc bodies of elliptic cross section; several example pressure distributions for these bodies are presented. The cone pressure distributions are compared to the nonlinear theoretical calculations and experimental results given by Ferri.[6] Agreement is found to be good even for a cone that has a larger slope than that for which a slender theory appears applicable.

The wave drag of bodies having elliptic bases has been derived. It is shown that the wave drag of an elliptic base body with zero rate of change of eccentricity at the base is lower than the wave drag of the equivalent area body of revolution. A nonzero rate of change of eccentricity at the base of the body increases the wave drag of the body. The wave drag of the two elliptic cones calculated also agrees very well with the nonlinear results of Ferri.[6]

The Ward[7] slender theory is also applied to cones and parabolic arc bodies of revolution. Comparisons are made with the results of other linear theories and (for the cone) the nonlinear theory.

The application of the present elliptic cross-section body theory to bodies at angle of attack is also briefly indicated.

References

[1] Van Dyke, Milton D., *First- and Second-Order Theory of Supersonic Flow Past Bodies of Revolution*, Journal of the Aeronautical Sciences, Vol. 18, No. 3, pp. 161–178, March, 1951.

[2] von Kármán, Th., and Moore, Norton B., *Resistance of Slender Bodies Moving with Supersonic Velocities, with Special Reference to Projectiles*, Trans. A.S.M.E., Vol. 54, No. 23, pp. 303–310, December 15, 1932.

[3] Maslen, Stephen H., *Method for Calculation of Pressure Distributions on Thin Conical Bodies of Arbitrary Cross-Section in Supersonic Stream*, NACA TN No. 1659, July, 1948.

[4] Laporte, O., and Bartels, R. C. F., *An Investigation of the Exact Solutions of the Linearized Equations for the Flow Past Conical Bodies*, University of Michigan Bumblebee Report No. 75, February, 1948.

[5] Graham, Ernest W., *The Pressure on a Slender Body of Non-uniform Cross-Sectional Shape in Axial Supersonic Flow*, Journal of the Aeronautical Sciences, Vol. 17, No. 3, pp. 173–176, March, 1950.

[6] Ferri, Antonio, *The Linearized Characteristics Method and Its Application to Practical Non-Linear Supersonic Problems*, NACA TN No. 2515, October, 1951.

[7] Ward, G. N., *Supersonic Flow Past Slender Pointed Bodies*, Quart. Jour. Mech. and Applied Math., Vol. II, Pt. 1, pp. 74–97, 1949.

[8] Ferri, Antonio, *Elements of Aerodynamics of Supersonic Flows*; The Macmillan Company, New York, 1949.

[9] Munk, Max M., *The Aerodynamic Forces on Airship Hulls*, NACA Report No. 184, 1924.

[10] Jones, R. T., *Properties of Low-Aspect-Ratio Pointed Wings at Speeds Below and Above the Speed of Sound*, NACA Report No. 835, 1946.

[11] Milne-Thompson, L. M., *Theoretical Hydrodynamics*, pp. 156–158; Macmillan and Company, London, 1938.

[12] Bateman, H., *Partial Differential Equations of Mathematical Physics*, p. 430; Dover, New York, 1944.

[13] Pipes, Louis A., *Applied Mathematics for Engineers and Physicists*, pp. 402–405, 83–84; McGraw-Hill Book Company, Inc., New York, 1946.

[14] Taylor, G. I., and Maccoll, J. C., *The Air Pressure on a Cone Moving at High Speeds*, Proc. Roy. Soc. (A), Vol. 139, pp. 278–311, 1933.

[15] von Kármán, Th., *The Problem of Resistance in Compressible Fluids*, Atti dei Convegni 5, R. Accad. d'Italia, pp. 222–277, 1936.

[16] Jones, Robert T., and Margolis, Kenneth, *Flow over a Slender Body of Revolution at Supersonic Velocities*, NACA TN No. 1081, August, 1946.

[17] Broderick, J. B., *Supersonic Flow Round Pointed Bodies of Revolution*, Quart. Jour. Mech. and Applied Math., Vol. II, pp. 98–120, 1949.

[18] The Staff of the Computing Section, Center of Analysis (under the direction of Zdenek Kopal), *Tables of Supersonic Flow Around Cones*, M.I.T., Center of Analysis, Technical Report No. 1, 1947.

[19] Lighthill, M. J., *Supersonic Flow Past Bodies of Revolution*, R. & M. 2003, British A.R.C., 1945.

Appendix (A)—Evaluation of Coefficient c_0

The coefficient c_0, which occurs in Eq. (11), will be evaluated herein. Using Eq. (6), it may be determined that

$$\xi = \frac{1}{2}\cosh^{-1}\left[\left(\frac{r}{c}\right)^2 + \sqrt{\left[1-\left(\frac{r}{c}\right)^2\right]^2 + 4\left(\frac{r}{c}\right)^2 \sin^2\theta}\right]$$

$$\xi = \ln \frac{r}{c} + \frac{1}{2} \ln \left[1 + \sqrt{\left[1 - \left(\frac{c}{r} \right)^2 \right]^2 + 4 \left(\frac{c}{r} \right)^2 \sin^2 \theta} + \sqrt{2 \left[1 - \left(\frac{c}{r} \right)^2 \cos 2\theta + \sqrt{\left[1 - \left(\frac{c}{r} \right)^2 \right]^2 + 4 \left(\frac{c}{r} \right)^2 \sin^2 \theta} \right]} \right]$$

$$= \ln (r/c) + (1/2) \ln G(c/r, \theta) \tag{A-1}$$

where $G(c/r, \theta)$ is defined by Eqs. (A-1). Eq. (11) may now be written [using Eqs. (22a)] as

$$\varphi = \frac{S'(s)}{2\pi} \ln r + c_0 + \frac{S'(s)}{4\pi} \ln \frac{1}{c^2} G\left(\frac{c}{r}, \theta \right) + \frac{\frac{a^2}{4} \frac{d\epsilon}{ds} e^{2\xi_0} \cos 2\eta}{\left(\frac{r}{c} \right)^2 G\left(\frac{c}{r}, \theta \right)}$$

$$= \frac{S'(s)}{2\pi} \ln r + c_0 + f_1(r, \theta) + f_2(r, \theta) \tag{A-2}$$

From the general solution of Ward's Eq. (3), the above equation must have the following form:

$$\varphi = \frac{S'(s)}{2\pi} \ln r + c_0 + d_0 + \sum_{n=1}^{\infty} a_n r^{-n} \cos (n\theta + \beta_n) \tag{A-3}$$

where the last two terms of Eq. (A-3) are equal to the last two terms of Eq. (A-2). Thus, since

$$0 \leq |\cos 2\eta| \leq 1$$

and since $e^{2\xi_0}$ is finite for finite ξ_0, then

$$d_0 = \lim_{r \to \infty} (f_1 + f_2) = \frac{S'(s)}{2\pi} \ln \frac{2}{c} \tag{A-4}$$

Comparing Eqs. (3) and (A-3) and using Eq. (A-4), there results

$$c_0 = -d_0 + b_0 = \frac{S'(s)}{2\pi} \ln \frac{c}{2} + b_0 \tag{A-5}$$

with b_0 given by Eq. (4).

Appendix (B)—Pressure Coefficient on Circular Cones and Parabolic Bodies of Revolution

The pressure coefficient for circular cones and parabolic bodies of revolution at zero angle of attack will be derived here from the Ward-type slender theory, and comparisons will be made with more exact theories.

Since the potential φ for an axisymmetrical body is independent of the polar coordinate θ when the body is at zero angle of attack, the coefficients a_n of Eq. (3) are zero and

$$\varphi = [S'(s)/2\pi] \ln r + b_0 \tag{B-1}$$

For a cone of boundary radius $r = R(s)$

$$\begin{aligned} S(s) &= \pi R^2 \\ S'(s) &= 2\pi R(dR/ds) \\ S''(s) &= 2\pi (dR/ds)^2 = \text{const.} \\ S'''(s) &= 0 \end{aligned}$$

Thus, on the surface of the cone,

$$\frac{\partial \varphi}{\partial s} = [S''(s)/2\pi] \ln r + b_0' = \left(\frac{dR}{ds} \right)^2 \ln \frac{Br}{2s} \text{ [using Eq. (29)]} \tag{B-2}$$

$$\partial \varphi / \partial \nu = dR/ds \tag{B-3}$$

Since $dR/ds = \tan \mu$, where μ is the cone semivertex angle, then from Eqs. (B-2), (B-3), and (24)

$$C_p = -\tan^2 \mu [2 \ln (B \tan \mu/2) + 1] = C_D \tag{B-4}$$

It will be noted that the above equation is equivalent to the first two terms of Broderick's[17] series solution (Broderick expands the potential, which satisfies the nonlinear potential equation, in a power series in the thickness and logarithms of the thickness) for the cone. The Ward-type slender body solution, therefore, gives essentially the first-order solution to the problem. It is of interest to compare the circular cone pressure coefficient given by this slender theory with the results of higher order linear theories and the nonlinear theory. This comparison is made in Fig. 6 for cone semivertex angles of 5, 10, 15, and 20 deg. The other theories used are described below and are listed in order of estimated accuracy.

(*a*) *Nonlinear Taylor-Maccoll Theory.*[14]—The nonlinear theory is, of course, the most accurate of the theories listed. The values plotted in the figure were obtained from the M.I.T. Tables.[18]

(*b*) *von Kármán-Moore Linearized Theory.*—von Kármán and Moore[2] demonstrate that a solution to the linearized potential equation, Eq. (2), which satisfies the boundary conditions for a body of revolution at zero angle of attack, is

$$\varphi(s, r) = \int_0^{s - Br} \frac{f(\sigma)\, d\sigma}{\sqrt{(S - \sigma)^2 - B^2 r^2}} \tag{B-5}$$

The potential, thus, is that due to a supersonic source

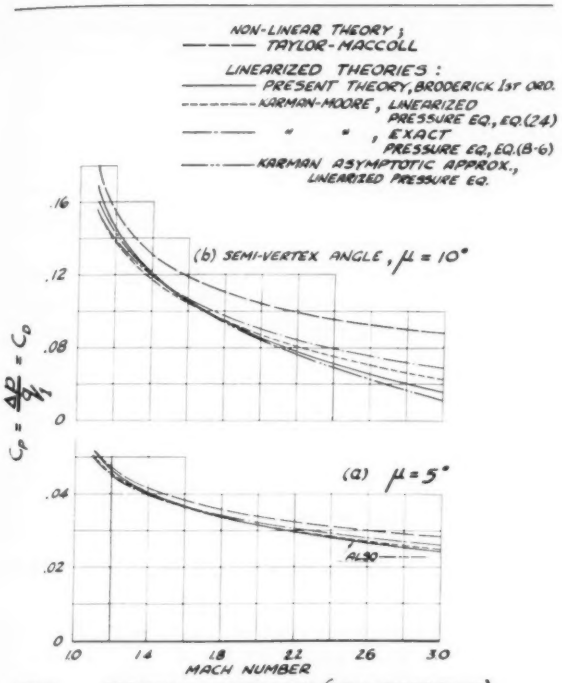

FIG. 6 PRESSURE COEFFICIENT (DRAG COEFFICIENT) ON CIRCULAR CONES ; COMPARISON OF VARIOUS THEORIES WITH PRESENT THEORY.

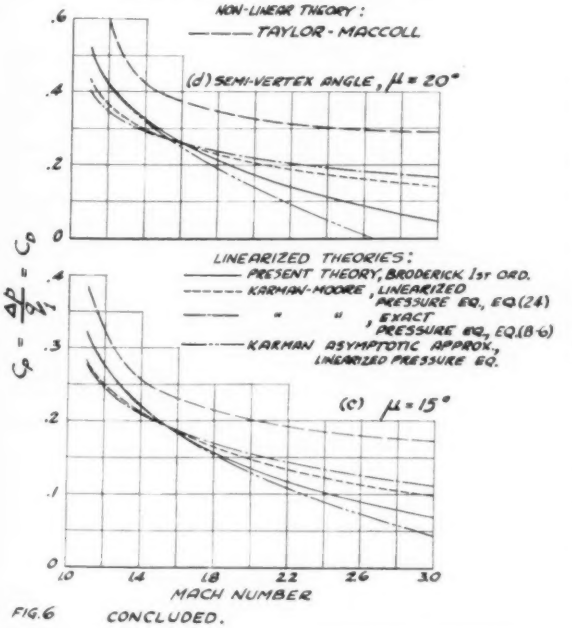
NON-LINEAR THEORY :
TAYLOR-MACCOLL
(d) SEMI-VERTEX ANGLE, μ = 20°
LINEARIZED THEORIES :
PRESENT THEORY, BRODERICK 1st ORD.
KARMAN-MOORE, LINEARIZED PRESSURE EQ., EQ.(24)
" " , EXACT PRESSURE EQ., EQ.(B-6)
KARMAN ASYMPTOTIC APPROX., LINEARIZED PRESSURE EQ.
(c) μ = 15°
MACH NUMBER

FIG. 6 CONCLUDED.

distribution, of local strength $f(s)$, extending downstream from the origin along the body axis. The upper limit of integration indicates that only that portion of the line source in the fore Mach cone of the point (s, r) affects the flow at the point. In the von Kármán-Moore theory, the boundary conditions are satisfied *exactly* at the *body surface*. This fact requires that a stepwise calculation be carried out for an arbitrary body of revolution; the line source is broken up into a number of discrete sources of constant value of $f'(s)$, the integral [Eq. (B-5)] being replaced by a corresponding summation formula. The source strength for each step can be calculated once the strengths of the sources upstream of the given source are known. The solution for a cone can be obtained in closed analytical form; the perturbation velocities are[2]

$$\varphi_s = -K_1 \cosh^{-1}(\cot \mu/B)$$

$$\varphi_r = K_1 B \sqrt{(\cot \mu/B)^2 - 1}$$

where

$$K_1 = \frac{\tan \mu}{\sqrt{\cot^2 \mu - B^2} + \tan \mu \cosh^{-1}(\cot \mu/B)}$$

Some controversy exists at the present time as to the pressure coefficient equation to be used with a linear theory once the perturbation velocities are obtained from the equation for the potential. Van Dyke[1] advocates the use of the exact pressure equation,

$$\frac{\Delta p}{q} = \frac{2}{\gamma M_1^2} \times \left\{ \left[1 + \frac{\gamma - 1}{2} M_1^2 (1 - \varphi_z^2 - \varphi_r^2) \right]^{\gamma/\gamma - 1} - 1 \right\} \quad \text{(B-6)}$$

where γ is the ratio of the specific heats. He recognizes, however, the inconsistency of its use, since the order of approximation of the linearized pressure equation [Eq. (24)] is not lower than that of the linearized potential equation. Results obtained using both pressure equations are plotted in Fig. 6.

(*c*) *von Kármán Asymptotic Approximation to the Solution of the Linearized Potential Equation.*[15]—This solution is obtained from the von Kármán-Moore[2] integral formula for the potential, Eq. (B-1), by satisfying the *linearized* body conditions, Eq. (22), rather than the exact boundary conditions, on the *body axis* rather than on the body surface. With this assumption, the source strength can be shown to be

$$f(s) = (1/2\pi) S'(s)$$

This relation substituted into Eq. (B-5) gives, for the potential,

$$\varphi(s, r) = \frac{1}{2\pi} \int_0^{s - Br} \frac{S'(\sigma)\, d\sigma}{\sqrt{(s - \sigma)^2 - B^2 r^2}} \quad \text{(B-7)}$$

Thus, if the body area is given in analytical form, the above equation may yield the potential in closed analytical form. It has been shown by Lighthill[19] that Eq. (B-7) gives φ with an error of $0(d)$. Thus, since Eq. (3) has an error term of $0(d^*)$, it is seen that the von Kármán asymptotic approximation leads to errors of the same order as the Ward-type slender theory.

The pressure coefficient for a cone given by the von Kármán theory, using the linearized pressure equation

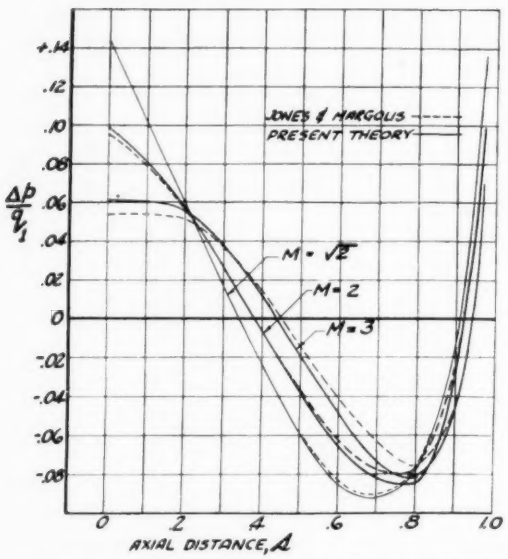

FIG. 7 PRESSURE DISTRIBUTION, PARABOLIC BODY OF REVOLUTION. EFFECTIVE THICKNESS RATIO 0.10.

[Eq. (24)], can be shown to be

$$\frac{\Delta p}{q} = \tan^2 \mu \left[2 \cosh^{-1}\left(\frac{1}{B \tan \mu}\right) - 1 \right]$$

In Fig. 6 it is indicated that the von Kármán-Moore solution with the exact pressure equation agrees most closely with the nonlinear results. As is expected the agreement of the linear theories is best for smaller cone angles; the agreement is also best at the lower Mach Numbers. The agreement between the von Kármán asymptotic approximation and the Ward-type or Broderick first-order solution is close, as expected except at the higher Mach Number range and for the larger cone angles. Here, the von Kármán solution appears to be inferior.

The slender theory pressure coefficient on a parabolic body of revolution of unit length, whose surface is characterized by the equation

$$R = 2d(1 - s)s$$

(d is the fineness ratio of the body), may be derived using Eqs. (B-2) and (29), with the result that

$$\partial\varphi/\partial s = 4d^2[(1 - 6s + 6s^2) \ln Bd(1 - s) + 3s(3s - 2)] \quad \text{(B-8)}$$

$$\partial\varphi/\partial\nu = 2d(1 - 2s) \quad \text{(B-9)}$$

The pressure coefficient calculated from the Eqs. (B-8), (B-9), and (26) for a body of fineness ratio of 0.10 is presented in Fig. 7 for flight Mach Numbers of $\sqrt{2}$; 2, and 3. In that figure is also indicated results of calculations using the von Kármán[15] asymptotic solution to the linear theory integral equation for φ [Eq. (B-7)], which was applied to the parabolic body of revolution by Jones and Margolis.[16] The agreement between the two methods is, as is expected, very good.

IAS Twenty-Second Annual Meeting

Authors wishing to have papers considered for presentation at this meeting should submit outlines or short abstracts to the Meetings Committee, 2 East 64th St., New York 21, N.Y., no later than September 15, 1953.

Three-Dimensional Laminar Boundary-Layer Flow

FRANKLIN K. MOORE*

Lewis Flight Propulsion Laboratory, NACA

SUMMARY

The possibilities for predicting steady three-dimensional boundary-layer behavior are inferred from detailed consideration of the case of a cone at angle of attack to a supersonic stream.

Qualitative features of the cone boundary layer are discussed, and solutions are presented in which (a) angle of attack is assumed small (a method of perturbations), thickening of the boundary layer on the lee side of the cone is indicated but no separation of the cross flow occurs; and (b) consideration is restricted to the plane of symmetry of the flow, with no restriction on angle of attack. On the lee side of the cone, unique solutions are limited to small angle of attack, and beyond a certain angle of attack, the boundary layer cannot remain thin.

The concepts of displacement thickness and flow separation are generalized to three dimensions, and failure of the thin boundary-layer assumptions is related to the formation of strong vortices in a separated region, for laminar or, more tentatively, turbulent flow.

INTRODUCTION

THE TECHNIQUES FOR PREDICTING the steady plane laminar flow of a viscous fluid are rather well developed. Interest in aircraft applications has centered attention on the boundary layer, which is a thin layer of fluid enveloping a body, to which the frictional and dissipative effects of viscosity are confined and beyond which the fluid behaves in a nonviscous manner, substantially unaffected by the presence of the boundary layer.

It is the purpose of the present paper to discuss the steady three-dimensional boundary layer. It is possible to attempt a general treatment, introducing particular problems for illustrative purposes only. This approach is largely frustrated by the great variety of aerodynamic effects which may arise in three-dimensional flows. The reverse approach is therefore adopted. Detailed consideration is given to a specific problem, which is intrinsically of interest, and from the results are drawn whatever general conclusions seem warranted. The particular problem treated concerns the laminar boundary layer of a semi-infinite circular cone at angle of attack to a supersonic stream (see Fig. 1). This choice is made for the following reasons:

(a) The semi-infinite cone is a useful idealization of the nose portion of a spike inlet or of the nose portion of the fuselage of a supersonic aircraft or missile. The aerodynamic performance of these configurations at angle of attack is of current interest.

(b) The limiting cases of small and large angle of attack illustrate available three-dimensional boundary-layer theories to which plane flow considerations are at least partially applicable.

(c) Cases intermediate between these two limits are in no way characteristic of plane flow and yet are amenable to analysis.

Presented at the Aerodynamics Session, Twenty-First Annual Meeting, IAS, New York, January 26–29, 1953.

* Aeronautical Research Scientist.

NOTATION

A_n, B_n, D_n	= functions of θ and M_s, see Eqs. (1)
C	= constant, see Eq. (3)
C_p	= specific heat at constant pressure
f, g	= flow functions, see Eqs. (5)
h	= overall local boundary-layer thickness
J	= gas constant
K	= function related to δ^*, see Eq. (12)
k	= parameter, see Eq. (16)
M, M_s	= Mach Number and free-stream Mach Number, respectively
p	= static pressure
q	= velocity vector in the boundary layer
R_x, R_y	= Reynolds Number ($= \rho_r u_r x/\mu_r$, $\rho_r u_r/\mu_r$)
T	= absolute static temperature
u, v, w	= velocity components in direction of x, y, and φ, respectively
x, y, φ	= coordinates along a generator of the cone, normal to the surface, and circumferentially around cone, respectively, see Fig. 1
α	= angle of attack, see Fig. 1
γ	= ratio of specific heats
δ_x, δ_φ	= lengths based on mass-flow defects, see Eqs. (13)
δ^*	= displacement thickness of boundary layer
θ	= semivertex angle of cone
λ	= similarity coordinate, see Eq. (6)
μ	= coefficient of viscosity
ρ	= density
Φ, Ψ, ψ	= flow functions

Subscripts

1 = conditions in flow at outer edge of boundary layer

r = reference condition

Subscript notation for partial differentiation is used where convenient.

Superscripts

(n) denotes order of approximation in perturbation method

Bar over quantity denotes evaluation of nonviscous flow at cone surface when $\alpha = 0$.

Primes denote ordinary differentiation.

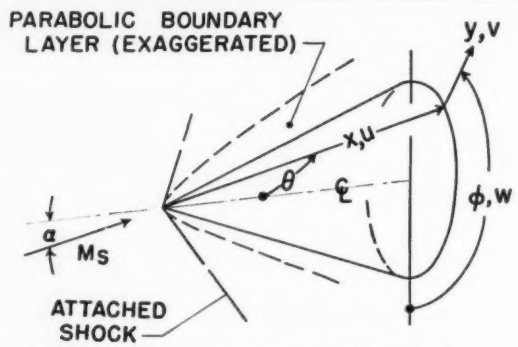

FIG. 1. Circular cone at angle of attack—notation.

GENERAL FEATURES OF THE PROBLEM

(1) *Nonviscous Flow Outside the Boundary Layer*

A circular cone at angle of attack to a steady supersonic stream is shown in Fig. 1. The nonviscous flow outside the boundary layer is assumed to be unaffected by the presence of the thin boundary layer and is conical in the Busemann sense (the shock is attached); all physical quantities are constant along rays from the apex and, in particular, along generators of the cone. Therefore, physical quantities at the outer edge of the boundary layer depend on φ but not on x. These circumferential variations govern the behavior of the boundary layer at its outer edge and therefore require specification. The most convenient representation of the nonviscous flow is provided by the M.I.T. tables.[1-3] Young and Siska[4] have elucidated the application of these tables at the cone surface (alternatively, at the outer edge of a thin boundary layer) and have made comparisons with experiment. At the cone surface,

$$\left.\begin{aligned} u_1/\tilde{u} &= 1 - \alpha A_1 \cos\varphi + \alpha^2(B_1 + D_1 \cos 2\varphi) + \ldots \\ w_1/\tilde{u} &= \alpha A_2 \sin\varphi + \alpha^2 D_2 \sin 2\varphi + \ldots \\ p_1/\tilde{p} &= 1 + \alpha A_3 \cos\varphi + \alpha^2(B_3 + D_3 \cos 2\varphi) + \ldots, \text{etc.} \end{aligned}\right\} \quad (1)$$

The A's, B's, and D's are functions only of θ and M_s and are obtainable from references 1, 2, and 3 via reference 4. Being the result of expansion in powers of α, Eqs. (1) may properly be used only for small or moderate α. A further limitation has been pointed out by Ferri,[5] who shows that Eqs. (1) are correct only if the outer flow may be considered isentropic (neither θ nor M_s too large).

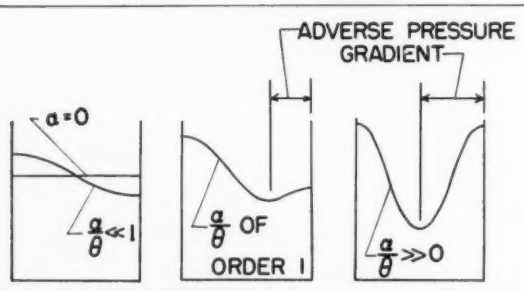

FIG. 2. Typical circumferential static pressure distributions on cone at angle of attack.

At zero angle of attack, the pressure is constant around the cone. For small positive angle of attack, the pressure is slightly higher at the bottom of the cone and slightly lower at the top, as shown by Eqs. (1) and Fig. 2. As the angle of attack is further increased, there is a region of rising pressure ("adverse pressure gradient") near the top of the cone. Finally, in the limit [beyond the scope of Eqs. (1)] of $\alpha/\theta \to \infty$, the pressure distribution approaches the form appropriate to the plane cross flow around a circular cylinder.

(2) *Secondary Flow in the Boundary Layer*

A stream line at the outer edge of the boundary layer would follow a course around the cone as shown in Fig. 3. Static pressure is constant across a thin boundary layer. Therefore, particles following a stream line within the boundary layer are subject to the same circumferential pressure gradient as are those following the outer stream line but, because of their lower inertia, tend to take a course conforming more closely to the direction of the circumferential pressure gradient, as shown by the dotted stream line in Fig. 3. This is the well-known phenomenon of "secondary flow" in the boundary-layer transverse to the outer flow and is characteristic of the three-dimensional boundary layer.

(3) *Boundary-Layer Similarity*

It may be shown[6,7] that the equations of motion, together with the fact that outer flow quantities are independent of x, permit the supposition of parabolic similarity in the laminar boundary layer—that is, physical quantities in the boundary layer depend only on the two variables $y/\sqrt{x}$ and φ. Accordingly, if the boundary layer is viewed in any meridional plane, flow quantities are constant along the family of parabolas originating at the apex of the cone and the boundary layer may be said to grow parabolically along generators of the cone,† as indicated in Fig. 1.

BOUNDARY-LAYER EQUATIONS FOR CONE

In plane or axisymmetric boundary-layer problems, it is customary to introduce a stream function in order to satisfy the continuity equation identically. In three-dimensional problems, a similar device may be employed.[7] In the coordinate system of the present problem, the steady continuity equation,

† This is a special case of the independent conclusions of Hayes[6] and the author[7] that parabolic boundary-layer similarity may be assumed along generators of any "conical" body (e.g., a cone of elliptic cross section). For this class of flows, therefore, an analysis (either experimental or theoretical) at any surface spherical about the apex may be used to infer the behavior of the complete laminar boundary layer.

$$\frac{1}{x}\frac{\partial}{\partial x}(\rho u x) + \frac{\partial \rho v}{\partial y} + \frac{1}{x \sin\theta}\frac{\partial \rho w}{\partial \varphi} = 0$$

is satisfied by the definition of new functions Ψ and Φ,

$$\left.\begin{aligned} \rho u x \sin\theta &\equiv \partial\Psi/\partial y \\ \rho v x \sin\theta &\equiv -\frac{\partial\Psi}{\partial x} - \frac{1}{x\sin\theta}\frac{\partial\Phi}{\partial\varphi} \\ \rho w x \sin\theta &\equiv \partial\Phi/\partial y \end{aligned}\right\} \tag{2}$$

Definitions (2) are substituted into the remaining equations (momentum, energy, and state), under the assumption of a thin laminar boundary layer and with the use of certain transformations[7]—viz.:

(a) A transformation due to Howarth confers the advantage that the transformed equations closely resemble the corresponding equations of incompressible flow. This transformation requires the assumption of the linear temperature-viscosity relation of Chapman and Rubesin:[8]

$$\mu/\mu_r = C(T/T_r) \tag{3}$$

where subscript r represents a reference condition and C is a constant chosen to match Eq. (3) to the more precise Sutherland formula at the body surface.

(b) A transformation based on that of Mangler[9] yields equations in nearly Cartesian form.

(c) A transformation expressing parabolic similarity along cone generators.

Further, it is assumed that the Prandtl Number is 1, that the ratio of specific heats is constant, and that there is no heat transfer through the cone surface. These assumptions permit the equation of constant enthalpy to be used in the boundary layer in place of the more complicated differential energy equation.

The following boundary-layer equations result:[7, 10]

momentum,

$$\left[f + \frac{p'(\varphi)}{3p\sin\theta}g + \frac{2}{3\sin\theta}g_\varphi\right]f_{\lambda\lambda} - \frac{2}{3\sin\theta}g_\lambda f_{\lambda\varphi} + \frac{2}{3}(g_\lambda)^2 + 2f_{\lambda\lambda\lambda} = 0 \tag{4a}$$

$$\left[f + \frac{p'(\varphi)}{3p\sin\theta}g + \frac{2}{3\sin\theta}g_\varphi\right]g_{\lambda\lambda} - \frac{2}{3\sin\theta}g_\lambda g_{\lambda\varphi} - \frac{2}{3}g_\lambda f_\lambda + 2g_{\lambda\lambda\lambda} = \frac{2}{3u_r^2\sin\theta}\frac{p'(\varphi)}{\rho} \tag{4b}$$

enthalpy,

$$C_pT + \frac{u_r^2}{2}[(f_\lambda)^2 + (g_\lambda)^2] = C_pT_1 + \frac{u_r^2}{2}\left[\left(\frac{u_1}{u_r}\right)^2 + \left(\frac{w_1}{u_r}\right)^2\right] \tag{4c}$$

state,

$$p(=p_1) = \rho JT \tag{4d}$$

Where $f(\lambda, \varphi)$ and $g(\lambda, \varphi)$ are related to the functions

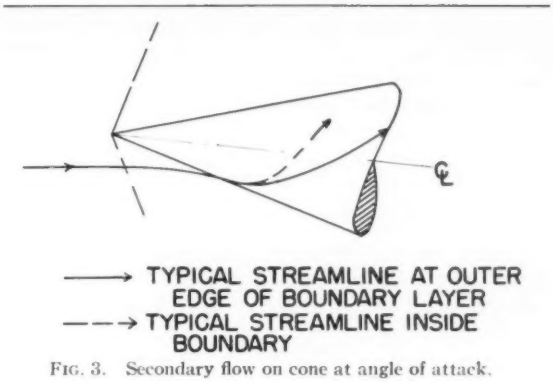

FIG. 3. Secondary flow on cone at angle of attack.

Ψ and Φ of Eqs. (2),

$$u/u_r \equiv f_\lambda; \quad w/u_r \equiv g_\lambda \tag{5}$$

The similarity coordinate λ is a function of $y/\sqrt{x}$,

$$\lambda \equiv \left(3\frac{p_r}{p}\frac{C}{R_r}\right)^{1/2}\int_0^{R_y/C}\frac{\rho}{\rho_r}\,d(R_y/C) \tag{6}$$

The boundary conditions are: At the outer edge of the boundary layer ($\lambda \approx \infty$), the u and w velocity components should take on their corresponding nonviscous values,

$$f_\lambda(\infty, \varphi) = \frac{u_1(\varphi)}{u_r}; \quad g_\lambda(\infty, \varphi) = \frac{w_1(\varphi)}{u_r} \tag{7a}$$

At the cone surface ($\lambda = 0$), u and w vanish,

$$f_\lambda(0, \varphi) = g_\lambda(0, \varphi) = 0 \tag{7b}$$

and the normal component v vanishes,†

$$f(0, \varphi) = g(0, \varphi) = 0 \tag{7c}$$

Eqs. (4) may be reduced to a pair of simultaneous equations with two independent and two dependent

† From Eqs. (2), the simplest way to make $v = 0$ at the cone surface is to require Ψ and Φ to vanish separately. This point is discussed more fully in reference 7.

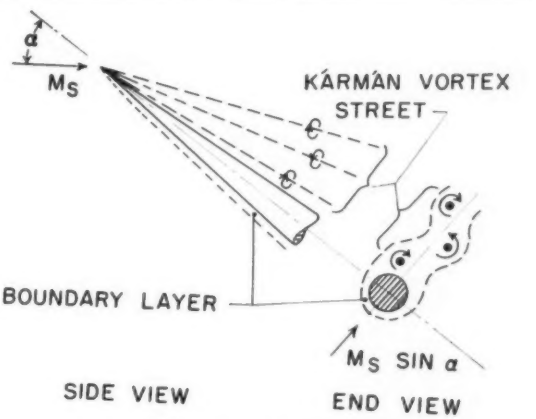

FIG. 4. Slender cone at large angle of attack.

variables and, despite the simplifications already made, present a rather formidable problem in general. Therefore, attention will be given to the special simplifications available in limiting cases.

Limiting Cases

(1) *Large Angle of Attack, Small Cone Angle*

In the special limiting case illustrated in Fig. 4 for which $\alpha/\theta \to \infty$ (in effect, $\theta \to 0$ in order that the shock may be considered attached), if the transformation

$$\Lambda \equiv \lambda/\sqrt{3 \sin \theta}; \quad F \equiv f/\sqrt{3 \sin \theta}; \quad G \equiv g/\sqrt{3 \sin \theta}$$

is substituted into Eqs. (4) and if terms of order θ/α are neglected, Eqs. (4) reduce[10] precisely to the equations for the laminar boundary layer on an infinite cylinder at angle of attack. Similarity exists in terms of the square root of the local radius of the cone ($x \sin \theta$). Thus, if the cone is sufficiently slender and the angle of attack is sufficiently large, it is correct to suppose that the boundary layer at any point is identical with the boundary layer that would exist on an infinite cylinder of constant radius equal to the local radius of the cone at that point. For the case of the infinite cylinder at angle of attack, Prandtl,[11] Sears,[12] and Jones[13] have shown that the profiles of velocity components lying in a cross-sectional plane may be obtained by plane-flow methods directly, as though the motion were that about a cylinder in a plane flow with a stream velocity equal to the cross-flow component of the actual stream (see Fig. 4). Although this result is strictly correct only for incompressible flow, the approach has been successfully exploited by Allen and Perkins[14] for the estimation of viscous cross-forces on slender bodies of revolution at large angle of attack in supersonic flow.

Thus, when $\alpha/\theta \to \infty$, the circumferential cross flow on a cone at angle of attack may be expected to exhibit plane-flow characteristics—in particular, separation in the form of a von Kármán vortex street† (Fig. 4).

(2) *Small Angle of Attack, Large Cone Angle*

Mangler[9] has shown that there is a transformation of variables which relates the laminar boundary layer on a body of revolution at angle of attack to an equivalent plane flow about (say) an airfoil section. A special case relates the laminar boundary layer on a circular cone at zero angle of attack in supersonic flow with the plane boundary layer on a semi-infinite flat plate. In effect, Mangler's transformation has been included in Eqs. (4), which therefore reduce to the Blasius flat-plate equation in the limit $\alpha/\theta \to 0$.

A Method of Perturbations

(1) *Differential Equations*

In certain problems of the three-dimensional boundary layer, solutions may be obtained by supposing that the flow is nearly plane or nearly axisymmetric. In the present instance, a solution is sought for small angle of attack ($\alpha/\theta \ll 1$) as a perturbation of the known axisymmetric flow at zero angle of attack. The functions f and g are written in a form chosen to be consistent (to first order in α) with the outer flow as represented in Eqs. (1),

$$\left.\begin{aligned} f &\equiv f^{(0)}(\lambda) - \alpha A_1 \cos \varphi f^{(1)}(\lambda) + \ldots \\ g &\equiv \alpha A_2 \sin \varphi g^{(1)}(\lambda) + \ldots \end{aligned}\right\} \tag{8}$$

Incorporation of Eqs. (8), (4c), and (4d) into Eqs. (4a) and (4b) and into boundary conditions (7) and collecting terms of zero and first order in α/θ separately yields

† An experimental study of shed vortices on the lee side of slender bodies of revolution is provided by Allen and Perkins.[14]

$$\text{zero order:} \quad \left\{\begin{aligned} & f^{(0)} f^{(0)\prime\prime} + 2 f^{(0)\prime\prime\prime} = 0 \\ & f^{(0)\prime}(\infty) = 1; \qquad f^{(0)\prime}(0) = f^{(0)}(0) = 0 \end{aligned}\right\} \tag{9}$$

$$\text{first order:} \quad \left\{\begin{aligned} & f^{(0)} g^{(1)\prime\prime} - \frac{2}{3} f^{(0)\prime} g^{(1)\prime} + 2 g^{(1)\prime\prime\prime} = -2\left(1 + \frac{\gamma - 1}{2} M_r^2 \left[1 - [f^{(0)\prime}]^2\right]\right) \\ & g^{(1)\prime}(\infty) = 1; \qquad g^{(1)\prime}(0) = g^{(1)}(0) = 0 \end{aligned}\right\} \tag{10}$$

and

$$\left\{\begin{aligned} & -\frac{2A_2}{3A_1 \sin \theta} f^{(0)\prime\prime} g^{(1)} + f^{(0)} f^{(1)\prime\prime} + f^{(0)\prime\prime} f^{(1)} + 2 f^{(1)\prime\prime\prime} = 0 \\ & f^{(1)\prime}(\infty) = 1; \qquad f^{(1)\prime}(0) = f^{(1)}(0) = 0 \end{aligned}\right\} \tag{11}$$

(The reference condition has here been taken to correspond to conditions in the nonviscous flow at the cone surface when $\alpha = 0$.)

(2) Results

Successive solution† of the ordinary boundary-value problems (9), (10), and (11) provide a complete description of the laminar boundary layer on a cone at small angle of attack. When $\alpha = 0$, the boundary-layer thickness is constant in any cross section. When there is a small angle of attack, the boundary layer is slightly thicker on the top and thinner on the bottom, because of the circumferential component of flow illustrated in Fig. 3. The formula for displacement thickness is

$$\delta^* = (\delta^*)_{\alpha=0}[1 - (\alpha/\theta)K(\theta, M_s)\cos\varphi + \ . \ . \ .] \quad (12)$$

The analysis yields K, which is shown in Fig. 5, together with a cross-sectional sketch of the circumferential variation of displacement thickness due to angle of attack. Roughly, the change in δ^* due to angle of attack is in the same proportion to $(\delta^*)_{\alpha=0}$ as α is to θ.

Further examination of the results of this perturbation procedure yields no indication whatever of cross-flow separation; this result might be anticipated in view of the favorable nature of the circumferential pressure gradient indicated for small angle of attack in Fig. 2.

Displacement Thickness

The definition of displacement thickness [Eq. (12)] of a three-dimensional boundary layer requires clarification.

The boundary layer is normally considered as a region wherein viscosity effects predominate and outside of which nonviscous laws apply. When the Reynolds Number is large, the boundary layer is assumed to be so thin that the nonviscous portion of the flow occurs as if there were no boundary layer. This assumption is strictly correct for infinite Reynolds Number. For large but finite Reynolds Number, however, the growth of the boundary layer causes the nonviscous flow to be deflected ("displaced") away from the body surface.

This displacement effect of a plane boundary layer is analyzed by equating the actual mass flow in the boundary layer

$$\int_0^h \rho u \, dy \quad (h \equiv \text{outer edge of boundary layer})$$

to the mass flow associated with a (fictitious) completely nonviscous flow terminated at δ^* rather than at the body surface,

$$\rho_1 u_1 (h - \delta^*)$$

yielding the usual definition of displacement thickness in terms of the "mass-flow defect" of the boundary layer,

$$\delta^* \equiv \int_0^h \left(1 - \frac{\rho u}{\rho_1 u_1}\right) dy$$

In three-dimensional flow, mass-flow defects occur with reference to both velocity components tangential to the surface; in the case of the cone at angle of attack, these are

$$\delta_x \equiv \int_0^\infty \left(1 - \frac{\rho u}{\rho_1 u_1}\right) dy$$

$$\delta_\varphi \equiv \int_0^\infty \left(1 - \frac{\rho w}{\rho_1 w_1}\right) dy \quad (13)$$

and it is not clear that either describes the displacement effects of the boundary layer.

A unique definition can be given[15] for the displacement thickness of a three-dimensional boundary layer: At the far outer edge (h) of any boundary layer, there is a certain distribution of the velocity component (v) normal to the body surface, determined by the characteristics of the boundary layer. The displacement thickness δ^* may then be defined as the local height of a fictitious impermeable surface that would deflect a completely nonviscous flow in just such a way as to produce at $y = h$ a distribution of normal velocity equal to that actually produced by the boundary layer. The continuity equation and the thin boundary-layer assumptions provide the equation for δ^*,

$$\text{div}\left[\rho_1 q_1 \delta^* - \int_0^\infty (\rho_1 q_1 - \rho q)\, dy\right] = 0 \quad (14)$$

(The divergence operator and the vector q have two components, both tangential to the surface.) Eq. (14) applies to turbulent, as well as laminar, boundary layers.

In the case of a cone at small angle of attack, Eq. (14) simplifies to

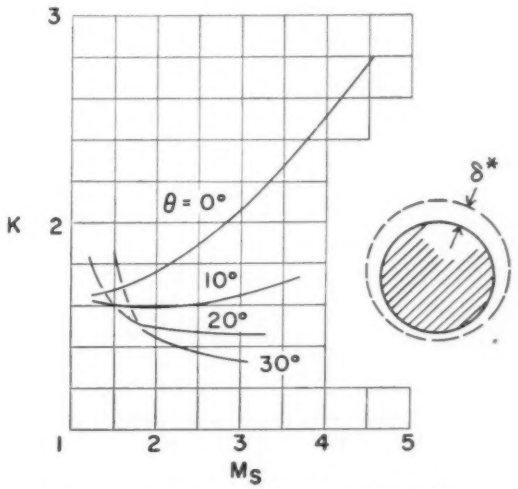

Fig. 5. Displacement thickness when $\alpha/\theta \ll 1$.

† Details are given in reference 10. The solution of Eqs. (9) is the well-known Blasius function.

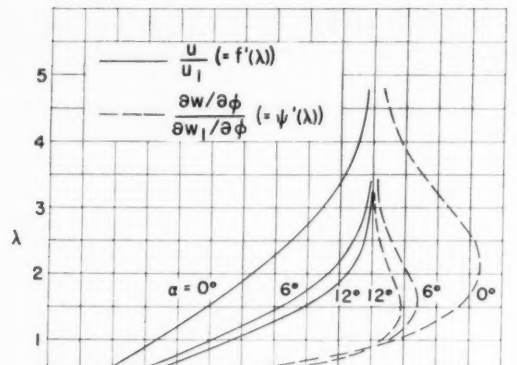

FIG. 6. Velocity profiles in plane of symmetry at bottom of cone.

$$\delta^* = \delta_x - \alpha \frac{2A_2}{3 \sin \theta} (\delta_x - \delta_\varphi) \cos \varphi + \quad . .$$

which is equivalent to Eq. (12).

Thus, δ^* depends on the two mass-flow defects defined in Eqs. (13) but is not equal to either.

BOUNDARY LAYER IN PLANE OF SYMMETRY

(1) *Differential Equations*

With reference to the important question of cross-flow separation, the analysis for small angle of attack provides only the information that the phenomenon must be sought at higher angles of attack than are contemplated in the perturbation analysis. A complete analysis would be difficult to carry out for large angle of attack. However, in common with many three-dimensional flows, the boundary layer on a cone at angle of attack has a plane of symmetry; the vertical meridional plane $\varphi = 0, \pi$. (See Fig. 1.) Eqs. (4) and (7) simplify[16] to ordinary differential equations if consideration is restricted to this plane, where $p'(\varphi) \equiv f_{\lambda\varphi} \equiv g_\lambda \equiv 0$,

$$\left.\begin{aligned} &(f + k\psi)f'' + 2f''' = 0 \\ &(f + k\psi)\psi'' + 2\psi''' - k(\psi')^2 - \frac{2}{3}\psi' f' + \\ &\qquad \left(k + \frac{2}{3}\right)\left\{1 + \frac{\gamma - 1}{2} M_1^2 [1 - (f')^2]\right\} \\ &f'(\infty) = \psi'(\infty) = 1 \\ &f'(0) = \psi'(0) = f(0) = \psi(0) = 0 \end{aligned}\right\} \quad (15)$$

where ψ is a new dependent variable and k is a parameter,

$$[w_{1\varphi}(0, \pi)/u_1(0, \pi)]\psi(\lambda) \equiv g_\varphi(\lambda; 0, \pi)$$
$$k \equiv [2/3 \sin \theta)(w_{1\varphi}(0, \pi)/u_1(0, \pi)] \quad (16)$$

(The reference condition is taken at the outer edge of the boundary layer at $\varphi = 0$ or π, depending on whether bottom or top of the cone is under consideration.) The parameter k depends essentially on α; the greater the angle of attack the greater the magnitude of $w_{1\varphi}$ and, hence, k. At the bottom of the cone k is positive; at the top, negative.

(2) *Results at Bottom of Cone*

Solution of Eqs. (15) yields, in the plane of symmetry, the profile of the velocity component along generators

$$u/u_1 = f'(\lambda)$$

and the circumferential gradient of the circumferential velocity in the boundary layer, as a fraction of the corresponding gradient just outside the boundary layer,

$$w_\varphi/w_1 = \psi'(\lambda) \ .$$

At the bottom of the cone, velocity profiles have been obtained[16] for various angles of attack, $M_s = 3.1$, and $\theta = 7.5°$. The outer flow was represented as in reference 10. The results (Fig. 6) show the expected thinning of the boundary layer as angle of attack is increased. The fact that the circumferential velocity within the boundary layer exceeds its stream value is presumably a consequence of the secondary flow illustrated in Fig. 3.

(3) *Limitations of Method When Applied at Top of Cone*

(*a*) *Uniqueness.*—At the top of the cone, solutions can be obtained only for rather small values of α. Beyond the angle of attack for which

$$k = -\frac{1}{3}\left(\frac{f'}{\psi'}\right)_{max.} \quad (\alpha \approx 0.5° \text{ when } M_s = 3.1, \theta = 7.5°) \quad (17)$$

solutions exist but are not unique.[16] The following is offered in explanation of this fact:

At the bottom of the cone, fluid is entrained by the thin boundary layer and is conveyed around the cone away from the plane of symmetry (see Fig. 7a). Here the condition of the boundary layer is uniquely determined by the characteristics of the outer flow at the plane of symmetry, and a thin boundary layer solution is unique, for all angles of attack.

At the top of the cone, for large α, fluid arrives in the vicinity of the plane of symmetry after having traveled around the body. Therefore, the boundary layer at the top depends not only on the outer flow in the plane of symmetry but on the influences to which the boundary layer has been subject during its passage around the body. A plane-of-symmetry analysis fails to yield a unique solution under these circumstances.

However, the true lateral region of influence of the plane of symmetry grows parabolically (Fig. 7b) along the top generator according to the law of simple molecular diffusion applicable in the present case. Therefore, at the top of the cone, while the flow is toward the plane

of symmetry for all angles of attack, in the sense of being transverse to cone generators, for a sufficiently small angle of attack the flow is outward from the parabolic region described, and uniqueness is expected. The foregoing argument yields Eq. (17), which gives the maximum angle of attack for which conditions in the plane of symmetry uniquely describe the flow at the top of the cone.

(*b*) *Existence.*—At the top of the cone, for angles of attack greater than that for which

$$k = -1 (\alpha = 6.2^\circ \text{ when } M_s = 3.1, \theta = 7.5^\circ) \quad (18)$$

no solution of Eqs. (15) exists which satisfies the boundary conditions. This fact was first pointed out by Hayes[6] in a discussion of the character of the laminar boundary layer on conical bodies in supersonic flow. Whereas the question of uniqueness discussed above is concerned only with the usefulness of a mathematical simplification, the existence of a critical angle of attack [Eq. (18)] beyond which a thin boundary-layer solution fails to exist would seem to be of more direct physical significance. If a thin boundary layer does not exist, then it follows that the actual boundary layer is so thick that the assumption of a thin laminar boundary layer is incorrect. Following Hayes,[6] one suspects that the critical condition (18) is connected with laminar separation of the circumferential flow.

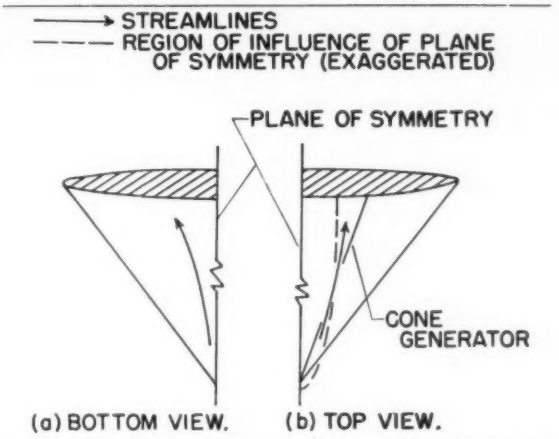

FIG. 7. Flow in boundary layer of cone near plane of symmetry.

SEPARATION

(1) General Considerations

To form a proper explanation of the critical condition (18), one must have a general view of the sort of information concerning three-dimensional separation which thin boundary-layer theory can provide.

In plane flow, the "separation point" is taken as the point at which a reverse-flow velocity profile appears, as in Fig. 8a. This criterion of separation has proved to be difficult to generalize to three dimensions. However, without specifying the velocity field inside the separated region, it may be observed that at the separation point the wall stream surface bifurcates, and at a point of reattachment (if such occurs) the two stream surfaces join again at the wall. Thus, as in Fig. 8a, there is embedded at the base of the boundary layer a distinct bubble that does not exchange fluid with the rest of the flow. Generalization to three dimensions may therefore be accomplished by defining a separated region as a bubble of fluid embedded in the boundary layer between the solid body and a stream surface meeting the body in a closed curve and containing a sheet pattern of vorticity the precise nature of which would depend on the particular problem. This sort of separation is predictable by thin boundary-layer analysis.

Of course, the sort of separation of greatest engineering importance occurs when the embedded vortex sheet coalesces to form strong concentrated vortices, with the consequence that the outer flow is greatly disturbed and large pressure effects occur. This process is not amenable to an analysis that presumes a thin boundary layer. However, thin boundary-layer theory may predict the circumstances under which coalescence occurs; if such an analysis predicts a thin boundary layer throughout the separated region, the associated vortex sheet would presumably tend to adhere to the body. If, however, the theory indicated infinite boundary-layer thickness anywhere in the separated region, there the coalescence process would most especially begin, finally engulfing most of the separated region.

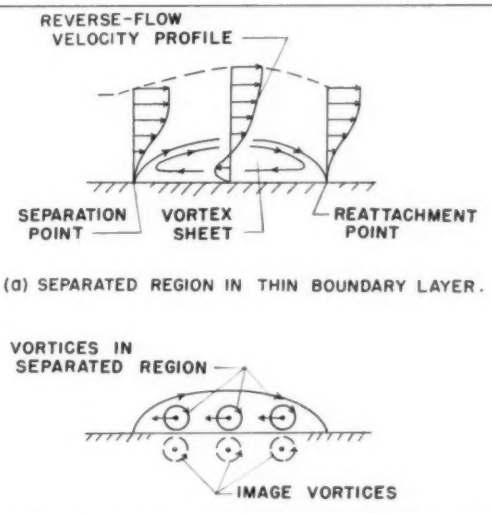

FIG. 8. Plane separation.

The process of coalescence may perhaps occur by the following mechanism: Let the vortex sheet of Fig. 8a be represented by a series of individual vortices as in Fig. 8b and represent the effect of the wall by the image vortices below the wall. Then, if the fluid above the wall

imposes no additional constraint (i.e., a boundary layer of locally infinite thickness), each vortex would move to the left toward the separation point under the influence of the induced field of its image.† Vortices initially near the separation point tend to remain fixed, however, because there the boundary layer is supposed to remain thin. Therefore, each vortex moving upstream tends to overtake the vortex ahead of it, and coalescence into a single strong vortex ensues.

A general criterion for the existence of a thin boundary layer would express the requirement that the boundary layer entrain fluid at its outer edge. If h represents the local overall thickness of the boundary layer and if it is recalled that the flow in the vicinity of h may be represented as the nonviscous flow over a fictitious displacement surface δ^*, the criterion may be written to specify that the fluid flux into the region between the surfaces h and δ^* in the fictitious nonviscous flow be positive.

$$\operatorname{div}[(h - \delta^*)\rho_1 q_1] > 0 \tag{19}$$

(2) *Examples*

(*a*) *Plane Cylinder.*—Taking x along the body, inequality (19) may be written

$$\frac{(d/dx)(h - \delta^*)}{h - \delta^*} > \frac{-\partial \rho_1 u_1/\partial x}{\rho_1 u_1} \tag{20}$$

As the rear stagnation point is approached, $u_1 \to 0$ and $-du_1/dx$ is finite and positive. Since $h - \delta^*$ is by definition greater than zero, inequality (20) can be satisfied only if

$$d(h - \delta^*)/dx \to \infty$$

in violation of the thin boundary-layer assumptions. This conclusion is reached with no detailed knowledge of the boundary layer and is, of course, obvious on the grounds that the boundary-layer fluid conveyed around the body must finally leave the body in the vicinity of the rear stagnation point and proceed downstream. A vortex sheet would be predicted to cover the after-portion of the body and, because of the infinitely thick boundary layer at the rear stagnation point, would coalesce to form a vigorous vortex system.

In three-dimensional flow, consideration of the outer flow is, in general, not sufficient to predict the certain "blow-up" of a thin boundary layer; information concerning the boundary layer itself is required. In the present instance, knowledge of parabolic similarity along generators permits inequality (19) to be written, near the top of the cone,

$$\frac{(\partial/\partial\varphi)(h - \delta^*)}{h - \delta^*} > \frac{-(dw_1/d\varphi) - (3/2)u_1 \sin\theta}{w_1} \tag{21}$$

indicating infinite boundary-layer thickness only if $w_1 = 0$ and, even then, only if $dw_1/d\varphi$ is less than zero (true at the top of the cone) and is larger in magnitude than $3/2u_1 \sin\theta$ or if $k < -1$ [cf. Eq. (18)]. This result may be explained as follows: For large angles of attack at the top of the cone, the boundary-layer fluid must leave the vicinity of the body and proceed downstream (Fig. 9a), just as in the case of a plane cylinder. However, the boundary layer is presumed to grow parabolically in the streamwise direction along generators of the cone. Thus, below some critical angle of attack ($k = -1$, as it turns out), the fluid conveyed around the cone toward the top may simply augment the growing boundary layer (Fig. 9c).

As the angle of attack is increased from zero, at first there is no vortex sheet and the boundary layer is everywhere thin. It may be shown that an adverse pressure gradient first appears at the top of the cone when $k = -2/3$ ($\alpha = 4.3°$ when $M_s = 3.1$, $\theta = 7.5°$). Possibly then, an imbedded vortex sheet appears in the range $-1 < k < -2/3$ for which the boundary layer may be regarded as thin. This possible (not proved) state of affairs is illustrated in Fig. 9d.

When the angle of attack is greater than that for which $k = -1$, the prediction of infinite boundary-layer thickness implies the freedom sufficient for coalescence of the vortex sheet. In the flow about a cone at moderate angle of attack, this coalescence gives rise to a steady symmetric vortex pair appearing as lobes at the top of the cone (Fig. 9b). Allen and Perkins[14] provide experimental demonstration of this type of separation, which is an essentially three-dimensional phenomenon to be distinguished from the unsteady vortex street (Fig. 4) produced in plane flow or on the cone when $\alpha/\theta \gg 1$.

Fig. 10 shows how the critical angle of attack ($k = -1$) varies with M_s and θ. The critical angle of attack is seen to be of the same order as the semivertex angle of the cone. The figure indicates the possibility of rather profound qualitative differences in the flows at high Mach Number about cones of different vertex angles.

† A familiar example of this induced motion is the spreading of a smoke ring that impinges on the wall of a room.

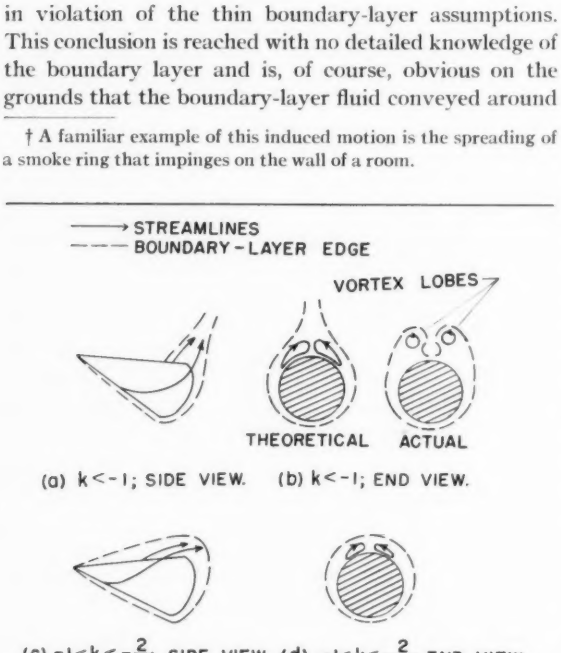

FIG. 9. Separation on cone at angle of attack.

Of course, the argument given herein for the significance of the critical point $k = -1$ is idealized. Physical significance should be attached not so much to the mathematical singularity at $k = -1$ as to the tendency to infinite thickness and the consequent tendency of a vortex sheet to coalesce when k approaches -1. Furthermore, possible effects connected with laminar instability are not considered.

(*b*) *Conical Bodies in General.*—Inequality (19) and the condition of parabolic boundary-layer similarity may be used to provide a criterion [equivalent to Eq. (18)] for the maximum angle of attack consistent with a thin boundary layer on any smooth conically symmetric body (e.g., a cone of elliptic cross section) in supersonic flow.

(*c*) *Turbulent Boundary Layer on a Cone.*—If similarity also holds for the turbulent boundary layer on a cone and if the similarity law is nearly linear because of the strong mechanical diffusion, vigorous separation would be indicated to occur at an angle of attack for which $k = -4/3$ (a higher angle than in the laminar case, for which the critical value is $k = -1$).

Concluding Remarks

(1) Summary Description of Cone Boundary Layer

At zero angle of attack, the laminar boundary-layer growth along generators may be studied by plane-flow methods. As the angle of attack is increased to a small positive value, the boundary layer tends to thicken at the top of the cone and to thin at the bottom in consequence of the circumferential flow due to angle of attack. Also, a circumferential component of skin friction provides a small viscous lift. There is no separation of this circumferential flow.

When the angle of attack is increased to the value for which $k = -2/3$ (about 4.3° when $\theta = 7.5°$, $M_s = 3.1$), an adverse circumferential pressure gradient first appears at the top of the cone. Presumably, at somewhat higher angle of attack, there appears a separated bubble embedded at the base of the boundary layer, growing in extent as the angle of attack is further increased.

The boundary layer may no longer be regarded as thin when the angle of attack is reached for which $k = -1$ (about 6.2° when $\theta = 7.5°$, $M_s = 3.1$). At and above this angle of attack, whatever flat vortex bubble exists at the top of the cone must be in the process of coalescence into a symmetric pair of strong steady vortices.

If the cone is sufficiently slender, at an extremely high angle of attack ($\alpha/\theta \gg 1$), the circumferential flow is qualitatively the same as the plane flow about a cylinder, and a von Kármán vortex street is shed at the top of the cone.

Similar considerations would apply for the general class of bodies with conical symmetry and for the fully turbulent boundary layer.

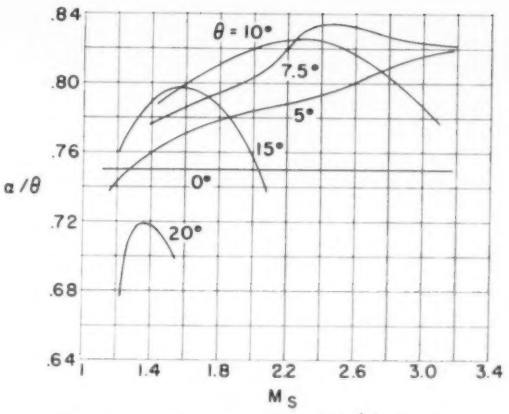

FIG. 10. Angle of attack for which $k = -1$.

(2) The Use of Boundary-Layer Theory

In the treatment of three-dimensional problems, reduction in the number of variables is of first importance. The number of dependent variables may be reduced by making various physical approximations and by defining a pair of functions such that continuity is satisfied identically. The number of independent variables (coordinates of the solution) are reduced by:

(a) Invoking similarity when possible (e.g., parabolic similarity in the cone case).

(b) Perturbing a known flow (e.g., $\alpha/\theta \ll 1$, in the cone case). This results in linear equations to which the method of separation of variables may often be applied.

(c) Restricting consideration to a plane of symmetry of the flow. As in the cone case, this method succeeds only when the boundary layer "starts" at the plane of symmetry.

It is felt that laminar boundary-layer analysis may prove more useful and realistic for many three-dimensional flows than for plane flow. For example, in cases of plane flow about cylinders, the question usually addressed to theory is: "At what point on the body does separation always occur?" The actual separation often so distorts the outer flow that boundary-layer calculations based on a theoretical pressure distribution do not give a reliable answer. On the other hand, in the case of the cone, the question may be: "At what angle of attack does separation first appear anywhere on the cone?" The answer to this question may reliably be given by theory because, at its first appearance, separation is apparently not violent.

References

[1] Anon., *Tables of Supersonic Flow Around Cones*, Tech. Rep. No. 1, Dept. Elec. Eng., M.I.T., 1947.

[2] Anon., *Tables of Supersonic Flow Around Yawing Cones*, Tech. Rep. No. 3, Dept. Elec. Eng., M.I.T., 1947.

[3] Anon., *Tables of Supersonic Flow Around Cones of Large Yaw*, Tech. Rep. No. 5, Dept. Elec. Eng., M.I.T., 1949.

(*Concluded on next page*)

[4] Young, G. B. W., and Siska, C. P., *Supersonic Flow Around Cones at Large Yaw*, Journal of the Aeronautical Sciences, Vol. 19, No. 2, pp. 111–119, February 19, 1952.

[5] Ferri, Antonio, *Supersonic Flow Around Circular Cones at Angles of Attack*, NACA TN No. 2236, 1950.

[6] Hayes, Wallace D., *The Three-Dimensional Boundary Layer*, NAVORD Rep. 1313, NOTS 384, U.S. Naval Ordnance Test Section (Inyokern), May 9, 1951. (Bur. Ordnance Task Assignment NOTS-36-Re3d-441-3.)

[7] Moore, Franklin K., *Three-Dimensional Compressible Laminar Boundary-Layer Flow*, NACA TN No. 2279, 1951.

[8] Chapman, Dean R., and Rubesin, Morris W., *Temperature and Velocity Profiles in the Compressible Laminar Boundary Layer with Arbitrary Distribution of Surface Temperature*, Journal of the Aeronautical Sciences, Vol. 16, No. 9, pp. 547–565, September, 1949.

[9] Mangler, W., *Boundary Layers on Bodies of Revolution in Symmetrical Flow*, Reps. and Trans. No. 55, GDC/689T, British M.A.P., April 15, 1946.

[10] Moore, Franklin K., *Laminar Boundary Layer on a Circular Cone in Supersonic Flow at a SmallAngle of Attack*, NACA TN No. 2521, 1951.

[11] Prandtl, L., *On Boundary Layers in Three-Dimensional Flow*, Reps. and Trans. No. 64, British M.A.P., May 1, 1946.

[12] Sears, W. R., *The Boundary Layer of Yawed Cylinders*, Journal of the Aeronautical Sciences, Vol. 15, No. 1, pp. 49–52, January, 1948.

[13] Jones, Robert T., *Effect of Sweepback on Boundary Layer and Separation*, NACA Report No. 884, 1947 (formerly NACA TN No. 1492).

[14] Allen, H. Julian, and Perkins, Edward W., *A Study of Effects of Viscosity on Flow Over Slender Inclined Bodies of Revoluton*, NACA Report No. 1048, 1951.

[15] Moore, Franklin K., *Displacement Effect of a Three-Dimensional Boundary Layer*, NACA TN No. 2722, 1952.

[16] Moore, Franklin K., *Laminar Boundary Layer on Cone in Supersonic Flow at Large Angle of Attack*, NACA TN No. 2844, 1952.

Suggestion for Binding
Issues of the Journal of the Aeronautical Sciences

Arrangements have been made so that our readers may have their issues of the JOURNAL bound carefully and economically in our authorized binding. Simply write for details to:

AIRE
P.O. Box 776
Highland Park, Illinois

Changes of Address

Since the Post Office Department does not as a rule forward magazines to forwarding addresses, it is important that the Institute be notified of changes in address 30 days in advance of publishing date to ensure receipt of every issue of the JOURNAL and REVIEW.

Notices should be printed legibly and sent directly to:

Institute of the Aeronautical Sciences, Inc.
2 East 64th Street, New York 21, New York

Critical Bending Stress for Flat Rectangular Plates Supported Along All Edges and Elastically Restrained Against Rotation Along the Unloaded Compression Edge

JAMES H. JOHNSON, JR.,* AND ROBERT G. NOEL†

North American Aviation, Inc.

ABSTRACT

A theoretical analysis of the critical bending stress for flat rectangular plates supported along all edges and elastically restrained along the unloaded compressive edge is presented. Critical buckling constants for four positions of the axis of zero stress are computed for all values of edge restraint and wave length. These four positions are locations of the axis of zero stress, varying from mid-depth of the plate to the unloaded tension edge. The latter location of the zero stress axis is that of triangular compressive loading.

A discussion of the effects of elastic restraint against rotation along the unloaded tension edge is given.

INTRODUCTION

IN THE DESIGN OF aircraft structural components, consideration must sometimes be given to the local instability of plate structures that are subjected to unsymmetrical bending loads. For example, unsymmetrical channel, I- and Z-section beams, fuselage rings, and multiweb box beams frequently buckle locally because of unsymmetrical distribution of bending loads.

The local instability stress of a structure composed of two or more plates joined at the unloaded edges can be found by the moment distribution method.[3, 4] In order to use this method, critical stress coefficients k must be known as a function of the edge-restraint coefficients ϵ and the half-length of buckle waves λ for all loaded plates in the system. These data are already given for plates in compression[5-7] and for plates subjected to symmetrical bending in the plane of the plate.[2] Also, the moment distribution method has been used to determine the local instability stresses for columns of various cross-sectional shapes[8, 9] and for multiweb box beams subjected to symmetrical bending loads.[2]

In the present paper, critical stress coefficients are given for all values of λ and ϵ for flat plates subjected to the general bending load of Fig. 1. The values presented herein can be used with the results of references 2, 5, 6, and 7 and the moment distribution method[3, 4] to determine the critical stresses of flat-plate structures subjected to loads resulting in unsymmetrical bending stress distributions.

Received July 15, 1952.

* Research Engineer, Aerophysics Laboratory.

† Stress Analyst, Aerophysics Laboratory.

SYMBOLS

D	=	flexural rigidity of plates, in.lbs. $[Et^3/12(1-\mu^2)]$
E	=	Young's modulus of elasticity, lbs. per sq.in.
N_0	=	intensity of compressive force in x direction at edge of plate $x = 0$ and $x = \lambda$, lbs. per in.
N_x	=	intensity of distributed forces in x direction at edges of plate $x = 0$ and $x = \lambda$, lbs. per in.
S_0	=	stiffness per unit length of elastic restraining medium or amplitude of sinusoidal applied moment divided by amplitude of resulting sinusoidal rotation of elastic medium in quarter radians, lbs.-in.
T	=	external work of applied forces during buckling
V	=	internal energy of deformation during buckling
a	=	length of plate in x direction, in.
a_1, a_n	=	Fourier coefficients of sin $(n\pi y/b)$
b	=	width of plate in y direction, in.
i, j, n	=	integers
m	=	number of half waves in x direction
k	=	nondimensional critical-stress coefficient that depends upon conditions of edge restraint and shape of plate
t	=	thickness of plate element, in.
w	=	plate-buckling deformation, normal to plane of the plate
x	=	plate coordinate in direction of stress
y	=	plate coordinate, perpendicular to direction of stress
α	=	numerical factor that depends upon the location of a plate axis of zero stress
β	=	ratio of half-wave length to plate width (λ/b)
γ	=	Lagrangian multiplier
μ	=	Poisson's ratio

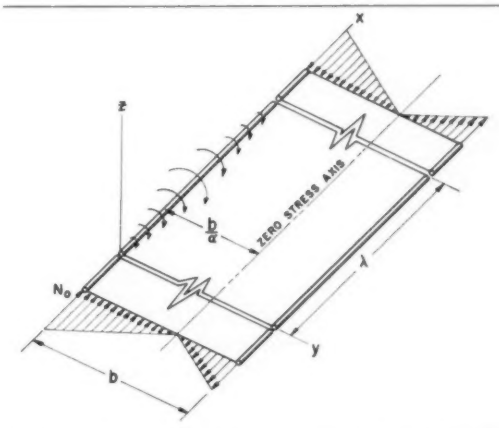

FIGURE 1. INFINITELY LONG FLAT PLATE UNDER BENDING FORCES-TENSION EDGE HINGED, COMPRESSION EDGE ELASTICALLY RESTRAINED

λ = half-wave length of buckles in longitudinal direction, in.
ϵ = nondimensional restraint coefficient given by $(4S_0b \div D)$
σ = longitudinal compressive stress, lbs. per sq.in.
θ = amplitude of sinusoidal edge rotation

Subscripts

p = plate
r = restraint
cr = critical

Theoretical Analysis

The energy method was used for the calculation of the critical stress of an infinitely long flat plate under bending forces in the plane of the plate. The plate was considered to be simply supported along the tension edge and elastically restrained by a restraining medium along the compression edge. It was assumed that the restraining medium was such that a sinusoidal restraint produced in-phase sinusoidal rotation of the restrained edge. This condition is satisfied by a rigid joint between two or more flat plates that buckle into the same wave length. The critical stress of the plate was determined from the condition of neutral stability in which the work of applied forces must equal the sum of the strain energy of the buckled plate and the energy of the restraining medium,

$$T = V_p + V_r \tag{1}$$

If w is the deflection normal to the plate at any point (x, y) in the plane of the plate shown in Fig. 1, T and V_p are given by the following equations [reference 1, Eqs. (201) and (199)]:

$$T = \frac{1}{2}\int_0^{\lambda}\int_0^{b}\left[N_x\left(\frac{\partial w}{\partial x}\right)^2 + N_y\left(\frac{\partial w}{\partial y}\right)^2 + 2N_{xy}\frac{\partial w}{\partial x}\frac{\partial w}{\partial y}\right]dx\,dy \tag{2}$$

$$V_p = \frac{D}{2}\int_0^{\lambda}\int_0^{b}\left\{\left(\frac{\partial^2 w}{\partial x^2} + \frac{\partial^2 w}{\partial y^2}\right)^2 - 2(1-\mu)\left[\frac{\partial^2 w}{\partial x^2}\frac{\partial^2 w}{\partial y^2} - \left(\frac{\partial^2 w}{\partial x\,\partial y}\right)^2\right]\right\}dx\,dy \tag{3}$$

The stiffness S_0 of a plate has been defined[4] as the ratio of moment per unit length at any point along the restrained edge to the rotation in quarter radians at that point when the moment is distributed sinusoidally. Since it was assumed that the restraining moment was in-phase with the rotation of the edge, plate stiffness S_0 is constant long the x axis. With this definition of S_0, V_r is given by the following equation [reference 5, Eq. (B-4)]:

$$V_r = 2S_0\int_0^{\lambda}\left[\left(\frac{\partial w}{\partial y}\right)_{y=0}\right]dx + 2S_0\int_0^{\lambda}\left[\left(\frac{\partial w}{\partial y}\right)_{y=b}\right]dx \tag{4}$$

The deflected surface may be represented by the Fourier series

$$w = \sin\frac{\pi x}{\lambda}\sum_{n=1}^{\infty} a_n \sin\frac{n\pi y}{b} \tag{5}$$

The intensity of distributed forces acting in the middle plane of the plate is given by the equation

$$N_x = N_0\,[1 - \alpha(y/b)] \tag{6}$$

Substitution of w and N_x from Eqs. (5) and (6) in Eqs. (2), (3), and (4) yields

$$T = \frac{N_0\pi^2 b}{8\lambda}\left(1 - \frac{\alpha}{2}\right)\sum_{n=1}^{\infty} a_n^2 + \frac{N_0\alpha b}{\lambda}\sum_{n=1}^{\infty}\sum_{i}^{\infty}\frac{a_n a_i ni}{(n^2 - i^2)^2} \tag{7}$$

$(n \pm i = \text{odd})$,

$$V_p = \frac{D\lambda b\pi^4}{8}\sum_{n=1}^{\infty} a_n^2\left(\frac{1}{\lambda^2} + \frac{n^2}{b^2}\right)^2 \tag{8}$$

$$V_r = S_0\theta^2\lambda \tag{9}$$

where θ is the amplitude of the sinusoidal edge rotation and is given by

$$\theta = \sum_{n=1}^{\infty} a_n\,(n\pi/b) \tag{10}$$

Substituting these expressions in Eq. (1) and making the substitutions

$$N_0 = k\,(\pi^2 D/b^2)$$

$$S_0 = D\epsilon/4b, \qquad \beta = \lambda/b$$

gives the following expression in k:

$$k\beta^2\left(1 - \frac{\alpha}{2}\right)\sum_{n=1}^{\infty} a_n^2 + \frac{8k\beta^2\alpha}{\pi^2}\sum_{n=1}^{\infty}\sum_{i}^{\infty}\frac{a_n a_i ni}{(n^2 - i^2)^2} = \sum_{n=1}^{\infty} a_n^2(1 + \beta^2 n^2)^2 + \frac{2\beta^4 b^2\epsilon\theta^2}{\pi^4} \tag{11}$$

$(n \pm i = \text{odd})$. The coefficients a_n must be so adjusted as to make the expression above for k a minimum with the constraining relationship of Eq. (10). To minimize k with its constraining relationship, construct the Lagrangian function

$$\mathfrak{L}(a_n,\theta) = \sum_{n=1}^{\infty} a_n{}^2(1+\beta^2n^2)^2 + \frac{2\beta^4b^2\epsilon\theta^2}{\pi^4} - \frac{8k\beta^2\alpha}{\pi^2}\sum_{n=1}^{\infty}\sum_{i}^{\infty}\frac{a_na_ini}{(n^2-i^2)^2} - k\beta^2\left(1-\frac{\alpha}{2}\right)\sum_{n=1}^{\infty}a_n{}^2 - \gamma\left(\theta - \sum_{n=1}^{\infty}a_n\frac{n\pi}{b}\right) = 0$$

$$\left.\begin{aligned} \frac{\partial\mathfrak{L}}{\partial a_n} &= 2a_n(1+\beta^2n^2)^2 - \frac{16k\beta^2\alpha}{\pi^2}\sum_{i}^{\infty}\frac{a_ini}{(n^2-i^2)^2} - k\beta^2\left(1-\frac{\alpha}{2}\right)(2a_n) + \gamma\frac{n\pi}{b} = 0 \\ \partial\mathfrak{L}/\partial\theta &= (4\beta^4b^2\epsilon\theta/\pi^4) - \gamma = 0 \end{aligned}\right\} \tag{12}$$

($n \pm i$ = odd). The equations of expression (12) with the constraining relation (10) give, after simplification, the following system of linear homogeneous equations:

$$\left.\begin{aligned} a_n\left[(1+\beta^2n^2)^2 - k\beta^2\left(1-\frac{\alpha}{2}\right)\right] - \frac{8k\alpha\beta^2}{\pi^2}\sum_{i}^{\infty}\frac{a_ini}{(n^2-i^2)^2} + \frac{n\pi}{2}\left(\frac{\gamma}{b}\right) = 0 \\ \sum_{n=1}^{\infty}na_n - \frac{\pi^3}{4\epsilon\beta^4}\left(\frac{\gamma}{b}\right) = 0 \end{aligned}\right\} \tag{13}$$

($n \pm i$ = odd).

The results presented in this paper were determined by neglecting all even a_n greater than a_6 or $a_{j+8} = 0$, where $j = 0, 2, 4, 6, \ldots, \infty$. The work of solving Eqs. (13) may be greatly reduced by evaluating the odd a's in terms of the even a's. Performing these operations and substituting in Eqs. (13) leads to the following set of stability equations:

$$\left.\begin{aligned} &a_n\left[(1+\beta^2n^2)^2 - k\beta^2\left(1-\frac{\alpha}{2}\right)\right] - \frac{64\alpha^2\beta^4k^2n}{\pi^4}\sum_{i=1,3,5}^{\infty}\frac{2i^2}{(n^2-i^2)^2\,[A]\,(i^2-4)^2}a_2 - \\ &\frac{64\alpha^2\beta^4k^2n}{\pi^4}\sum_{i=1,3,5}^{\infty}\frac{4i^2}{(n^2-i^2)^2[A]\,(i^2-16)^2}a_4 - \frac{64\alpha^2\beta^4k^2n}{\pi^4}\sum_{i=1,3,5}^{\infty}\frac{6i^2}{(n^2-i^2)^2\,[A]\,(i^2-36)^2}a_6 + \\ &\frac{n\pi}{2}\left[1+\frac{8\alpha\beta^2k}{\pi^2}\sum_{i=1,3,5}^{\infty}\frac{i^2}{(n^2-i^2)^2\,[A]}\right]\left(\frac{\gamma}{b}\right) = 0 \\ &\frac{8\beta^4}{\pi^3}\left[1+\frac{8\alpha\beta^2k}{\pi^2}\sum_{i=1,3,5}^{\infty}\frac{i^2}{(i^2-4)^2\,[A]}\right]a_2 + \frac{16\beta^4}{\pi^3}\left[1+\frac{8\alpha\beta^2k}{\pi^2}\sum_{i=1,3,5}^{\infty}\frac{i^2}{(i^2-16)^2\,[A]}\right]a_4 + \\ &\frac{24\beta^4}{\pi^3}\left[1+\frac{8\alpha\beta^2k}{\pi^2}\sum_{i=1,3,5}^{\infty}\frac{i^2}{(i^2-36)^2\,[A]}\right]a_6 - \left[\frac{1}{\epsilon}+\frac{2\beta^4}{\pi^2}\sum_{i=1,3,5}^{\infty}\frac{i^2}{[A]}\right]\left(\frac{\gamma}{b}\right) = 0 \end{aligned}\right\} \tag{14}*$$

(n = even), where

$$[A] = \{(1+\beta^2i^2)^2 - k\beta^2\,[1-(\alpha/2)]\}$$

* Note that Eqs. (14) reduce to Eqs. (A11) of reference 2 by setting $\alpha = 2$.

In order for the system of linear homogeneous Eqs. (14) to have other than the trivial solution, the determinant of the coefficients must vanish. The minimum value of k for which this determinant vanishes is the desired critical stress coefficient. Values of critical stress coefficients k satisfying this condition have been calculated and are given in Figs. 2, 3, 4, and 5 for all values of ϵ and β and for values of α of 7/4, 3/2, 5/4, and 1.

Plates of Finite Length

Critical stress coefficients for flat plates of finite length may be obtained by substituting a/mb for λ/b, where the number of half-wave lengths m must be chosen so that k is a minimum. Stress coefficients are given in Figs. 6 and 7 for finite plates having all edges simply supported and for finite plates having a fixed unloaded compressive edge. The curves given in Figs. 6 and 7 for intermediate values of α were obtained by cross-plotting the results calculated in the present paper and those of references 1 and 2.

Effects of Restraint Along Tension Edge

The results determined for this paper are for a long, flat rectangular plate under loading and restraint conditions of Fig. 1. This case was considered because it was assumed that restraint along the tension edge would have little effect on plate stiffness. To check the validity of this assumption, the critical stress coefficient for a plate simply supported along the compression edge and built in along the tension edge was determined for various a/b ratios. These results were compared with critical stress coefficients for a plate simply supported on all edges. This comparison is

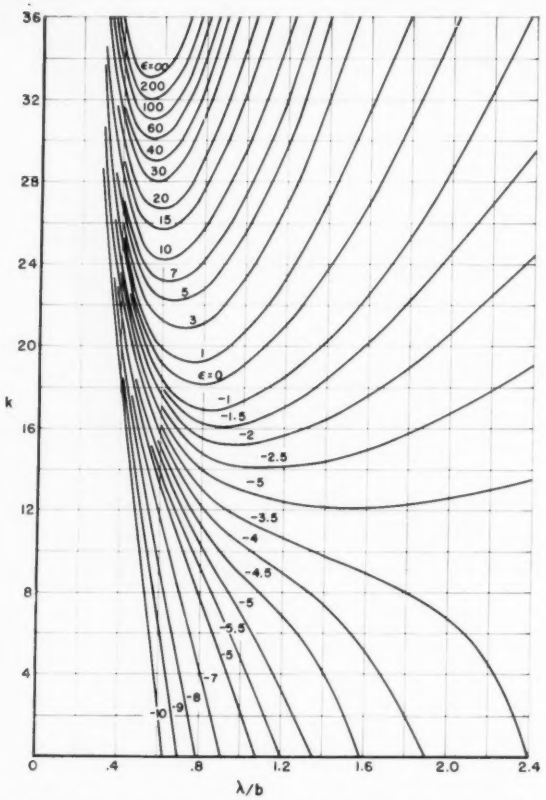

FIGURE 2. CRITICAL STRESS COEFFICIENTS FOR A FLAT PLATE IN BENDING IN THE PLANE OF THE PLATE WITH VARIOUS RESTRAINT COEFFICIENTS ϵ ALONG THE COMPRESSION EDGE AND $\alpha = 7/4$

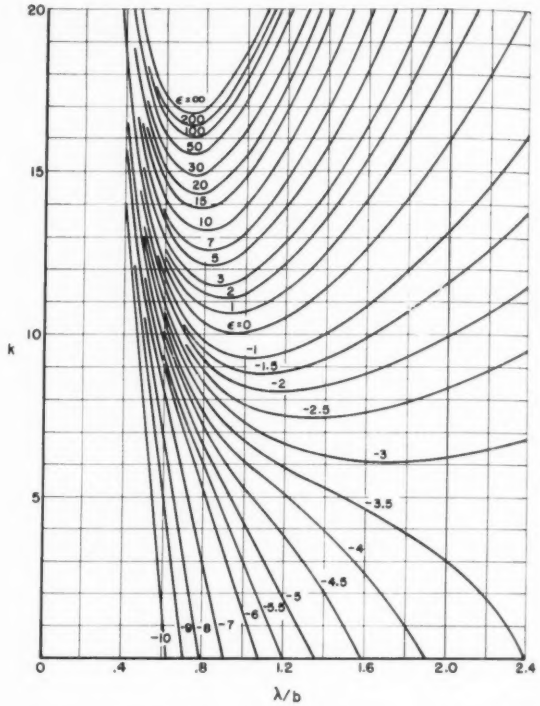

FIGURE 4. CRITICAL STRESS COEFFICIENTS FOR A FLAT PLATE IN BENDING IN THE PLANE OF THE PLATE WITH VARIOUS RESTRAINT COEFFICIENTS ϵ ALONG THE COMPRESSION EDGE AND $\alpha = 5/4$

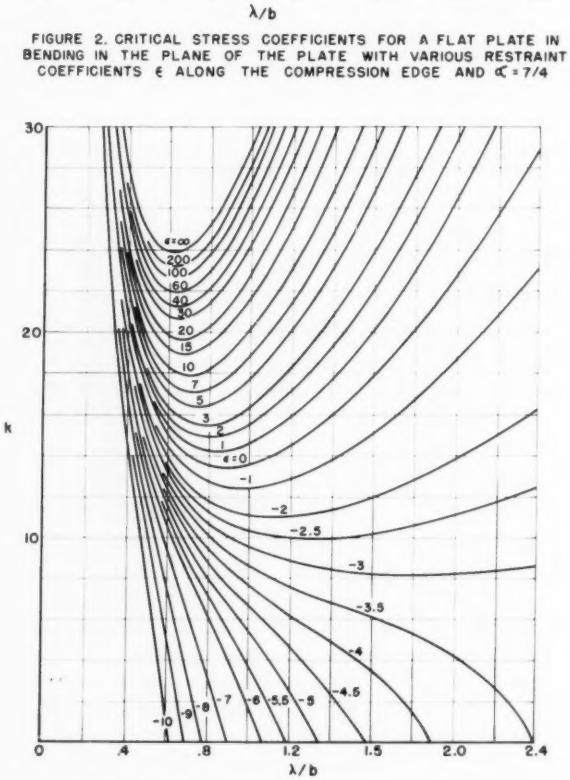

FIGURE 3. CRITICAL STRESS COEFFICIENTS FOR A FLAT PLATE IN BENDING IN THE PLANE OF THE PLATE WITH VARIOUS RESTRAINT COEFFICIENTS ϵ ALONG THE COMPRESSION EDGE AND $\alpha = 3/2$

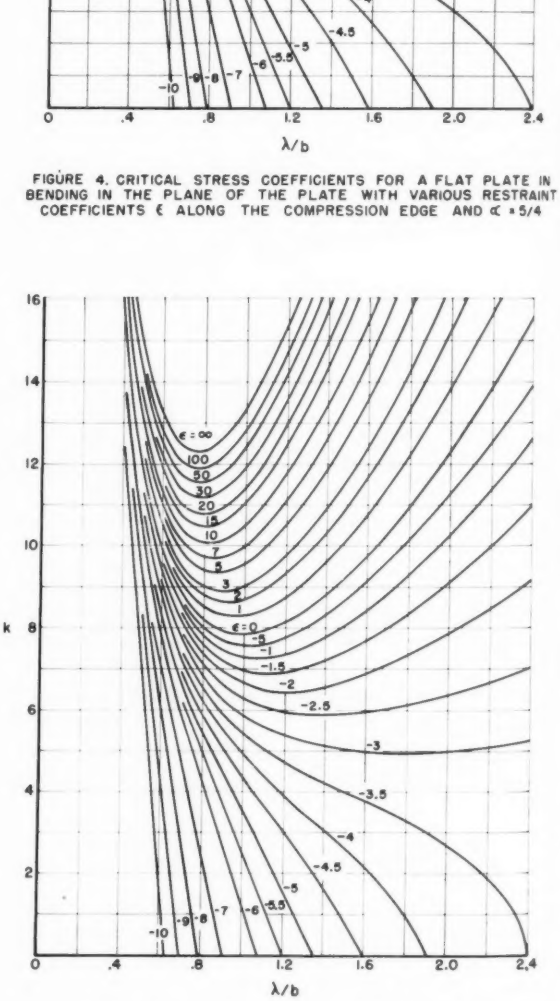

FIGURE 5. CRITICAL STRESS COEFFICIENTS FOR A FLAT PLATE IN BENDING IN THE PLANE OF THE PLATE WITH VARIOUS RESTRAINT COEFFICIENTS ϵ ALONG THE COMPRESSION EDGE AND $\alpha = 1$

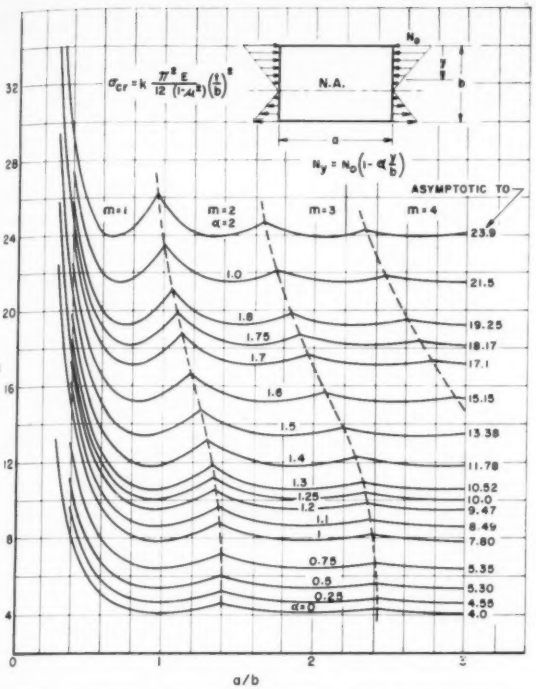

FIGURE 6. CRITICAL STRESS COEFFICIENTS FOR A FLAT PLATE IN BENDING IN THE PLANE OF THE PLATE—ALL EDGES SIMPLY SUPPORTED

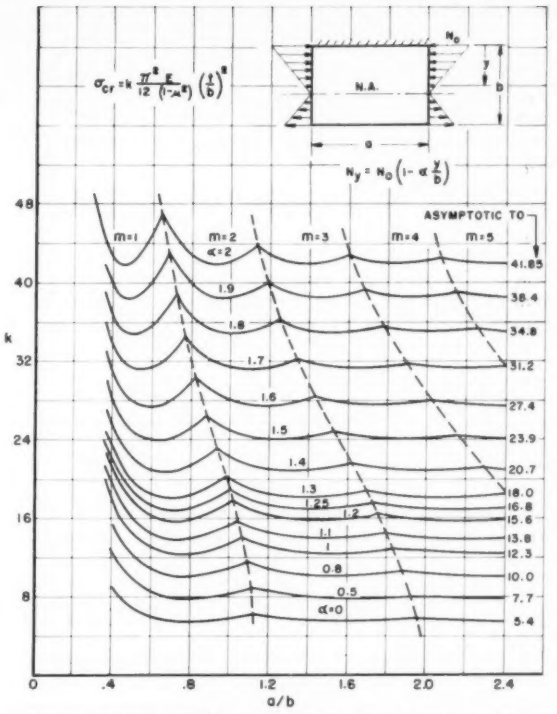

FIGURE 7. CRITICAL STRESS COEFFICIENTS FOR A PLATE IN BENDING IN THE PLANE OF THE PLATE—UNLOADED EDGE ON COMPRESSION SIDE FIXED, ALL OTHER EDGES SIMPLY SUPPORTED

shown in Fig. 8. For all α, it can be seen that restraint along the tension edge increases the plate stiffness and, thereby, the critical stress coefficient. The amount of this increase varies with the a/b ratios and α. An assumption of simple support along the tension edge gives conservative values for the critical stress coefficient for values of $\alpha > 1$. The degree of conservatism is not so great as indicated in Fig. 8, because the condition of built-in edge cannot be attained in any practical structural design. Therefore, an assumption of simple support along the unloaded tension edge of a plate in bending would lead to results slightly conservative for practical designs.

Conclusions

(1) The curves of Figs. 2, 3, 4, and 5 provide sufficient data with the results of references 2, 6, and 7 for use in computing the critical bending stresses of beams by use of the moment distribution method of reference 4.

(2) The stress coefficients given in Figs. 6 and 7 should be used to compute the critical bending stresses of flat rectangular plates of finite length having the particular edge conditions shown.

(3) In the practical case, the assumption of simple support along the unloaded tension edge of a plate in bending gives slightly conservative critical stresses.

References

[1] Timoshenko, S., *Theory of Elastic Stability;* McGraw-Hill Book Company, Inc., New York, 1936.

(*Concluded on next page*)

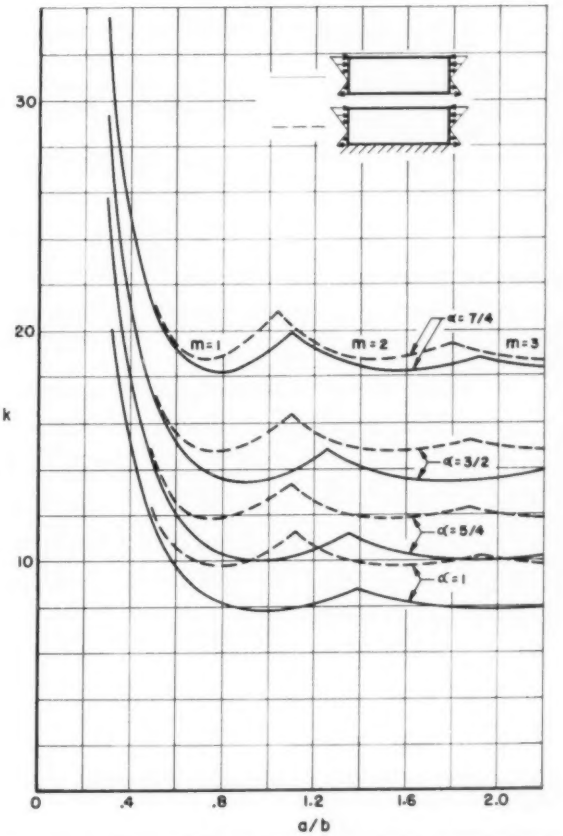

FIGURE 8. COMPARISON OF CRITICAL STRESS COEFFICIENTS FOR HINGED AND FIXED TENSION EDGE

[3] Schuette, E. H., and McCulloch, J. C., *Charts for the Minimum-Weight Design of Multiweb Wings in Bending*, NACA TN No. 1323, June, 1947.

[4] Lundquist, E. E., *Stability of Structural Members under Axial Load*, NACA TN No. 617, 1937.

[5] Lundquist, E. E., Stowell, E. Z., and Schuette, E. H., *Principles of Moment Distribution Applied to Stability of Structures Composed of Bars or Plates*, NACA ARR 3K06, November, 1943.

[6] Lundquist, E. E., and Stowell, E. Z., *Critical Compressive Stress for Flat Rectangular Plates Supported along all Edges and Elastically Restrained against Rotation along the Unloaded Edges*, NACA Report No. 733, 1942.

[6] Lundquist, E. E., and Stowell, E. Z., *Critical Compressive Stress for Outstanding Flanges*, NACA Report No. 734, 1942.

[7] Kroll, W. D., *Tables of Stiffness and Carry-over Factor for Flat Rectangular Plates under Compression*, NACA ARR 3K27, November, 1943.

[8] Kroll, W. D., Fisher, G. P., and Heimerl, G. J., *Charts for Calculation of the Critical Stress for Local Instability of Columns with I-, Z-, Channel, and Rectangular-Tube Section*, NACA ARR 3K04, November, 1943.

[9] Hu, Pai C., and McCulloch, J. C., *The Local Buckling Strength of Lipped Z-Columns with Small Lip Width*, NACA TN No. 1335, June, 1947.

Notice to Contributors

Manuscripts submitted for publication *must* be double- or triple-spaced originals. There should be wide margins on both sides of the sheets and triple spacing around formulas to allow for the marking of directions to the printer.

Original drawings (jet black India ink on white paper or tracing cloth) should accompany the manuscript. (*Blueprints are not acceptable.*) Photographs *must* be on glossy paper. The smallest lettering on 8- by 10-in. figures should be no less than 1/4 in. high.

Only the simplest formulas should be typewritten, all others should be carefully written in pen and ink. The difference between capital and lower-case letters and Greek symbols should be clearly distinguished.

See Inside Back Cover of this issue for further details.

Changes of Address

Since the Post Office Department does not as a rule forward magazines to forwarding addresses, it is important that the Institute be notified of changes in address 30 days in advance of publishing date to ensure receipt of every issue of the JOURNAL and REVIEW.

Notices should be printed legibly and sent directly to:

Institute of the Aeronautical Sciences, Inc.

2 East 64th Street, New York 21, New York

The Aerodynamic Characteristics of Low Aspect Ratio Wing-Body Combinations in Steady Subsonic Flow*

H. R. LAWRENCE†

Cornell Aeronautical Laboratory, Inc.

SUMMARY

The linearized flow field about a thin wing of arbitrary twist mounted on an infinite inclined circular cylinder in a uniform incompressible free stream is formulated as the solution of a pair of simultaneous integral equations in two variables.

By making use of an extended form of the slender-body approximation, the simultaneous integral equations are shown to be equivalent to a single integral equation valid on the wing surface.

The method employed by the writer in references 9 and 15 is used to approximate this two-variable integral equation by a single-variable integral equation for the chordwise lift distribution. The chordwise lift distribution on the wing-body configuration is shown to be identical with that of a wing with the same exposed plan form but altered twist distribution. A procedure for computing the distribution of lifting pressures is presented.

Methods for extending this result to bodies of finite length and to account for the effects of compressibility are discussed.

LIST OF SYMBOLS

a	= body radius
$b(x)$	= local semispan of wing-body configuration measured from body centerline
b_0	= maximum semispan of wing-body configuration
c	= semichord of wing at wing-body intersection
$F(x, \zeta)$	= $\phi + i\psi$ [see Eq. (54)]
$f(x)$	= [see Eq. (28)]
$g(x)$	= [see Eq. (36)]
$H(\zeta)$	= [see Eq. (56)]
$l(x, y)$	= lift per unit area on wing
$L_B(x)$	= lift per unit chord on body
$L_W(x)$	= lift per unit chord on wing
$L(x)$	= lift per unit chord on wing-body configuration
$P(\eta)$	= [see Eq. (33) and Appendix]
p_0	= free-stream static pressure
p	= static pressure
$Q(x, y)$	= (see Eq. (31)]
R_W	= projection of wing on xy plane
R_B	= projection of body on xy plane
r, θ	= polar coordinates in yz plane
U	= free-stream velocity
$u(x, y)$	= $l(x, y)/2\rho U^2$
$\omega_a(x, y)$	= aerodynamic angle of attack, see Eq. (49)
$\omega_g(x, y)$	= geometric angle of attack, see Eq. (48)
$\omega_i(x, y)$	= induced angle of attack, see Eq. (50)
x, y, z	= cartesian coordinates
ζ, η	= Cartesian coordinates corresponding to x, y, respectively
$\alpha(x, y)$	= angle of attack distribution on wing
α_0	= angle of attack of body
$\beta(x)$	= $b(x) - a$, local exposed semispan of wing
β_0	= $b_0 - a$, maximum exposed semispan of wing
∇^2	= Laplacian operator
$\phi^{(0)}, \phi^{(1)}, \tilde{U}\phi$	= velocity potentials
μ	= [see Eq. (53)]
ζ	= $y + iz$

INTRODUCTION

The problem of calculating the aerodynamic characteristics of a wing-body configuration was first considered by Lennertz.[1] The case of a high aspect ratio wing mounted on an infinite circular cylinder was investigated by making use of the Prandtl[2] lifting-line theory in conjunction with the concept of image vortices in the Trefftz plane. A formula was obtained for the lift on a wing with uniform loading, and the twist distribution for minimum induced drag was computed. Multhopp[3] investigated the case of a high aspect ratio wing mounted on an infinite cylinder of arbitrary cross section. Following Lennertz, he assumed that the wing can be considered as a lifting line. Multhopp then proved that the wing-body problem can be reduced to the solution of the Prandtl lifting-line integral equation by conformal transformation of the wing-body configuration in the Trefftz plane. Although the wing-body problem for cases where the Prandtl wing theory is valid is solved in principle by this method, analytic difficulties and laborious numerical calculations are encountered in practical application of the Multhopp procedure. Flax and Treanor[4] have developed a variational procedure that appears to avoid these computational problems.

The aerodynamic theory of high aspect ratio wings mounted on infinite cylindrical bodies appears to be reasonably complete for cases where the Prandtl lifting-line theory is valid. Development of a method for computing the aerodynamic characteristics of high aspect ratio swept-wing-body configurations remains as a subject for further research.

A method for computing the aerodynamic characteristics of low aspect ratio wing-body configurations was first presented by Spreiter.[5] The method is restricted to cases in which accelerations in the stream direction can be neglected in the Laplace equation. This type of solution will be called the "very low aspect ratio" case,

Received January 8, 1953.

* This investigation was carried out under sponsorship of the Flight Research Laboratory, Air Material Command, to which the author is appreciative for permission to publish the results.

† Assistant Head, Aerodynamic Research Department.

since the same assumption, when applied to a wing alone, leads to the Jones[6] theory, valid for aspect ratios below one-half. Spreiter solves the wing-body problem by conformal transformation, thus reducing the problem to the Jones case. Although the transformation used is identical with that employed by Multhopp, the analysis proceeds with little difficulty because of the simple character of the Jones solution. Relatively simple analytic solutions are obtained for many cases of interest. Ward[7] has derived the Spreiter results for the supersonic case by a more rigorous procedure based on the Laplace transform and has cleared up certain discrepancies in the Spreiter theory. Adams and Sears[8] have clarified the discrepancies of the Spreiter theory in the subsonic case by an adaptation of the Ward technique in which the Fourier transform replaces the Laplace transform. The objective of the present paper is to develop a method for computing the aerodynamic characteristics of wing-body configurations at small angles of attack in a subsonic flow field. The results will be restricted to low aspect ratio wings (say 0 to 4) with straight trailing edges and arbitrary twist mounted on finite bodies of circular cross section at arbitrary angles of incidence. The body radius will be assumed constant along the wing-body intersection.

The problem will be attacked by considering the case of a wing mounted on an infinite circular cylinder in an incompressible flow. Slender-body theory may then be used to generalize the result to bodies of finite length, and the Prandtl-Glauert transformation may be applied to remove the restriction to incompressible flow.

Formulation as a Boundary-Value Problem

Consider a thin wing with straight trailing edge mounted on an infinite circular cylinder embedded in a uniform incompressible free stream of velocity U in the positive x direction. The wing and body axes lie approximately in the plane $z = 0$ with angles of attack $\alpha(x, y)$ and α_0, respectively, relative to the free stream. The wing-body configuration is assumed to possess a plane of symmetry $y = 0$.

The flow field about the infinite cylinder of radius a, when the wing is not present, may be described by the velocity potential $\phi^{(0)}$ defined below.

$$\phi^{(0)}(x, r, \theta) = Ux + U\alpha_0 \cos\theta(a^2/r) \tag{1}$$

where (r, θ), the polar coordinates in the yz planes, are defined by the formulas

$$z = r\cos\theta, \qquad y = r\sin\theta \tag{2}$$

The velocity potential $\phi^{(1)}$, which describes the flow field about the wing-body configuration, is considered to be the sum of the potential $\phi^{(0)}$ due to the body and a perturbation potential $U\phi$ due to the presence of the wing. The angles $\alpha(x, y)$ and α_0 are assumed to be small so that the approximations of linearized lifting-surface theory may be employed.

The conditions that (1) the potential function $\phi^{(1)}$ be harmonic outside rigid bodies and their wakes, (2) the flow through rigid surfaces vanish, and (3) the effects of the wings vanish far upstream may be stated in the following manner:

$$\Delta^2\phi^{(1)} = 0 \qquad \text{(in flow field)} \tag{3}$$
$$\phi_z^{(1)} = -U\alpha(x, y) \qquad \text{(on wing surface)} \tag{4}$$
$$\phi_r^{(1)} = -U\alpha_0\cos\theta \qquad \text{(on body surface)} \tag{5}$$
$$\phi^{(1)} = \phi^{(0)} \qquad (\text{at } x = -\infty) \tag{6}$$

Upon making use of the definition $\phi^{(1)} = \phi^{(0)} + U\phi$ and Eq. (1) for $\phi^{(0)}$, the above conditions may be rewritten in terms of ϕ as follows:

$$\Delta^2\phi = 0 \qquad \text{(in flow field)} \tag{7}$$
$$\phi_z = -\alpha(x, y) - \alpha_0\frac{a^2}{y^2} \qquad \text{(on wing surface)} \tag{8}$$
$$\phi_r = 0 \qquad \text{(on body surface)} \tag{9}$$
$$\phi = 0 \qquad (\text{at } x = -\infty) \tag{10}$$

Since only the differences in pressure between the upper and lower surfaces of the wing or body will be computed, the nonlinear terms in the Bernoulli equation may be neglected.

The linearized Bernoulli equation reduces to the following relationship between the static pressure p and the perturbation velocity potential $U\phi$:

$$p_0 - p = \rho U^2\phi z \qquad \text{(in flow field)} \tag{11}$$

where p_0 is defined as the static pressure in the free stream.

The boundary problem is uniquely specified by the conditions (7), (8), (9), and (10) when supplemented by the Kutta condition. The forces acting on rigid surfaces may be computed from Eq. (11).

Formulation as an Integral Equation

Consider the function $\phi(x, y, z)$ defined in terms of the undetermined function $u(x, y)$ by the formula

$$\phi(x, y, z) = \frac{1}{2\pi}\int\int_{\infty}\frac{d\xi\, d\eta\, zu(\xi, \eta)}{(y-\eta)^2 + z^2} \times \left[1 + \frac{x-\xi}{\sqrt{(x-\xi)^2 + (y-\eta)^2 + z^2}}\right] \tag{12}$$

where the integration is taken over the entire plane $z = 0$. It is evident that $\phi(x, y, z)$ satisfies Eqs. (7) and (10). Upon differentiating Eq. (12) with respect to x and allowing z to approach zero from above and below, there results the formulas

$$\phi_x(x, y, 0+) = u(x, y) \tag{13}$$
$$\phi_x(x, y, 0-) = -u(x, y) \tag{14}$$

By making use of Eq. (11), the lift per unit area $l(x, y)$ acting on a thin wing located in the plane $z = 0$ may be expressed in the form

$$l(x, y) = \rho U^2[\phi_x(x, y, 0+) - \phi_x(x, y, 0-)] \tag{15}$$

or, with the aid of Eqs. (13) and (14),

$$l(x, y) = 2\rho U^2 u(x, y) \tag{16}$$

Eq. (16) shows that the undetermined function $u(x, y)$ may be interpreted as proportional to the lift per unit area acting on a thin wing in the plane $z = 0$. Let R_W and R_B be defined as the projections of the wing and body, respectively, on the plane $z = 0$. Since the lift and, hence, $u(x, y)$ must vanish at all points off $R_W + R_B$ in the plane $z = 0$, the region of integration in Eq. (12) can be at most $R_W + R_B$.

The boundary condition (8) may be reformulated by differentiating Eq. (12) with respect to z and, after some manipulation, allowing z to approach zero. The final result of this process is the integral equation

$$\alpha(x, y) + \alpha_0 \frac{a^2}{y^2} = \frac{1}{2\pi} \frac{\partial}{\partial y} \int\int_{R_W + R_B} \frac{d\xi\, d\eta\, u(\xi, \eta)}{y - \eta} \left[1 + \frac{\sqrt{(x - \xi)^2 + (y - \eta)^2}}{x - \xi}\right] \tag{17}$$

valid on the wing surface R_W.

Eq. (12) may be rewritten in polar coordinates defined by Eqs. (2) as shown,

$$\phi(x, r, \theta) = \frac{r \cos\theta}{2\pi} \int\int_{R_W + R_B} \frac{d\xi\, d\eta\, u(\xi, \eta)}{r^2 - 2r\eta \sin\theta + \eta^2} \left[1 + \frac{x - \xi}{\sqrt{(x - \xi)^2 + r^2 - 2r\eta \sin\theta + \eta^2}}\right] \tag{18}$$

Upon differentiating with respect to r, simplifying the resultant expression by partial integration, and substituting $r = a$, there results the formula

$$\phi_r(x, a, \theta) = \frac{\cos\theta}{2\pi} \frac{\partial}{\partial y} \int\int_{R_W + R_B} \frac{d\xi\, d\eta\, y(\xi, \eta)(a^2 - \eta^2)}{2\eta(\eta^2 - 2y\eta + a^2)} \left[1 + \frac{x - \xi}{\sqrt{(x - \xi^2) + \eta^2 - 2y\eta + a^2}}\right] -$$
$$\frac{\cos\theta}{2\pi} \frac{\partial}{\partial y} \int\int_{R_W + R_B} \frac{d\xi\, d\eta\, u(\xi, \eta)}{2\eta} \left[\frac{x - \xi}{\sqrt{(x - \xi)^2 + \eta^2 - 2y\eta + a^2}}\right] \tag{19}$$

where y is defined as $a \sin\theta$. An integral equation valid on the region R_B is obtained from the boundary condition (9) by setting $\phi_r(x, a, \theta)$ equal to zero in Eq. (19). The integral equations (17) and (19) represent a complete formulation of the wing-body problem when combined with the Kutta condition and Eq. (11) for the pressure.

In order to simplify the analysis, an approximate integral equation valid on R_B will be derived to replace Eq. (19). It will be assumed that the radical occurring in the integrands of Eq. (19) may be replaced by $|x - \xi|$. This is equivalent to the assumption that the wing-body configuration is slender insofar as satisfying the boundary condition on the body is concerned. The final result, however, is not restricted to slender configurations. At large values of η where the inequality $|x - \xi| > |\eta|$ no longer holds, the integrand approaches zero as $1/\eta$, and all wing-body configurations appear to be slender with respect to the boundary condition on the body. This conclusion is restricted, of course, to the case of slender bodies. The approximation employed will be further justified by comparison with known results valid for high aspect ratio wings in combination with cylindrical bodies.

Upon defining $\phi(x, y)$ as the integral from $-\infty$ to x of $u(\xi, y)$, the approximate integral equation valid on the region R_B may be written in the form

$$0 = \frac{\partial}{\partial y} \int_{-b(x)}^{b(x)} \frac{d\eta\, \phi(x, \eta)(a^2 - \eta^2)}{2\eta(\eta^2 - 2y\eta + a^2)} \tag{20}$$

where $b(x)$ is the wing semispan when $b(x) > a$ and $b(x) = a$ otherwise. Eqs. (17) and (20) represent the integral equation formulation of the wing-body problem, which will be employed in subsequent developments.

The Chordwise Lift Distribution

The lift per unit area on the wing $l(x, y)$ is expressed in terms of the function $u(x, y)$ by Eq. (16). The lift per unit chord $L_W(x)$ acting on the wing is therefore given by the formula

$$L_W(x) = 4\rho U^2 \int_a^{b(x)} dy\, u\,(x, y) \tag{21}$$

where the integration region has been halved by consideration of symmetry about the plane $y = 0$. By using the Eq. (11), the lift per unit chord acting on the body $L_B(x)$ may be written in the form

$$L_B(x) = \rho U^2 \int_0^{2\pi} d\theta\, a \cos\theta\, \phi_r(x, a, \theta) \tag{22}$$

The function $\phi_r(x, a, \theta)$ may be evaluated in terms of $u(x, y)$ by making use of Eq. (18). As in the case of the boundary condition on the body surface, the radical in Eq. (18) will be approximated by $|x - \xi|$. Then, upon differentiating Eq. (18) with respect to x, substituting a for r, and integrating over the variable ξ, there results the formula

$$\phi_x(x, a, \theta) = \frac{a \cos\theta}{\pi} \int_{-b(x)}^{b(x)} \frac{d\eta\, u\,(x, \eta)}{a^2 - 2a\eta \sin\theta + \eta^2} \quad (23)$$

Eq. (23) for $\phi_x(x, a, \theta)$ is now substituted in Eq. (22), and the order of integration is interchanged to give the result

$$L_B(x) = \frac{\rho U^2 a^2}{\pi} \int_{-b(x)}^{b(x)} d\eta\, u(x, \eta) \times \int_0^{2\pi} \frac{d\theta \cos^2\theta}{a^2 - 2a\eta \sin\theta + \eta^2} \quad (24)$$

The integration over θ can be performed by substituting $\theta' + (\pi/2)$ for θ and expanding the integrand in a Fourier series. The following formula is obtained:

$$\int_0^{2\pi} \frac{d\theta' \sin^2\theta'}{a^2 - 2a\eta \cos\theta' + \eta^2} = \frac{\pi}{a^2} \quad (|\eta| < a)$$

$$= \frac{\pi}{\eta^2} \quad (|\eta| > a)$$

and substituting in Eq. (24) the lift per unit chord acting on the body may be written in the form

$$L_B(x) = 2\rho U^2 \left[\int_0^a d\eta\, u(x, \eta) + \int_a^{b(x)} d\eta \frac{a^2}{\eta^2} u(x, \eta) \right] \quad (25)$$

Development of a Single-Variable Integral Equation

The first step in developing a single-variable integral equation will be to reduce the simultaneous integral equations (17) and (20) to a single integral equation. It will be shown that by suitably relating the values of $\phi(x, y)$ on R_B and R_W. Eq. (20) is satisfied identically. The method employed is closely related to the use of images. Eq. (20) is rewritten in the form

$$\frac{\partial}{\partial y}\left[\int_{-a}^{a} \frac{d\eta\, \phi(x, \eta)(a^2 - \eta^2)}{2\eta(\eta^2 - 2y\eta + a^2)} + \int_{-b}^{-a} + \int_{a}^{b} \frac{d\eta\, \phi(x, \eta)(a^2 - \eta^2)}{2\eta(\eta^2 - 2y\eta + a^2)} \right] = 0$$

The variable $\eta' = a^2/\eta$ is introduced in the second term to give the result

$$\frac{\partial}{\partial y}\left[\int_{-a}^{a} \frac{d\eta\, \phi(x, \eta)(a^2 - \eta^2)}{2\eta(\eta^2 - 2y\eta + a^2)} + \int_{+a}^{+a^2/b} + \int_{-a^2/b}^{-a} \frac{d\eta\, \phi(x, a^2/\eta)}{2\eta(\eta^2 - 2y\eta + a^2)} \right] = 0$$

It is evident that the above equation will be satisfied identically if the following relations hold:

$$\left.\begin{aligned} \phi(x, y) &= 0 \qquad (|y| < a^2/b) \\ \phi(x, a^2/y) &= \phi(x, y) \qquad (a^2/b < |y| < b) \end{aligned}\right\} \quad (26)$$

Eqs. (26) may be used to reduce the region of integration of Eq. (17) from $R_W + R_B$ to R_W alone. There results the integral equation shown below in which the region of integration and the region of validity are identical.

$$\frac{a^2\alpha_0}{y^2} + \alpha(x, y) = \frac{1}{2\pi}\frac{\partial}{\partial y} \int\int_{R_W} \frac{d\xi\, d\eta\, u(\xi, \eta)}{y - \eta}\left[1 + \frac{\sqrt{(x - \xi)^2 + (y - \eta)^2}}{x - \xi}\right] + \frac{1}{2\pi}\frac{\partial}{\partial y} \int\int_{R_W} \frac{d\xi\, d\eta\, u(\xi, \eta)}{y - (a^2/\eta)} \frac{a^2}{\eta^2}\left\{1 + \frac{\sqrt{(x - \xi)^2 + [y - (a^2/\eta)]^2}}{x - \xi}\right\} \quad (27)$$

In order to obtain a single-variable integral equation, Eq. (27) will be multiplied by a weighting factor and integrated over the wing span.[9] Following reference 10, a solution for the case of very low aspect ratio,

$$\sqrt{[b + (a^2/b)]^2 - [y + (a^2/y)]^2}$$

will be chosen as the appropriate weighting factor for the case on hand. Upon multiplying (27) by this weighting factor and making use of the definitions

$$f(x) = \int_{-b}^{-a} + \int_{a}^{b} dy \left[\alpha(x, y) + \frac{\alpha_0 a^2}{y^2}\right] \sqrt{\left(b + \frac{a^2}{b}\right)^2 - \left(y + \frac{a^2}{y}\right)^2} \quad (28)$$

$$Q(x, y) = \int_{-c}^{c} d\xi \int_{-b}^{-a} + \int_{a}^{b} \frac{d\eta\, u(\xi, \eta)}{y - \eta}\left[1 + \frac{\sqrt{(x - \xi)^2 + (y - \eta)^2}}{x - \xi}\right] + \int_{-c}^{c} d\xi \int_{-b}^{-a} + \int_{a}^{b} \frac{d\eta\, u(\xi, \eta)}{y - (a^2/\eta)} \frac{a^2}{\eta^2}\left\{1 + \frac{\sqrt{(x - \xi)^2 + [y - (a^2/\eta)]^2}}{x - \xi}\right\} \quad (29)$$

there results the relationship

$$f(x) = \frac{1}{2\pi}\int_{-b}^{-a} + \int_{a}^{b} dy \sqrt{\left(b + \frac{a^2}{b}\right)^2 - \left(y + \frac{a^2}{y}\right)^2}\,\frac{\partial}{\partial y}\,Q(x, y) \tag{30}$$

where c is the wing semichord at the intersection of the wing and body.

In evaluating the integral expression (29) for $Q(x, y)$, the radicals will be approximated by the expression

$$(1/2)[|x - \xi| + \sqrt{(x - \xi)^2 + (b - a)^2}]$$

It is evident that when $|x - \xi|$ is large compared with the span, this approximation is satisfactory. The limiting case in which the aspect ratio approaches infinity will be discussed later. It will be shown that, for a rectangular wing, the integral equation to be derived by this approximation approaches a proper limiting form.

When the approximate value for the radicals in Eq. (29) is introduced and the spanwise symmetry is taken into account, the formula for $Q(x, y)$ may be written in the form

$$Q(x, y) = 2\int_{-c}^{c} d\xi \int_{a}^{d} d\eta\, u\,(\xi, \eta)\left[1 + \frac{|x - \xi| + \sqrt{(x - \xi)^2 + (b - a)^2}}{2(x - \xi)}\right]\left[\frac{y}{y^2 - \eta^2} + \frac{a^2}{\eta^2}\,\frac{y}{y^2 - (a^4/\eta^2)}\right] \tag{31}$$

The integral equation (30) will now be transformed by integrating the right-hand side by parts with respect to y. Since $Q(x, \pm a)$ vanishes, as seen from Eq. (31), and the radical vanishes at $y = \pm b$, there results the form

$$f(x) = \frac{1}{\pi}\int_{a}^{b} \frac{dyQ(x, y)}{y^3}\,\frac{(y^4 - a^4)}{\sqrt{[b + (a^2/b)^2] - [y + (a^2/y)^2]}} \tag{32}$$

Upon substituting Eq. (31) for Q in Eq. (32), interchanging the order of integration, and making use of the definition

$$P(\eta) = \int_{a}^{b} \frac{dy}{y^3}\,\frac{y^4 - a^4}{\sqrt{[(b + (a^2/b)]^2 - [y + (a^2/y)^2]}}\left[\frac{y}{y^2 - \eta^2} + \frac{a^2}{\eta^2}\,\frac{y}{y^2 - (a^4/\eta^2)}\right] \tag{33}$$

Eq. (32) may be written as follows:

$$f(x) = \frac{1}{\pi}\int_{-c}^{c} d\xi\left[2 + \frac{|x - \xi| + \sqrt{(x - \xi)^2 + (b - a)^2}}{(x - \xi)}\right]\int_{a}^{b} d\eta\, u(\xi, \eta)P(\eta) \tag{34}$$

The integral expression (33) for $P(\eta)$ is evaluated in the Appendix. There results the formula

$$P(\eta) = (\pi/2)[1 + (a^2/\eta^2)] \tag{35}$$

It is convenient to define the function $g(x)$ as follows:

$$g(x) = 2\int_{-c}^{x} d\xi \int_{a}^{b} d\eta\, u(\xi, \eta)\left(1 + \frac{a^2}{\eta^2}\right) \tag{36}$$

The integral equation (34) may be written in terms of $g(x)$ in the form

$$f(x) = \frac{1}{2}\,g(x) + \frac{1}{4}\int_{-c}^{c} d\xi\, g'(\xi)\left[1 + \frac{\sqrt{(x - \xi)^2 + (b - a)^2}}{x - \xi}\right] \tag{37}$$

The function $g'(x)$ may be interpreted physically in terms of the lift per unit chord of the wing-body configuration. The conditions of Eq. (26) are employed to transform the expression (25) for the body lift per unit chord to the form

$$L_B(x) = 4\rho U^2 \int_{a}^{b(x)} dn\,\frac{a^2}{\eta^2}\,u(x, \eta)$$

Upon adding the above formula for L_B to Eq. (21) for the wing lift per unit chord, the total lift per unit chord $L(x)$ is given by the expression

$$L(x) = 4\rho U^2 \int_{a}^{(b)x} d\eta\, u(x, \eta)\left(1 + \frac{a^2}{\eta^2}\right) \tag{38}$$

and making use of Eq. (36)

$$L(x) = 2\rho U^2 g'(x) \tag{39}$$

The Kutta condition is applied as a spanwise average by the condition that $g'(x)$ vanish at the trailing edge of the wing. The integral equation (37) together with the Kutta condition $g'(c) = 0$ and Eq. (28) for the function $f(x)$ are sufficient to determine the function $g(x)$ when the plan form and angle of attack of the wing-body configuration are specified. The lift per unit chord is then determined from Eq. (39).

Comparison with Other Theories for Limiting Cases

When the aspect ratio of the exposed wing is small, the integral equation (37) is seen to reduce to the form

$$g(x) = f(x) = 2\int_a^{b(x)} dy \left[\alpha(x, y) + \frac{\alpha_0 a^2}{y^2}\right] \sqrt{\left(b + \frac{a^2}{b}\right)^2 - \left(y + \frac{a^2}{y}\right)^2} \tag{40}$$

This result is identical with the solution obtained by Flax[10] for vanishing aspect ratio. The special case when $\alpha_0 = 0$ is given by Puckett and Morikawa.[11] If the angle of attack of the wing $\alpha(x, y)$ and body α_0 are equal, the well-known result of Spreiter[5] and Ward[7] is obtained.

The limiting form of the integral equation (37) as the span becomes large will be evaluated. In order to simplify the analysis, a rectangular untwisted wing will be specified. Furthermore, the wing and body will be assumed to be at the same angle of attack. The integral defining the function $f(x)$ may be evaluated explicitly in this case so that the integral equation (37) may be written as follows:

$$\frac{\pi}{2} b_0^2 \alpha_0 \left(1 - \frac{a^2}{b_0^2}\right)^2 = \frac{1}{2} g(x) + \frac{1}{4}\int_{-c}^{c} d\xi\, g'(\xi) \left\{1 + \frac{\sqrt{(x - \xi)^2 + b_0^2 [1 - (a/b_0)]^2}}{x - \xi}\right\} \tag{41}$$

where b_0 is the semispan of the configuration. When the span becomes large, the above integral equation reduces to the limiting form

$$\frac{1}{\pi}\int_{-c}^{c} \frac{d\xi\, g'(\xi)}{x - \xi} = 2\alpha_0(b_0 - a)\left(1 + \frac{a}{b_0}\right)^2 \tag{42}$$

Eq. (42) is the well-known integral equation of two-dimensional airfoil theory. The solution for $g(c)$, when the Kutta condition $g'(c) = 0$ is specified, is given in reference 12 as

$$g(c) = 2\pi[1 + (a/b_0)]^2 \alpha_0 (b_0 - a)c \tag{43}$$

and the lift coefficient based on exposed wing area is given by the formula

$$C_L = 2\pi\alpha_0[1 + (a/b_0)]^2 \tag{44}$$

This result agrees with the results of reference 4 to within 4 per cent for a/b_0 ratios up to 0.4.

Solution of the Single-Variable Integral Equation

The solution of the integral equation (37) will be shown to depend in a simple manner upon the solution of the problem for a twisted wing without a body. A method for solving this wing-alone case has been presented in reference 9, and hence, most of the numerical work required for the solution of the wing-body problem is available.

The exposed semispan of the wing will be denoted by $\beta(x) = b(x) - a$. The integral equation (37) may be rewritten in the form

$$f(x) = \frac{1}{2} g(x) + \frac{1}{4}\int_{-c}^{c} d\xi\, g'(\xi) \left[1 + \frac{\sqrt{(x - \xi)^2 + \beta^2(x)}}{x - \xi}\right] \tag{45}$$

It is evident that Eq. (45) for $g(x)$ is identical with the integral equation (43) of reference 9 when the known function $k(x)$ defined therein is replaced by $f(x)$, defined by Eq. (28). Furthermore, $f(x)$ reduces to $k(x)$ as the body radius approaches zero. Hence, the integral equation (45) may be said to contain the integral equation (43) of reference 9 as a special case.

For the case of a flat wing at angle of attack α_0 equal to the body angle of attack, the function $f(x)$ may be written as follows:

$$f(x) = (\pi/2)\alpha_0 b^2 [1 - (a^2/b^2)]^2 \tag{46}$$

where b is, in general, a function of x. In the special case of a rectangular wing, $f(x)$ is a constant, and the solution for the wing-alone and the wing-body problems differs only by a constant factor.

Calculation of the Pressure Distribution

The distribution of lifting pressures may be computed by applying the procedure developed in reference 15. The integral equation (27) is rewritten in the form

$$\omega_a(x, y) = \frac{2}{\pi}\frac{\partial}{\partial y}\int_a^b d\eta\, \phi(x, \eta)\left[\frac{y}{y^2 - \eta^2} + \frac{a^2}{\eta^2}\frac{y}{y^2 - (a^4/\eta^2)}\right] \tag{47}$$

where the following definitions are used:

$$\omega_g(x, y) = \alpha(x, y) + (a^2\alpha_0/y^2) \tag{48}$$

$$\omega_a(x, y) = \omega_g(x, y) - \omega_i(x, y) \tag{49}$$

$$\omega_i(x, y) = \frac{1}{2\pi}\frac{\partial}{\partial y}\int\int_{R_W} d\xi\, d\eta\, u(\xi, \eta)\left[\frac{\sqrt{(x - \xi)^2 + (y - \eta)^2} - |x - \xi|}{x - \xi}\right]\left[\frac{1}{y - \eta} + \frac{a^2/\eta^2}{y - (a^2/\eta)}\right] \tag{50}$$

If the aerodynamic angle of attack $\omega_a(x, y)$ were known, Eq. (47) would be the governing integral equation for a very low aspect ratio wing. The solution of this integral equation is well known. (See, for example, reference 11.)

The aerodynamic angle of attack $\omega_a(x, y)$ may be approximated in the following manner: It is evident from Eq. (50) that the induced angle of attack $\omega_i(x, y)$ vanishes as the aspect ratio approaches zero and represents a small correction to the geometric angle $\omega_g(x, y)$ for wings of low aspect ratio. Following reference 15, the induced angle of attack will be assumed to be constant over the span or $\omega_i(x, y) = \omega_i(x)$ only. It will be noted that this assumption is analogous to assuming that the downwash is constant over the wing chord in the Prandtl[2] lifting-line theory. Eq. (47) may be rewritten in the form

$$\omega_g(x, y) - \omega_i(x) = \frac{2}{\pi}\frac{\partial}{\partial y}\int_a^b d\eta\, \phi(x, \eta)\left[\frac{y}{y^2 - \eta^2} + \frac{a^2}{\eta^2}\frac{y}{y^2 - (a^4/\eta^2)}\right] \tag{51}$$

In order to compute the induced angle $\omega_i(x)$, Eq. (51) is multiplied by

$$\sqrt{[b + (a^2/b)]^2 - [y + (a^2/y)]^2}$$

and integrated over the wing semispan. Upon performing certain integrations and making use of Eqs. (28) and (36), the following formula is obtained:

$$\omega_i(x) = [f(x) - g(x)]/(\pi/2)b^2\mu(a/b) \tag{52}$$

where $\mu(a/b)$ is given by the expression

$$\begin{aligned}\mu &= \frac{4}{\pi b^2}\int_a^b dy\, \sqrt{\left(b + \frac{a^2}{b}\right)^2 - \left(y + \frac{a^2}{y}\right)^2} \\ &= 1 + \frac{a^4}{b^4} - \frac{2}{\pi}\frac{a}{b}\left(1 - \frac{a^2}{b^2}\right) - \frac{1}{\pi}\left(1 + \frac{a^2}{b^2}\right)^2 \sin^{-1}\left[\frac{2(\alpha/b)}{1 + (a^2/b^2)}\right]\end{aligned} \tag{53}$$

The aerodynamic angle of attack may thus be expressed by Eqs. (48), (49), (52), and (53) in terms of the geometry of the configuration and the solution $g(x)$ to the integral equation (37).

The pressure distribution may be computed from Eq. (11) when the potential function ϕ is known. ϕ may be written as the real part of the complex potential F, or

$$F(x, \zeta) = \phi + i\psi, \qquad \zeta = y + iz \tag{54}$$

The complex potential function F may be calculated from the formula (see, for example, reference 11)

$$F(x, \zeta) = \frac{1}{\pi}\int_a^b d\eta\, \omega_a(x, \eta) \log\left[\frac{H(\zeta) + H(\eta)}{H(\zeta) - H(\eta)}\right] \tag{55}$$

where H is defined as follows:

$$H(\zeta) = \sqrt{[b + (a^2/b)]^2 - [\zeta + (a^2/\zeta)]^2} \tag{56}$$

Results and Extensions

The primary result of this paper is a method for calculating the symmetric lift distribution on a configuration consisting of a wing with straight trailing edge and arbitrary twist mounted on an infinite circular cylinder at arbitrary angle of attack in steady uniform linearized incompressible flow. The following engineering problems can be solved by suitable modifications of this result:

(1) The three-dimensional Prandtl-Glauert transformation may be used to compute the lift distribution at high Mach Numbers. In the case of low aspect ratio thin-wing slender-body configurations, the results appear to be applicable almost up to Mach Number unity. The calculation is so nearly identical to the well-known wing-alone case that it will not be presented.

(2) The restriction to infinitely long bodies of constant radius may be partially removed by a slight extension of the theory. Consider the case where the body radius is constant along the wing-body intersection. If the body forward of the wing-body intersection is slender, the lift distribution of this forebody may be computed by slender-body theory and added to the result for an infinite body-wing configuration without loss in accuracy. For the case of a slender body of variable radius aft of the wing trailing edge, the situation is somewhat more complex because of the interaction of the wing wake and body. This case has been analyzed by Adams and Sears.[8] The resulting lift distribution may be added to the lift distribution for the forebody and the infinite body-wing configuration.

(3) The effects of flaps and camber on the chordwise lift distribution may be computed in exactly the same way as for a wing alone. The wing-alone problem has been discussed in detail in reference 9.

(4) The theory developed in this paper is strictly applicable to low aspect ratio wings. However, as noted previously, the predictions of this theory are satisfactory for all aspect ratios in the case of a rectangular wing-body configuration. The assumptions made in the present analysis are essentially the same as those employed in reference 9 for the wing-alone case. Since the predictions of reference 9 for wing alone are found to agree with test data for aspect ratios from 0 to 4 at all taper ratios, there is good reason to believe that a similar situation will apply to the wing-body theory presented herein.

Appendix

Evaluation of $P(\eta)$

The integral expression for $P(\eta)$ given in Eq. (33) may be evaluated by substituting a new variable of integration t, where

$$2t = y + (a^2/y) \qquad (y = t + \sqrt{t^2 - a^2})$$

and making use of the definitions

$$2s = \eta + (a^2/\eta) \quad [2r = \beta + (a^2/\beta)]$$

to reduce the integral to the form

$$P(\eta) = \frac{2s}{\eta} \int_a^r \frac{dtt}{t^2 - s^2} \sqrt{\frac{t^2 - a^2}{r^2 - t^2}}$$

The substitution of a new variable $z = \sqrt{t^2 - a^2} \div \sqrt{r^2 - t^2}$ reduces $P(\eta)$ to the form

$$P(\eta) = \frac{2s}{\eta} \int_0^\infty dz \left[\frac{1}{1 + z^2} - \frac{1}{1 - \left(\frac{r^2 - s^2}{s^2 - a^2}\right) z^2} \right]$$

The second term of the integral vanishes when interpreted as a Cauchy principal value, whereas the first term is easily integrated to give the result

$$P(\eta) = (\pi\ 2)[1 + (a^2/\eta^2)]$$

References

[1] Lennertz, J., "Influence of the Airplane Body on the Wings," Durand's *Aerodynamic Theory*, Vol. IV, Division K, Chapt. III.

[2] Prandtl, L., *Tragflügeltheorie I. Mitteilung Nachrichten der K. Gesselschaft der Wissenschaften zu Göttingen*, Math.-Phys. Klasse, pp. 451–477, 1918.

[3] Multhopp, H., *Aerodynamics of the Fuselage*, Luftfahrtforschung, Vol. 18, No. 2-3, March, 1941 (NACA TM No. 1036).

[4] Flax, A. H., and Treanor, C., *A Variatonal Calculation of Subsonic Wing-Body Interference According to Lifting-Line Theory*, Cornell Aeronautical Laboratory, Inc. (to be published).

[5] Spreiter, John R., *Aerodynamic Properties of Slender Wing-Body Combinations at Subsonic, Transonic and Supersonic Speeds*, NACA TN No. 1662, 1948.

[6] Jones, R. T., *Properties of Low-Aspect-Ratio Pointed Wings at Speeds Below and Above the Speed of Sound*, NACA TN No. 1032, 1946.

[7] Ward, G. N., *Supersonic Flow Past Slender Pointed Bodies*, Quarterly Journal of Mechanics and Applied Mathematics, Vol. II, Part 1, 1949.

[8] Adams, Mac C., and Sears, W. R., *Slender Body Theory: Review and Extensions*, Journal of the Aeronautical Sciences, Vol. 20, No. 2, p. 85, February, 1953.

[9] Lawrence, H. R., *The Lift Distribution on Low Aspect Ratio Wings at Subsonic Speeds*, Journal of the Aeronautical Sciences, Vol. 18, No. 10, p. 683, October, 1951.

[10] Flax, A. H., *Integral Relationships in the Linearized Theory of Wing-Body Interference*, Cornell Aeronautical Laboratory, Inc. (to be published).

[11] Puckett, A. E., and Morikawa, G. K., *Equivalence of the Spanwise Lift Distribution to the Spanwise Lift-Influence Function for Slender Wings and Wing Bodies*, Readers' Forum, Journal of the Aeronautical Sciences, Vol. 18, No. 7, p. 503, July, 1951.

[12] Munk, Max M., *General Theory of Thin Wing Sections*, NACA TR No. 142, 1922.

[13] Lawrence, H. R., and Gerber, E. H., *The Aerodynamic Forces on Low Aspect Ratio Wings Oscillating in an Incompressible Flow*, Journal of the Aeronautical Sciences, Vol. 19, No. 11, p. 769, November, 1952.

[14] Munk, Max M., *The Aerodynamic Forces on Airship Hulls*, NACA TR No. 184, 1924.

[15] Lawrence, H. R., *The Pressure Distribution on Low Aspect Ratio Wings in Steady or Unsteady Incompressible Flow*, Readers' Forum, Journal of the Aeronautical Sciences, Vol. 20, No. 3, p. 218, March, 1953.

A Constant-Area, Constant-Temperature Combustor*

PHILIP ROSEN† AND R. W. HART†
The John Hopkins University

ABSTRACT

The theoretical performance of a piloted constant-area, constant-temperature combustor with mass addition is studied. Perpendicular injection of mass at constant injection velocity and temperature is assumed. Mixing between the injected mass and the main stream is regarded as instantaneous, and the flow is regarded as one-dimensional. The effect of chemical kinetics is considered by the use of a simple rate equation. The exit velocity corresponding to maximum throughput is found to be $\sqrt{RT}$. The combustor length required to accelerate the gases to this velocity is found to depend on the reaction rate constants, flame temperature, input flow variables, and the temperature of combustion. It is determined that there exists a lower limit on the temperature below which the combustor is unstable.

(I) INTRODUCTION

EARLY RAM-JET COMBUSTION CHAMBERS consisted basically of a fuel injector and a "flameholder" at the upstream end of a cylindrical pipe. A fuel mixture was injected into the air stream and ignited. The flameholder—an obstacle to airflow such as a strut(s) or disc(s)—provided eddy regions where motion of the gases was slow enough to permit rather complete burning and consequent pilot action. It was found that these combustion chambers are stable over a range of fuel and flow variables but that the stability range was exceedingly difficult to predict and depended on fuel injector geometry and flameholder geometry.

Most research in ram-jet combustion problems has been concerned with a search for empirical relations between flow, fuel, and geometry variables, because of the difficulty in characterizing theoretically compressible turbulent flow; the effect of flameholder and injector geometry on the flow; the effect of mixing and heat transfer; and the chemical kinetics of the reactions. Several investigators made simplified theoretical analyses of cylindrical pipe operation.[1–4] One-dimensional flow and addition of heat were assumed. By using the equations of conservation of mass, energy, and momentum with the equation of state of an ideal gas, useful information, particularly limiting velocities and mass flows, was obtained. The effects of fuel properties on operations of flameholder-type ram-jets—which enter the problem through kinetics of reaction—or mixing and geometry effects have apparently not been treated theoretically. In the idealized cylindrical pipe combustors, where the above-mentioned theory is valid, heat transfer and mixing are perfect and instantaneous throughout any cross-sectional element, but no transfer takes place along any direction parallel to the cylinder axis (cf. reference 5).

In this report we will consider the cylindrical combustor from a similar point of view but will introduce the effect of fuel type by considering the rate of heat production to be described by a simple reaction rate equation of arbitrary order and by assuming that the temperature in the combustor is a fixed constant. A similar approach to a constant-pressure constant-temperature can-type combustor has been used by Avery and Hart.[5] An additional simplification is made by assuming that the combustor receives a known mass flow of stoichiometric composition from a pilot and through the cylindrical walls. With these assumptions the rate of heat production given by a rate equation is then required to equal the heat rate required (a) to warm the injected mixture up to the combustor operating temperature and (b) to increase the velocity of the injected mixture, as well as the velocity of the original gases. Application of the conservation equations then yields relationships that must exist between rate of addition of unburned fuel to the burner and rate of combustion to determine the burner length and range of stability.

(II) THEORETICAL ANALYSIS

(*1*) *The Conservation Equations.*—The differential equations expressing conservation of energy, momentum, and mass are:[6]

Neglecting heat losses, diffusion, and burner drag, the energy conservation is

$$\frac{d\dot{Q}}{dx} = \frac{V^2 - V_u^2}{2} + C_p(T - T_u)\frac{d\dot{m}}{dx} + \frac{\dot{m}\,d\,V^2}{2\;dx}$$

The conservation of momentum equation is

$$-A(dp/dx) = (d/dx)\,(\rho A V^2)$$

The equation of conservation of mass is

$$(d/dx)\,(\rho A V) = d\dot{m}/dx$$

Received February 27, 1953.

* Supported by the Bureau of Ordnance, U.S. Navy, under Contract NOrd 7386. The authors wish to express their appreciation to Dr. W. H. Avery for many helpful discussions. The authors also would like to acknowledge the aid given them by R. E. Walker.

† Senior Physicist, Applied Physics Laboratory.

where

$d\dot{Q}/dx$ = rate of production of heat (per unit length) caused by chemical reaction
$\dot{m}$ = rate of mass flow through the cylinder at x
A = cross-section area of the cylindrical combustor
P = static pressure of gases in the combustor
C_p = average heat capacity of fuel-air mixture and combusted products
T = absolute temperature = constant
V_u = velocity of injected mixture, assumed perpendicular to the cylinder walls and constant
T_u = temperature of injected mixture

With the constant values of V_u, T_u, and A, all of the conservation equations can be integrated,

$$\dot{m}\left[\frac{V^2 - V_u^2}{2} + C_p(T - T_u)\right] + C = \dot{Q} \quad (1a)$$

where C is the constant of integration,

$$P + \rho V^2 = P_0 + \rho_0 V_0^2 = \text{constant} = F \quad (1b)$$

(The subscript zero indicates evaluation at the upstream end of the combustor.)

$$\dot{m} = \rho A V \quad (1c)$$

These three equations and the equation of state $P = \rho RT$ constitute four equations relating five unknowns ($\dot{Q}$, P, ρ, V, and $\dot{m}$). The temperature, T, and the area, A, are specified. The rate equation will relate heat production, $\dot{Q}$, to the other four variables and therefore permit us to determine the behavior of P, T, ρ, V, $\dot{m}$, and $\dot{Q}$.

(2) *Limiting Exit Flow Velocity.*—Just as in the case of a cylindrical combustor with heat addition and without mass addition, an important limiting flow condition can be determined without considering details of the chemical reaction. It will now be shown that the constant-temperature combustor has maximum "throughput"† when the exit Mach Number is $(\gamma)^{-1/2}$.

Differentiation of Eq. (1c) with respect to x, and elimination of the density by means of Eq. (1b) and the equation of state yield a relation between the rate of mass addition and the rate of change of velocity,

$$\frac{d\dot{m}}{dx} = \frac{AF(RT - V^2)}{(RT + V^2)^2}\frac{dV}{dx} = \frac{AF(1 - \gamma M^2)}{RT(1 + \gamma M^2)^2}\frac{dV}{dx} \quad (2a)$$

where γ is the specific heat ratio and M is Mach Number of the flow.

A second differentiation yields

$$\left.\frac{d^2\dot{m}}{dx^2}\right|_{V=\sqrt{RT}} = \frac{-AF}{2(RT)^{3/2}}\left(\frac{dV}{dx}\right)^2\Bigg|_{V=\sqrt{RT}} \quad (2b)$$

† Total mass flow through the combustor exit.

The constant F is greater than zero, so that the mass flow rate has a maximum at $V^2 = RT$ or $M^2 = 1/\gamma$‡ (unless dV/dx is zero with $d^2V/dx^2 < 0$). But it is easy to show that the requirement that heat be generated (i.e., that $d\dot{Q}/dx$ be positive) requires that dV/dx be positive for V^2 less than RT. Using Eq. (1a) with $\dot{m} = AFV/(RT + V^2)$ following from Eqs. (1b) and (1c), we find

$$0 < \frac{d\dot{Q}}{dx} = \frac{d\dot{m}}{dx}\left[c_p(T - T_u) + \frac{1}{2}(V^2 - V_u^2)\right] + \frac{dV}{dx}\frac{AFV^2}{RT + V^2} \quad (2c)$$

and using $d\dot{m}/dx$ from Eq. (2a),

$$0 < \frac{d\dot{Q}}{dx} = \frac{dV}{dx}\left\{\frac{AF\gamma M^2}{(1 + \gamma M^2)} + \frac{AF\gamma}{\gamma - 1}\frac{1 - \gamma M^2}{(1 + \gamma M^2)^2} \times \left[1 - \frac{T_u}{T} + \frac{\gamma - 1}{2}\left(M^2 - \frac{T_u}{T}M_u^2\right)\right]\right\} \quad (2d)$$

Now, evaluating at $V^2 = RT$,

$$0 < \left.\frac{d\dot{Q}}{dx}\right|_{V^2=RT} = \frac{AF}{2}\left.\frac{dV}{dx}\right|_{V^2=RT} \quad (2e)$$

The condition that the rate of heat generation $d\dot{Q}/dx$ be greater than zero requires that dV/dx be positive according to Eq. (2d). (The region V^2 greater than RT is of no significance in the investigation of this combustor, since it has now been shown that $d\dot{m}/dx$ becomes negative in this region, corresponding to mass subtraction.) It is easily shown, further, that dV/dx is positive for all velocities less than $(RT)^{1/2}$ when heat is generated in the combustor. From Eq. (2d), this condition obviously can immediately determine that, for all velocities less than this critical velocity, the bracketed term is positive. The operating temperature of the combustor (T) is necessarily greater than the temperature of the injected fuel-air mixture (T_u), and the Mach Number with which the fuel-air mixture enters the combustion chamber (M_u) is, in any case, less than sonic, so that whenever the term $(1 - \gamma M^2)$ is positive the bracketed term is also positive. In the limiting case when there is no unburned fuel beyond a certain point in the combustor, $d\dot{Q}/dx$ will be zero and so dV/dx will be zero.

It is easily shown that the ratio of mass throughput to mass flow input from the pilot increases with decreasing input Mach Number. From Eqs. (1b) and (1c),

$$\frac{\dot{m}}{\dot{m}_0} = \frac{M}{M_0}\left[\frac{RT + V_0^2}{RT + V^2}\right] = \frac{M}{M_0}\left[\frac{1 + \gamma M_0^2}{1 + \gamma M^2}\right]$$

‡ A similar phenomenon occurs at the same Mach Number in the analysis of a constant-area combustor given by Chambre and Linn (reference 1, p. 537).

Since this ratio increases with increasing V, we obtain maximum throughput by inserting the velocity, $V = \sqrt{RT}$, and

$$\dot{m}_{\text{exit}}/m_0 = (1 + M_0^2)/2\sqrt{\gamma}\, M_0 \qquad (2f)$$

(3) Combustion Efficiency.—We will now investigate the combustion efficiency η, which the conservation equations require to exist in this constant-temperature combustor—without regard to the type of heat-producing reaction.

Let η equal mass flow rate of completely combusted fuel-air mixture divided by total mass flow rate. Then the heat flow rate $\dot{Q}$ is given in terms of the heat of combustion by

$$\dot{Q} = \eta H\dot{m}$$

where H is the energy released per unit mass by complete combustion of the injected fuel-air mixture. (Nitrogen in the fuel air mixture is to be included in the combustion products.)

Eq. (1a) specifies the rate at which heat must be produced in order to maintain the combustor temperature constant. Rewriting this equation, we find

$$\eta = \frac{C}{\dot{m}H} + \frac{C_p(T - T_u)}{H} + \frac{V^2 - V_u^2}{2H} \qquad (3a)$$

It is evident that, downstream from the pilot where the mass flow rate is much greater than the input mass flow from the pilot, the term $C/\dot{m}$ tends toward zero, and the combustion efficiency tends to become independent of the integration constant C. The combustion efficiency approaches as a limit the value

$$\frac{C_p(T - T_u)}{H} + \frac{V^2 - V_u^2}{2H} = \frac{T - T_u}{T_f - T_u} + \left(\frac{M^2T - M_u^2T_u}{T_f - T_u}\right)\frac{\gamma - 1}{2} \qquad (3b)$$

The downstream limit combustion efficiency, η^*, corresponding to maximum throughput is obtained by substituting $V^2 = RT$ into this equation, and letting

$$\left.\begin{aligned} H &= C_p(T_f - T_u) \\ \eta^* &= \frac{T - T_u}{T_f - T_u} + \frac{T - \gamma M_u^2 T_u}{T_f - T_u}\left(\frac{\gamma - 1}{2\gamma}\right) \end{aligned}\right\} \qquad (3c)$$

which is relatively insensitive to changes in the temperature (T_u) and Mach Number (M_u) of the injected mixture, provided T_u is much less than T and that the injection Mach Number is small. [Note that the flame temperature, T_f, is here defined by $C_p(T_f - T_u) = H =$ heat of combustion.] Since part of the heat results in accelerating the gas, the burner temperature can never reach T_f. The integration constant C is determined by the composition, temperature, and velocity of the pilot output. It is easily shown that the amount of fuel that can be burned in a combustor operating at maximum throughput corresponding to the pilot temperature T, $\dot{m} = FA/2\sqrt{RT}$, is independent of the choice of C, although the combustor length does depend on C. We calculate $(m_{\text{exit}})\,(\eta_{\text{exit}}) - m_0\eta_0 =$ mass burned per second in the combustor. Substituting the expression for efficiency derived above, and $V^2 = RT$, we find that the mass burned per second depends on the pilot temperature but does not depend on the choice of C. The required combustor length to attain $V^2 = RT$ does, however, depend on the choice of C. The burner analysis is simplified by selecting a pilot for which $C = 0$. This can be effected, for example, by regarding the pilot as an extension of the combustor.

With $C = 0$,

$$\eta = \frac{C_p}{H}(T - T_u) + \frac{V^2 - V_u^2}{2H} \qquad (3d)$$

If $\eta = 1$, an upper limit V^* is set on the velocity,

$$V^* = \sqrt{2H + V_u^2 - 2C_p(T - T_u)} = \sqrt{2C_p(T_f - T) + V_u^2} \qquad (3e)$$

The highest temperature (T^*) possible with maximum exit velocity $V = \sqrt{RT}$ is found from Eq. (3e) setting $V^* = \sqrt{RT}$,*

$$T^* = [2\gamma/(3\gamma - 1)]T_f \qquad (3f)$$

when $M_u \ll 1$.

(4) Kinetics of Reaction.—We now express the rate of heat production per unit length, $d\dot{Q}/dx$, in terms of the state and flow variables; then, in the following section, the conservation equations are solved for these variables, with the aid of an assumed Nth-order reaction.

Assume a simple Nth-order reaction—i.e., the time rate of change of concentration of fuel (C_f) due to chemical reaction is

$$\partial C_f/\partial t = -K'e^{-E/RT}C_f^N$$

The concentration of fuel is readily expressed in terms of the air-to-fuel ratio (a/f) and the concentration of unreacted fuel-air mixture by

$$C_f = \rho(1 - \eta)/[1 + (a/f)]$$

The air-to-fuel ratio will be assumed stoichiometric so that (a/f) is constant throughout the combustor.

The amount of heat produced per second per unit length is proportional to the mass of fuel-air mixture reacted per unit length—i.e.,

$$\frac{d\dot{Q}}{dx} = \frac{d}{dx}(\eta H\dot{m}) = \frac{-\partial C_f}{\partial t} AH\left[1 + \frac{a}{f}\right]$$

so that under steady-state conditions

$$\frac{d}{dx}(\eta H\dot{m}) = AK'e^{-E/RT}\left[\frac{\rho(1 - \eta)}{1 + (a/f)}\right]^N [1 + (a/f)]H \qquad (4a)$$

This differential equation is rewritten as a differential equation in velocity by substituting η from Eq. (3a) and $\dot{m}$ from Section (2), $m = AFV/(RT + V^2)$.

$$\frac{d}{dx}\left[\left(\frac{C_p}{H}(T - T_u) + \frac{V^2 - V_u^2}{2H}\right)\left(\frac{V}{RT + V^2}\right)\right] = \frac{K' e^{-E/RT}}{F}\left(1 + \frac{a}{f}\right)^{1-N}\left(\frac{F}{RT + V^2}\right)^N\left[1 - \frac{C_p}{H}(T - T_u) - \frac{V^2 - V_u^2}{2H}\right]^N \quad (4b)$$

Eq. (4b) can be rewritten in simpler form by using Eq. (3e). We obtain

$$\frac{[V^4 + (3RT - 2H + V^{*2})V^2 + RT(V^{*2} - 2H)](V^2 + RT)^{N-2}}{[V^2 - V^{*2}]^N} dV = \frac{(-1)^N}{(2H)^{N-1}} K F^{N-1} e^{-E/RT} dx \quad (4c)$$

where $K = K'/[1 + (a/f)]^{N-1}$.

A solution of this equation gives the velocity as a function of position in the combustor for an Nth-order reaction. Other flow and state variables are expressed in terms of V,

$$\dot{m} = AFV/(RT + V^2), \quad \rho = F/(RT + V^2)$$

$$P = FRT/(RT + V^2), \quad \eta = [C_p(T - T_u)/H] + [(V^2 - V_u^2)/2H] \quad (4d)$$

(5) *Solution of the Velocity Differential Equation for a Second-Order Reaction* ($N = 2$).—With $N = 2$, Eq. (4c) is readily integrated. We find

$$\left\{(V - V_0) + \left[\frac{V^{*4} + (RT - H)V^{*2} + RTH}{V^{*2}}\right]\left(\frac{V}{V^{*2} - V^2} - \frac{V_0}{V^{*2} - V_0^2}\right)\right\} - \left[\frac{2V^{*4} + (2RT - H)V^{*2} - HRT}{2V^{*3}}\right]\ln\left[\left(\frac{V^* + V}{V^* - V}\right)\left(\frac{V^* - V_0}{V^* + V_0}\right)\right] \equiv \Phi(V, V_0, V_u, T, T_u, T_f) = \frac{K'[P_0 + \rho_0 V_0^2]e^{-E/RT}}{2H[1 + (a/f)]}(x - x_0) \quad (5a)$$

where $x - x_0$ = length of combustor.

Eq. (5a) indicates the behavior of velocity as a function of position. The relationship is too complicated, however, to visualize readily, although it is clear that the limiting velocity V^* (corresponding to $\eta = 1$) is reached only at infinite distances. It has already been shown that $(V^*)^2 > RT$, $dv/dx > 0$.

For $C \neq 0$, we obtain the following expression, which is also integrable, although somewhat more complicated:

$$\int_{V_0}^{V} \frac{[(V^4 + 3RT - 2H + V^{*2})V^2 + RT(V^{*2} - 2H)V^2]\,dV}{\left(V^3 + \frac{2CV^2}{AF} - VV^{*2} + \frac{2RCT}{AF}\right)^2} = \frac{K_e^{-E/RT}}{2H}F(x - x_0)$$

In this study we concern ourselves only with the simpler case $C = 0$ corresponding to

$$\eta_0 = [(V_0^2 - V_u^2)/2H] + [(T - T_u)/(T_f - T_u)]$$

Fig. 1 shows a plot of $\log_e(\Phi\ e^{E/RT})$ against T. Curves A and B are for $E = 33{,}000$ cal. per mole and $M_0 = 0$ and 1/10, respectively, where $M_0 = V_0 \div (\gamma RT)^{1/2}$. Curves C and D are for $E = 25{,}000$ cal. per mole and for $M_0 \cong 0$ and 1/10, respectively. These curves show what one would expect—namely, the length required is larger for higher activation energies and slightly larger for smaller incident Mach Numbers for constant T. The effect of M_0 is not great if $M_0 \ll 1$. Consequently, for large throughput, $\dot{m}_{exit.}/\dot{m}_0$, the length is relatively insensitive to increases of $\dot{m}_{exit.}/\dot{m}_0$.

In the above and following calculations, we have used values for the constants as indicated below:

R = 2/30 = gas constant = 1/15 cal. per Gm. °K. for air ≃ 2 cal. per mole °K.

γ = 1.3
T_f = 2,400°K.
C_p = 0.288889 cal. per Gm. °K.
P_0 = 1/5 atmosphere
T_u = 480°K.
a/f = 16
K' = $(a/f)B'$
B' = 5×10^{12} cc. per Gm.sec.
V_u = V_0

(6) *Minimum Operating Temperature and Stability.*—Before we study further calculations, it is illuminating to consider the temperature range within which the combustor is capable of stable operation. We have already seen that the maximum attainable temperature is given (for small M_0) by $T^* = [2\gamma/(3\gamma - 1)]T_f$ and

that this temperature corresponds to an exit velocity V^* which is only attained at infinite length where the combustion becomes complete [Eq. (5a)]. A minimum stable operating temperature must exist, because the rate of chemical reaction decreases rapidly (essentially exponentially) with decreasing temperature, whereas the heat required to warm and accelerate the incoming mixture decreases relatively slowly (nearly linearly for the range of Mach Numbers considered). This means that below a critical temperature a disturbance that causes a drop in temperature may cause the heat generated to fall below the heat required to maintain energy balance and the temperature continues to fall.

It is easily shown that this combustor is unstable to changes in pilot temperature for temperatures less than that corresponding to the minimum of the curve of Fig. 1. This is so because, to the left of these minimums, a drop in the combustor temperature increases the length required to maintain that temperature and, since the length is fixed, the temperature must fall further. To the right of the minimums, a slight drop in temperature decreases the length required, and this will tend to bring the temperature back to what it was before. Similarly, a slight rise in temperature will increase the length required, and this will also tend to bring the temperature back. Thus, at first thought, we could consider our lower limit of temperature as corresponding to the value just beyond the minimum to the right. There is, however, a more severe stability criterion that yields somewhat higher minimum temperature.

Let us consider a perturbation in which an extra amount of mass is added at some point in the combustor. This will lower the local temperature suddenly. If this additional mass does not burn, then $\delta(d\eta\dot{m}/dx) = 0$. If it does burn, then $\delta(d\eta\dot{m}/dx) > 0$. Thus, from Eq. (4a), for a second-order reaction

$$\delta[\rho^2(1-\eta)^2 e^{-E/RT}] \geq 0$$

If we consider that pressure and velocity remain (roughly) constant, then,

$$\delta\rho = (\rho/T)\delta T, \quad \delta\eta = \delta T/(T_f - T_u)$$

and, thus,

$$\frac{-2}{T}\delta T - \frac{2\delta T}{(1-\eta)(T_f - T_u)} + \frac{E}{RT^2}\delta T \geq 0$$

or, since $\delta T < 0$,

$$\frac{2}{T} + \frac{2}{(1-\eta)(T_f - T_u)} - \frac{E}{RT^2} \geq 0 \qquad (6a)$$

If we choose $\eta = \eta_0$ then we find that

$$T \geq T_f/[1 + (2RT_f/E)]$$

If $T_f = 2{,}400$ and $E = 33{,}000$ cal. per mole, then $T \geqslant 1{,}860°\text{K.} \geqslant 0.775T_f$.

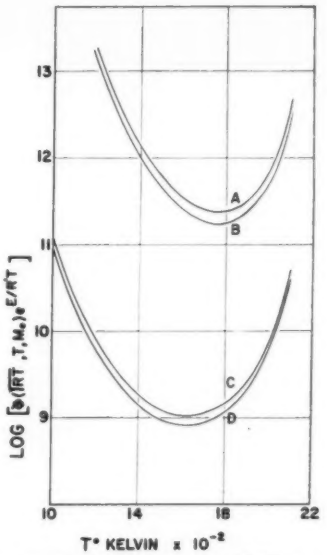

FIG. 1. The log of the length factor $\Phi e^{E/RT}$ is plotted against temperature; Curves A and B, $E = 33{,}000$ cal. per mole, $M_0 \cong 0$ and 0.1, respectively; Curves C and D, $E = 25{,}000$ cal. per mole, $M_0 \cong 0$ and 0.1, respectively.

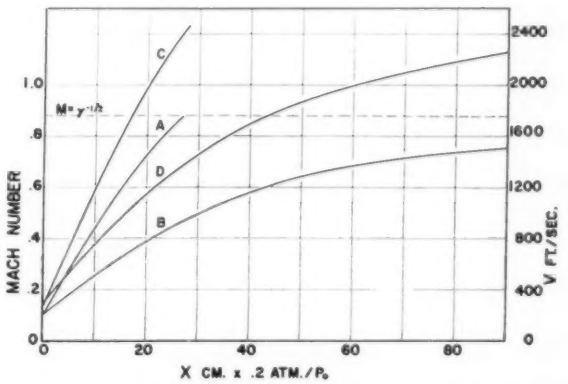

FIG. 2. The Mach Number and velocity are plotted against distance in the combustor; Curves A and B are Mach Number at $T = 1{,}860°$ K. and 2,152°K., respectively; Curves C and D are the corresponding velocities.

If η is closer to unity, then the minimum temperature is below this value, as can easily be seen from Eq. (6a). This is as one would expect, since, if the burning gas were unstable at the pilot, it would be unstable further downstream. This lower limit was obtained graphically by Avery and Hart for an activation energy of $E = 33{,}000$ cal. per mole.

(7) *Results.*—Let us consider $E = 33{,}000$ cal. per deg. mole and $M_0 = 1/10$ and calculate the length of the burner at the lower limit of the stability region $T = 1{,}860°$K. At this lower limit, we find $L = 26.5$ cm. At the upper limit $T = 2{,}152°$K., the length is infinite.

In Fig. 2 Curves A and B are plots of Mach Number in the burner vs. x, when $P_0 = 1/5$ atmosphere, for $T = 1{,}869°$K. and 2,152°K., respectively. We see that for $T = 1{,}860$, the Mach Number increases monotoni-

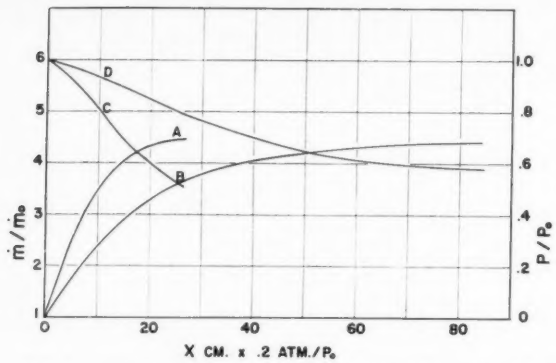

FIG. 3. The ratios of mass flow rate to initial flow rate and of pressure to initial pressure are plotted against distance in the combustor; Curves A and B are $\dot{m}/\dot{m}_0$ for T = 1,860°K. and 2,152°K., respectively; Curves C and D are P/P_0 for T = 1,860°K. and 2,152°K., respectively.

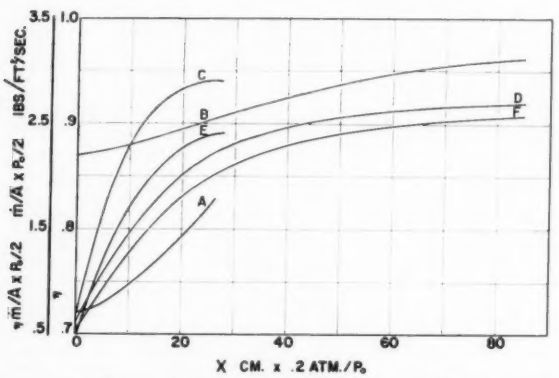

FIG. 4. The combustion efficiency, total mass flow rate per unit area, and the mass flow rate of burned gases per unit area are plotted against distance; Curves A and B are efficiency for T = 1,860°K. and 2,152°K., respectively; Curves C and D are corresponding curves for $\dot{m}/A$ and Curves E and F are $\eta\dot{m}/A$ for the above temperatures, respectively.

cally until it reaches $M = (1/\gamma)^{1/2}$ at x = 26.5 cm., while for T = 2,152°K. the Mach Number approaches $(1/\gamma)^{1/2}$ asymptotically at infinity. Also plotted in Fig. 2 are the actual velocities in feet per second. Curve C is for T = 1,860°K. and Curve D is for T = 2,152°K. At T = 1,860°K. the velocity starts at 270 ft. per sec. and rises to 2,400 ft. per sec., while for T = 2,152°K. the velocity starts at 295 ft. per sec. and approaches 2,575 ft. per sec. at infinity. The velocity difference between these two cases at the exit is relatively small considering the difference in length.

In Fig. 3 Curves A and B are plots of the ratio $\dot{m}/\dot{m}_0$ vs. x at P_0 = 1/5 atmosphere for T = 1,860°K. and 2,152°K., respectively. On Curve A, $\dot{m}/\dot{m}_0$ reaches a maximum of 4.44; at Curve B $\dot{m}/\dot{m}_0$ approaches the same value asymptotically at ∞. Curves C and D are plots of the ratio of pressure at any station to entrance pressure vs. x at T = 1,860°K. and 2,152°K., respectively. On Curve C, P/P_0 reaches a value of 0.505, and on Curve D P/P_0 approaches the same value at infinity.

In Fig. 4, Curves A and B are plots of η vs. x for P_0 = 1/5 atmosphere for T = 1,860°K. and 2,152°K., respectively. On Curve A, η reaches the value of 0.83 from a value of 0.72 at the pilot. On Curve B, η approaches the value unity at infinity from a value of 0.87 at the pilot.

Curves C and D are plots of mass per unit area per unit time in pounds per foot second, for P_0 = 1/5 atmosphere for T = 1,860° and 2,152°K., respectively. On Curve C, $\dot{m}/A$ increases from 0.66 lbs. per sq.ft. sec. to a definite maximum of 2.9 lbs. per sq.ft. sec. On Curve D, $\dot{m}/A$ approaches a value of 2.7 lbs. per sq.ft sec. from an initial value of 0.61 lbs. per sq.ft. sec. Here again we would gain nothing with a higher temperature.

Curves E and F are plots of $\eta\,\dot{m}/A$ for T = 1,860°K. and 2,152°K., respectively, at P_0 = 1/5 atmosphere. On Curve E, $\eta\,\dot{m}/A$ starts from a value of 0.47 lbs. per sq.ft. sec. and increases to a value of 2.4 lbs. per sq.ft. sec. On Curve F, $\eta\dot{m}/A$ approaches 2.7 lbs. per sq.ft. sec. at infinity from a value of 0.53 lbs. per sq.ft. sec.

REFERENCES

[1] Chambre, P., and Linn, C. C., Journal of the Aeronautical Sciences, Vol. 13, pp. 537–542, 1947.

[2] Foa, J. V., and Rudinger, G., Journal of the Aeronautical Sciences, Vol. 16, pp. 84–94, 1949.

[3] Hicks, B. L., Montgomery, D. J., and Wasserman, R. H., J.A.P., Vol. 18, pp. 891–902, 1947.

[4] Szczeniowski, B., Can. J. Res., Vol. 23A, pp. 1–11, 1945.

[5] Avery, W. H., and Hart, R. W., *Combustor Performance with Instantaneous Mixing*, Ind. & Eng. Chem., to be published.

[6] *Handbook of Supersonic Aerodynamics*, Section 4, Bureau of Ordnance Publication, NAVORD Report 1488, Vol. 1.

Studies of Some Effects of Airplane Configuration on the Response to Longitudinal Control in Landing Approaches

RALPH W. STONE, JR.,* AND WILLIAM BIHRLE, JR.*

Langley Aeronautical Laboratory, NACA

SUMMARY

The investigation reported in this paper was undertaken to see whether there are inherent differences in the response of the flight-path angle to control movements between swept-wing airplanes having no horizontal tail and using trailing-edge flaps for longitudinal control and conventional airplanes that are known to have satisfactory response characteristics. Particular emphasis is placed on the final few seconds of the landing approach.

This study shows that the only difference in the short-time response of the flight path between the two types of airplanes is in a time lag in the flight-path angle response of the swept-wing airplanes. This time lag was found to result from two factors: first, a relatively small value of the parameter,

$$(VC_{L_\alpha}/2\mu c)\,(V^2C_{m_{\delta_e}}/2\mu k_y^2)\Delta\delta_e$$

which is a measure of the effectiveness of the control in changing the flight-path angle and, second, a relatively large value of the parameter

$$(VC_{L_{\dot{\delta}_e}}/2\mu c)\Delta\delta_e$$

which is a measure of the amount of undesirable change in lift accompanying the control deflection required to change the angle of attack. It had been suspected that the relatively large change in drag with angle of attack, of low aspect ratio swept-wing airplanes having no horizontal tails, would be an important factor in the flight-path angle response, but this was found not to be the case for the short time intervals under consideration.

The importance of the differences found in the response characteristics between the two types of airplanes studied can only be evaluated by flight experience. Other factors such as range of vision, control feel, the pilot's reaction to the relatively large nose-up attitudes of the low aspect ratio swept-wing airplanes, and psychological influences associated with new type airplanes may be of equal or greater importance.

INTRODUCTION

WITH THE DEMAND FOR HIGH-SPEED FLIGHT, airplane configurations have changed appreciably, and necessary compromises have led to some flight difficulties particularly at low speeds. One such difficulty was reported in reference 1 for free-flying airplane models having low aspect ratio wings and no horizontal tails. The models responded uncertainly to elevator control movements, particularly when flying beyond the angle of attack of maximum L/D ratio. It was felt that troubles may be encountered on similar airplanes at low speeds, particularly in landing approaches where small height corrections may be needed. A theoretical investigation of the responses to longitudinal control of airplanes having low aspect ratio wings and no horizontal tails, therefore, was undertaken at the NACA's Langley Aeronautical Laboratory to evaluate the effects of aerodynamic differences between this type of airplane and other more conventional airplanes that are known to have satisfactory response characteristics in landing approaches.

Other factors such as the range of vision, control feel, pilots' reaction to the relatively large nose-up attitude of low aspect swept-wing airplanes and psychological influences associated with new type airplanes also may have considerable influence on pilots' opinions regarding the landing approach characteristics of such airplanes. The theoretical investigation, however, was made without regard to any such possible psychological influences.

Motions in response to longitudinal control movements were computed, on an analog computer, for two swept-wing airplanes having no horizontal tails and for a conventional airplane that was known to have good height control in landing approaches.

SYMBOLS AND COEFFICIENTS

The longitudinal motions presented herein were calculated about the stability axes.

S	=	wing area, sq.ft.
c	=	mean aerodynamic chord, ft.
W	=	weight of airplane
m	=	mass of airplane, slugs (W/g)
k_y	=	radius of gyration about Y-body axis, ft.
ρ	=	air density, slugs per cu.ft.
μ	=	airplane relative-density coefficient, $m/\rho Sc$
V	=	velocity, ft. per sec.
g	=	acceleration due to gravity, 32.2 ft./sec.^{2}
L	=	lift, lbs.
D	=	drag, lbs.
M	=	pitching moment, ft.lbs.
C_L	=	lift coefficient, $L/(1/2)\rho V^2S$
C_D	=	drag coefficient, $D/(1/2)\rho V^2S$
C_m	=	pitching-moment coefficient, $M/(1/2)\rho V^2Sc$

Presented at the Aerodynamics Session, Twenty-First Annual Meeting, IAS, New York, January 26–29, 1953.

* Aeronautical Research Scientist.

TABLE 1

Mass, Dimensional, and Aerodynamic Parameters (Aerodynamic Parameters for Airplanes B and C Generally Given Relative to Those for Airplane A)

Airplane	$\frac{W}{S}$	$\frac{k_y}{\bar{c}}$	$\frac{C_{m_q}}{(C_{m_q})_A}$	$\frac{C_{m_{\delta_e}}}{(C_{m_{\delta_e}})_A}$	$\frac{C_{L_{\delta_e}}}{(C_{L_{\delta_e}})_A}$	$\frac{C_{D_{\delta_e}}}{(C_{D_{\delta_e}})_A}$	$\frac{C_{m_\alpha}}{(C_{m_\alpha})_A}$	$\frac{C_{L_\alpha}}{(C_{L_\alpha})_A}$	$\frac{C_{L_{trim}}}{C_{L_{max}}}$
A	49.1	0.99	...	...	...	...	...	...	0.63
B	42.7	0.57	0.12	0.29	1.71	1.61	0.65	0.62	0.79
C	26.1	0.46	0.04	0.18	1.50	1.70	0.39	0.57	0.65

C_{L_0} = lift coefficient at $\alpha = 0°$ with an elevator deflection that would be required to trim at landing approach speed

C_{m_0} = pitching-moment coefficient at $\alpha = 0°$ with an elevator deflection that would be required to trim at landing approach speed

T = thrust, lbs.

Z = height, ft. $\left(\int_0^t V \sin\gamma \, dt\right)$

α = angle of attack, deg. ($\alpha = \theta - \gamma$)

γ = flight-path angle, deg.

θ = angle of pitch, deg.

δ_e = elevator deflection, deg.

ΔZ = increment of height from trimmed condition

$\Delta\alpha$ = increment of angle of attack from trimmed condition

$\Delta\gamma$ = increment of flight-path angle from trimmed condition

$\Delta\theta$ = increment of angle of pitch from trimmed condition

ΔV = increment of velocity from trimmed condition

$\Delta\delta_e$ = increment of elevator deflection from trimmed condition

$\dot{\theta}$ or q = pitching angular velocity, rad. per sec.

$\dot{V}$ = rate of change of velocity V with time

$C_{L_{\delta_e}} = \partial C_L/\partial\delta_e$, per deg.

$C_{D_{\delta_e}} = \partial C_D/\partial\delta_e$, per deg.

$C_{m_{\delta_e}} = \partial C_m/\partial\delta_e$, per deg.

$C_{L_\alpha} = \partial C_L/\partial\alpha$, per deg.

$C_{D_{(\alpha)}}$ = coefficient of drag as a nonlinear function of α

$C_{m_\alpha} = \partial C_m/\partial\alpha$, per deg.

$C_{m_q} = \partial C_m/\partial(q\bar{c}/2V)$

AIRPLANES INVESTIGATED

The airplanes for which motion calculations were made are referred to herein as airplanes A, B, and C. Airplane A is a conventional straight-wing airplane that has good response characteristics in the landing approach. Airplane B is a swept-wing airplane having no horizontal tail, and airplane C, which also has no horizontal tail, is generally similar to airplane B but has a lower aspect ratio and different mass characteristics. Pertinent aerodynamic, mass, and dimensional information on airplanes A, B, and C is given in Table 1.

PROCEDURE

For this investigation, the three longitudinal equations of motion were used in the analog computer:

$$\dot{V} = -\frac{V^2}{2\mu\bar{c}}(C_{D_{(\alpha)}} + C_{D_{\delta_e}}\delta_e) - g\sin\gamma + \frac{T}{m}\cos\alpha \quad (1a)$$

$$\dot{\gamma} = \frac{V}{2\mu\bar{c}}(C_{L_\alpha} + C_{L0} + C_{L_{\delta_e}}\delta_e) - g\cos\gamma + \frac{T}{m}\sin\alpha \quad (1b)$$

$$\ddot{\theta} = \frac{V^2}{2\mu k_y{}^2}(C_{m_\alpha}\alpha + C_{m0} + C_{m_{\delta_e}}\delta_e) + \frac{V}{4\mu k_y{}^2}C_{m_q}\bar{c}\dot{\theta} \quad (1c)$$

The equations were not linearized in that the thrust and gravitational forces were introduced in their nonlinear form. The lift, drag, and pitching-moment coefficients were introduced as functions of angle of attack and of elevator deflection. All of the airplanes were trimmed in level flight at 110 knots (185.8 ft. per sec.) at the beginning of the motions, and the slopes of the lift and pitching-moment coefficients with angle of attack were taken in the vicinity of the angle of attack for trimmed flight at 110 knots. The drag coefficient [$C_{D(\alpha)}$] was introduced as a nonlinear function of angle of attack. The lift, drag, and pitching-moment coefficients, as functions of elevator deflection, were introduced as linear functions of δ_e; the slopes were taken as mean values between the elevator deflection for trim and the maximum up-elevator deflection. The elevator deflections and therefore the values of $C_{L_{\delta_e}}\delta_e$, $C_{D_{\delta_e}}\delta_e$, and $C_{m_{\delta_e}}\delta_e$ were introduced as step functions. The thrust and the airplane damping derivative, C_{m_q}, were held constant for any given calculation.

In order to evaluate the response to longitudinal control for the three airplanes, the following procedure was used: As previously mentioned, the three airplanes were initially trimmed in steady level flight at a landing approach speed of 110 knots. The initial trim values are given in Table 2. A disturbance from this condition was initiated by deflecting the elevator down and holding it down for a short time (2 sec.), after which an attempt to stop the ensuing descent was made by deflecting the elevator full-up. The amount of down-elevator deflection used initially for airplane A resulted in a loss of altitude which might be desired for a final height correction during an approach, approximately 10 ft. For comparison purposes, it was desired to make the initial pushover flight paths the same for airplanes B and C as for airplane A, so that when the final up-elevator deflection was used in an attempt to stop the descent all three airplanes would be in approximately the same flight condition. This was attempted by de-

flecting the elevators down on airplanes B and C by an amount that would result in approximately the same initial rate of change of normal acceleration for all three airplanes. The amount that the elevator was deflected down from the initial trim deflection for all three airplanes is given in Table 3. As previously mentioned, the elevator on each airplane was deflected full-up after the initial pushover motion. The maximum full-up elevator was used so that it would give the maximum acceleration in pitch possible on each airplane, and any other correction by use of up-elevator would be proportional to that given by full-up elevator. It is realized that the use of full-up elevator and of step input functions does not simulate the actual conditions used by a pilot, but it was felt that the method does reveal any difference in response due to inherent differences in stability and control characteristics which exist among airplanes A, B, and C. In order that the airplanes would not trim at an angle of attack beyond maximum lift, the elevator was returned after a given time from full-up to a deflection that would trim the airplanes at maximum lift.

Simplified Analytical Considerations

The calculations performed in this paper, as previously noted, are based on the three longitudinal equations of motion and are accurate to the extent of the completeness and accuracy of the aerodynamic data used. Short-period oscillation in longitudinal motions may be studied, within required accuracy, by consideration of only two degrees of freedom, assuming the velocity to be constant. It is possible, therefore, that factors pertinent to short-time responses to longitudinal control movement also may be obtained from consideration of only two degrees of freedom. These degrees of freedom are expressed in the equations of the pitching and normal accelerations given previously as Eqs. (1b) and (1c). It can be shown that changes in the gravitational and thrust forces in Eq. (1b) are of only secondary importance, and, if neglected, the equations when simplified to changes from the initial trimmed conditions may be solved simultaneously for the flight-path angle γ, a pertinent parameter to changes in height, when the change in height may be expressed as

$$\Delta Z = \int^t V \sin \gamma \, dt \tag{2}$$

The solution for γ gives the following result:

$$\gamma = \frac{VC_{L_{\delta_e}}}{2\mu\bar{c}}\left(\frac{a}{b} + \frac{\lambda_2^2 e^{\lambda_1 t} - \lambda_1^2 e^{\lambda_2 t}}{b\sqrt{a^2 - 4b}}\right)\Delta\delta_e + \left(\frac{VC_{L_{\delta_e}}}{2\mu\bar{c}}\right)\left(\frac{V^2 C_{m_\alpha}}{2\mu K_y^2}\right)\left[\frac{\lambda_2^2 e^{\lambda_1 t} - \lambda_1^2 e^{\lambda_2 t}}{b^2\sqrt{a^2 - 4b}} - \left(\frac{t}{b} - \frac{a}{b^2}\right)\right]\Delta\delta_e - \left(\frac{VC_{L_\alpha}}{2\mu\bar{c}}\right)\left(\frac{V^2 C_{m_{\delta_e}}}{2\mu k_y^2}\right)\times\left[\frac{\lambda_2^2 e^{\lambda_1 t} - \lambda_1^2 e^{\lambda_2 t}}{b^2\sqrt{a^2 - 4b}} - \left(\frac{t}{b} - \frac{a}{b^2}\right)\right]\Delta\delta_e \tag{3}$$

where

$$a = \left(\frac{VC_{L_\alpha}}{2\mu\bar{c}} - \frac{VC_{m_q}\bar{c}}{4\mu k_y^2}\right)$$

TABLE 2

Initial Trim Values for Steady Level Flight at 185.8 Ft. per Sec. (110 Knots)

Airplane	α, Deg.	γ, Deg.	θ, Deg.	T, lbs.	δ_e, Deg.
A	4.40	0	4.40	2,642	5.0 (1.5° up stabilizer)
B	21.85	0	21.85	4,770	−20.0
C	15.97	0	15.97	2,781	−1.5 (30° up trimmer)

TABLE 3

Elevator Deflections Used and Comparison of Resulting Parameters Affecting Longitudinal Motion (Parameters for Airplanes B and C Given Relative to Those for Airplane A)

Airplane	Push-Down $\Delta\delta_e$, Deg. (From Trim Elevator Deflection)	Pull-Up $\Delta\delta_e$, Deg. (From Push-Down Elevator Deflection)	$\Delta\delta_e$ $(\Delta\delta_e)_A$ (for Pull-Up)	(a) $\frac{V^2 C_{m_{\delta_e}}\,\Delta\delta_e}{2\mu k_y^2}\,\frac{VC_{L_\alpha}}{2\mu\bar{c}}$ / $\left(\frac{V^2 C_{m_{\delta_e}}\,\Delta\delta_e}{2\mu k_y^2}\,\frac{VC_{L_\alpha}}{2\mu\bar{c}}\right)_A$	(b) $\frac{VC_{L_{\delta_e}}\,\Delta\delta_e}{2\mu\bar{c}}$ / $\left(\frac{VC_{L_{\delta_e}}\,\Delta\delta_e}{2\mu\bar{c}_A}\right)_A$
			Original Elevator Deflection		
A	1.86	−24.86	...	...	...
B	(c) 4.33	−14.33	0.58	0.25	1.14
C	(c) 2.45	−20.95	0.84	0.64	2.37
			Increased Up-Elevator Deflection		
B	(c) 4.33	(c) −57.81	2.33	1.00	...
C	(c) 2.45	(c) −32.71	1.32	1.00	...

(a) Parameter indicates total available elevator effectiveness in causing a rate of change of flight-path angle (neglecting change in lift due to elevator deflection).

(b) Parameter indicates change in lift due to elevator deflection.

(c) These $\Delta\delta_e$ values resulted in the initial increment of $\ddot{\gamma}$ being approximately the same as for airplane A (neglecting change in lift due to elevator deflection).

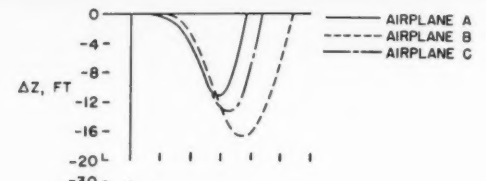

(a) ΔZ and $\Delta\delta_e$

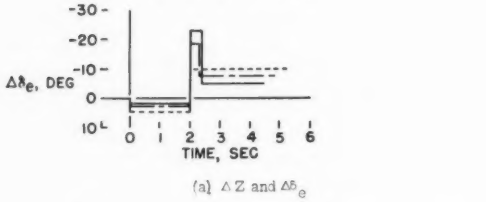

(b) $\Delta\alpha$ and $\Delta\theta$

Figure 1.- Comparison of short time responses of airplanes A, B, and C with available up-elevator deflection.

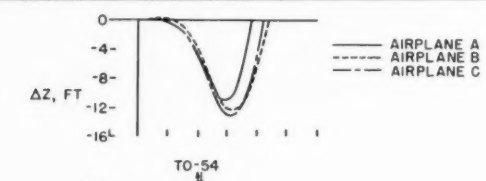

(a) ΔZ and $\Delta\delta_e$

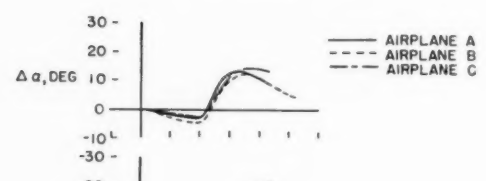

(b) $\Delta\alpha$ and $\Delta\theta$

Figure 2.- Comparison of short time responses of airplanes A, B, and C. Airplanes B and C with increased up-elevator deflection.

$$b = -\left(\frac{V^2 C_{L_\alpha} C_{m_q}}{8\mu^2 k_y^2} + \frac{V^2 C_{m_\alpha}}{2\mu k_y^2}\right)$$

$$\lambda_1 = -(a/2) - (\sqrt{a^2 - 4b}/2)$$

$$\lambda_2 = -(a/2) + (\sqrt{a^2 - 4b}/2)$$

If the velocity were constant as assumed in this simplified solution, γ as expressed in Eq. (3) is of prime importance to an understanding of factors pertinent to the short-time longitudinal responses of airplanes. If the lift due to elevator deflection, $C_{L_{\delta_e}}$, were zero, then γ, all its derivatives, and any height changes would be proportional to the factor

$$(VC_{L_\alpha}/2\mu\bar{c})\ (V^2 C_{m_{\delta_e}}/2\mu k_y^2)\Delta\delta_e$$

The down-elevator deflections required for airplanes B and C to obtain the same rate of change of normal acceleration in the initial pushover, previously discussed, were based on making this parameter the same as for airplane A.

Another factor that may have important influence on the motion is the change in lift due to elevator deflection ($C_{L_{\delta_e}}$), where an up-elevator deflection causes an immediate loss in lift proportional to the deflection. It should be noted that for a short coupled airplane such as airplanes B and C, which have no horizontal tails, a much larger change in lift is required in order to get a given pitching moment than is required on a conventional airplane with a horizontal tail.

Results and Discussion

Comparison of Airplanes A, B, and C

A fundamental comparison of the results of all three airplanes is given in Fig. 1. Here the maximum available full-up elevator was used on each airplane to stop the descent following the initial pushover. In Fig. 1a is shown the change in height obtained and the elevator control movements used. The initial flight paths in the pushover were about the same as was desired, although airplanes B and C required about two and one-third and one and one-third times as much increment in down-elevator, respectively, as did airplane A to accomplish this (see Table 3). Corrective action by the use of full-available up-elevator was attempted after the elevator was held down for 2 sec. The amount of the increment of up-elevator available on airplane B was a little more than one-half of that of airplane A, whereas the amount of the increment of up-elevator available on airplane C was about three-fourths of that of airplane A. After a short period of time, the elevators of airplanes A and C were moved down so as not to trim above maximum lift, whereas full-up elevator on airplane B trimmed the airplane at about maximum lift.

All three airplanes responded to the up-elevator deflection in that the descent was stopped and the lost height was regained. It took approximately twice as much time, however, for airplane B to stop its descent or to regain its lost height after up-elevator movement as it did for airplane A. In addition, airplane B lost about 50 per cent more height and traveled some 180 ft. further before the descent was stopped than did airplane A. It is possible that a pilot may become aware of such differences when making height correction in short-time periods. Further, presuming the airplanes were retrimmed at the bottom of the descents, the 6-ft. increment in height between them could represent as sent as much as, say, 100 ft. in the touchdown point; such an increment might be of concern. Airplane C responded more quickly than did airplane B but not so quickly as airplane A.

Fig. 1b shows the variations of angle of attack and angle of pitch for the motions just discussed. Of primary importance in changing height is, of course, the lift and how fast it can be changed. The angle of attack of airplane A changes at a rate about twice as fast as does airplane B. Because of the difference in wing loading and C_{L_α}, airplane A changed its normal acceleration about three times as fast as did airplane B, and it is this acceleration that the pilot feels. What the pilot does is to pitch the airplane, and what he sees is the motion of the horizon. The rate of change of the pitch angle for airplane A is also about twice as great as that of airplane B. These differences account for the differences in response as measured by the height changes previously discussed. Here, also, the results for airplane C fall between those for the other two airplanes. Although not shown here, because the values of angle of pitch presented are increments from the trimmed values, the initial trimmed pitch or attitude angle of airplane A was about 4°, whereas that for airplane B was well over 20° and that for airplane C was about 16°. Such differences in attitudes may influence a pilot's feelings with regard to an airplane's characteristics.

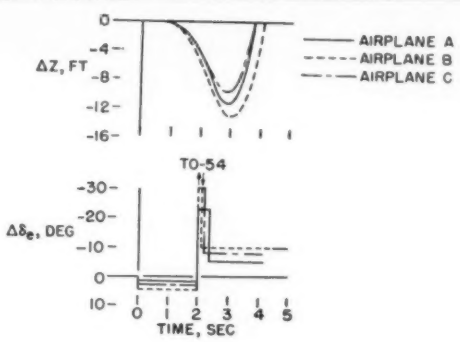

(a) ΔZ and $\Delta\delta_e$

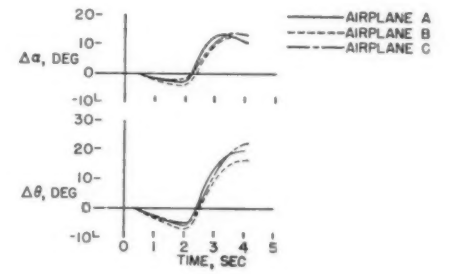

(b) $\Delta\alpha$ and $\Delta\theta$

Figure 3.- Comparison of short time responses of airplanes A, B, and C. Airplanes B and C with increased up-elevator deflections and the change in lift due to elevator deflection eliminated.

Effect of Increasing Total Elevator Effectiveness

In order to demonstrate reasons for these differences in height response, the total elevator effectiveness of airplanes B and C was increased to approximately that of airplane A by making the total elevator effectiveness parameter,

$$(C_{L_\alpha}/2\mu\bar{c})\ (C_{m_{\delta_e}}/2\mu k_y^2)\ \Delta\delta_e$$

previously discussed, the same for all airplanes. The total elevator effectiveness as used herein refers to the effectiveness of the elevator in causing an initial rate of change of flight-path angle, neglecting the effect of the change in lift due to elevator deflection. Making this parameter the same is done arbitrarily by assuming the factor to be increased by increasing the full-up-elevator deflections, based on the same slopes of the pitching moment with elevator deflection previously used. The maximum full-up-elevator deflection of airplane B was increased from −30° to about −74°, whereas for airplane C the deflection was increased from −20° to about −30°. It was realized that the increase in elevator deflection on airplane B was excessively large and beyond the linear range of $C_{m_{\delta_e}}$

The results of calculations with the total elevator effectiveness, the same for all three airplanes, are shown on Fig. 2. Here there is a great deal of improvement in the response of airplane B, Fig. 2a, the time for the airplane to respond to up-elevator deflection is now only slightly larger than that of airplane A, and the increment in height between them has been reduced to only about 2 ft. There was only slight improvement in airplane C, but, of course, less improvement and less correction was required.

The variations of the angle of attack and angle of pitch are shown in Fig. 2b. Here the rate of change of angle of attack, as indicated by its slope with time, is more nearly the same for airplane B as for airplane A than before. Similarly, airplane B pitched much more rapidly than before when only its normal full-up elevator was used. The changes on airplane C are only slight in that the required change in elevator deflection was much less extreme.

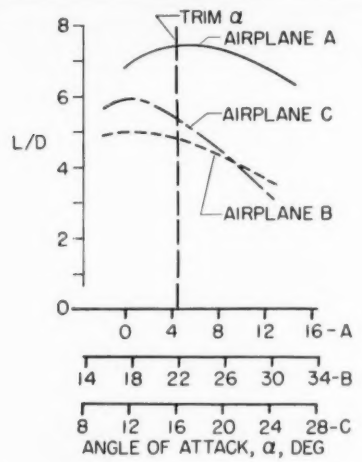

Figure 4.- Variations of lift-to-drag ratio with angle of attack for airplanes A, B, and C.

Effect of Eliminating the Lift Due to Elevator Deflection

The lift due to elevator deflection is a force in opposition to the desired force. This force is larger on short-coupled airplanes, such as airplanes B and C, than on conventional airplanes, as was previously discussed. It was reasoned that eliminating this factor may show some improvement on the height responses of airplanes B and C. The results of calculations with this force neglected and with the total elevator effectiveness increased in amounts as previously discussed are shown in Fig. 3.

The height changes and control deflections are shown on Fig. 3a. The response of airplanes B and C now compare favorably with those for airplane A. The improvement due to neglecting the lift due to elevator deflection was greatest for airplane C.

The time to respond to the up-elevator movement—that is, the time to stop the descent—are all about the same, although the actual changes in height are somewhat different.

The variations in the angle of attack and pitch angle with time for airplanes B and C, Fig. 3b, are also similar to those of airplane A, accounting at least in part for the similarity in height response just discussed. Thus, the differences in short-time responses to elevator control for two widely different types of airplanes (airplane A representing conventional straight-wing types and airplanes B and C representing swept-wing types having no horizontal tails) are primarily the results of differences in total elevator effectiveness and the increment of lift due to elevator deflection.

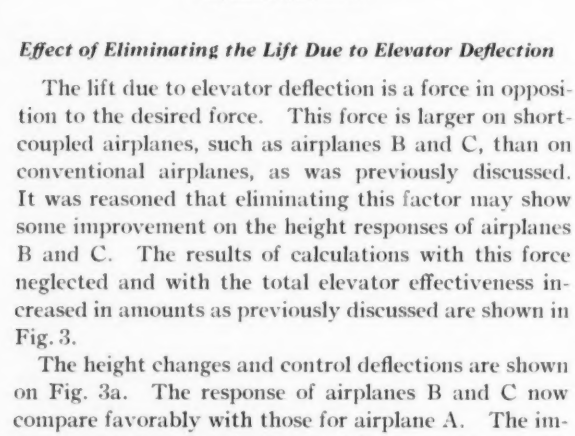

Figure 5.- Comparison of the change in height for long time periods of airplanes A, B, and C. Airplanes B and C with increased up-elevator deflections and the change in lift due to elevator deflection eliminated.

Effects of Other Parameters

It has been reasoned that other parameters than those previously discussed also may influence the short-time responses of the airplanes. It was felt that the great differences in the L/D ratios of airplane A and airplanes B and C could affect the results in that airplanes B and C would tend to trim in much steeper glide path angles following the up-elevator movement (see reference 1). A comparison of the L/D ratios of airplanes A, B, and C is shown on Fig. 4. Airplanes B and C have much smaller L/D ratios for the landing conditions, but of even more importance the variations of L/D with angle of attack from the trimmed angle of attack are much larger than for airplane A. The results previously discussed, however, indicate that these differences in L/D ratio do not influence the short-time responses, primarily because there was no appreciable variation in the velocity during the short times. The effect of the increased drag causing the larger variations in L/D on airplanes B and C is to reduce the velocity more rapidly on airplanes B and C than on airplane A. This is primarily a long-period effect, however, and may be expected to affect only the changes in height after long periods. Fig. 5 shows the relatively long time variations of height for airplanes A, B, and C with the airplanes in the same conditions previously shown in Fig. 3. The total elevator effectiveness of airplanes B and C was increased, and the lift due to elevator deflection was eliminated for airplanes B and C for the calculations of Fig. 5, as it was in Fig. 3. The change in height for the first 4 sec. in Fig. 5 is the same as that shown on Fig. 3. From this time until the end of the motion shown, there is developed a great difference in the height for the three airplanes, airplane A gaining the most altitude. All airplanes appear to be in a long-period or phugoid motion and, at the end of the motion shown, are descending because of the increased drag at the angle of attack of maximum lift. Airplane C, having the least L/D ratio, is descending most rapidly.

Other parameters that may be considered as important to the motion are the stability derivatives C_{m_α} and C_{m_q}. The effects of increasing the value of the damping derivative, C_{m_q}, on airplane B was studied, but the results are not shown here. Increasing the

TABLE 4

Comparison of Parameters Affecting Longitudinal Motion (Parameters for Airplanes B and C Given Relative to Those for Airplane A)

Airplanes	$\frac{1}{2\mu k_y^2}\left(\frac{1}{2\mu k_y^2}\right)_A$ (a)	$\frac{C_{m_{\delta_e}}}{(C_{m_{\delta_e}})_A}$ (a)	$\frac{V^2C_{m_{\delta_e}}}{2\mu k_y^2}\left(\frac{V^2C_{m_{\delta_e}}}{2\mu k_y^2}\right)_A$ (a)	$\frac{1}{2\mu\bar{c}}\left(\frac{1}{2\mu\bar{c}}\right)_A$ (a)	$\frac{C_{L_{\delta_T}}}{(C_{L_{\delta_T}})_A}$ (b)	$\frac{VC_{L_{\delta_T}}}{2\mu\bar{c}}\left(\frac{VC_{L_{\delta_T}}}{2\mu\bar{c}}\right)_A$ (b)	$\frac{C_{L_\alpha}}{(C_{L_\alpha})_A}$ (c)	$\frac{VC_{L_\alpha}}{2\mu\bar{c}}\left(\frac{VC_{L_\alpha}}{2\mu\bar{c}}\right)_A$ (c)	$\frac{V^2C_{m_{\delta_T}}}{2\mu k_y^2}\left(\frac{V^2C_{m_{\delta_e}}}{2\mu k_y^2}\right)_A$ (c)	$\frac{VC_{L_\alpha}}{2\mu\bar{c}}\left(\frac{VC_{L_\alpha}}{2\mu\bar{c}}\right)_A$ (c)
B	2.06	0.29	0.60	1.15	1.71	1.97	0.62	0.71	0.43	
C	3.94	0.18	0.71	1.88	1.50	2.82	0.57	1.07	0.76	

(a) Parameter indicates elevator effectiveness in causing a rate of change of pitch angle.
(b) Parameter indicates change in lift due to elevator deflection.
(c) Parameter indicates elevator effectiveness in causing a rate of change of flight-path angle (neglecting change in lift due to elevator deflection).

value of C_{m_q} did not appreciably influence the time at which the descent, following the pushover and then pull-up, was checked. The primary effect was to reduce the rate of change of the pitch angle and angle of attack, and thus in the pushover and subsequent pull-up the height changes were reduced, with increasing C_{m_q}.

No specific calculations were made to determine the effect of changes in the static stability derivative, C_{m_α}. From the simplified analytical considerations, previously discussed, however, the parameter in which C_{m_α} is dominate (assuming the lift due to elevator deflection, $C_{L_{\delta_e}} = 0$) is

$$[(V^2C_{L_\alpha}C_{m_q}/8\mu^2k_y^2) + (V^2C_{m_\alpha}/2\mu k_y^2)]$$

The values of these parameters for airplanes A, B, and C are nearly the same. The motions for all three airplanes were also nearly the same when the total elevator effectiveness of airplanes B and C was increased to that of airplane A and the lift due to control deflection, $C_{L_{\delta_e}}$, was eliminated. It may be reasoned, however, that reducing the static stability, C_{m_α}, would allow an airplane to pitch faster, to increase its angle of attack faster, and thus to respond more quickly to elevator deflection. Increasing C_{m_α} would, of course, have the opposite effect.

General Discussion

Examination of some of the parameters involved in longitudinal motions may give an understanding of the results just shown. Some of these parameters for airplanes B and C are compared relatively to those of airplane A in Table 4. From the simplified analytical consideration, it is indicated that these parameters are indicative, comparatively, of the motion to be expected at the time of control movement. The parameter $V^2C_{m_{\delta_e}}/2\mu k_y^2$ indicates the effectiveness of the elevator on the rate of changing the angle of the pitch. Airplanes B and C were less effective than airplane A. The parameter $VC_{L_\alpha}/2\mu\bar{c}$ indicates the ability, when pitched, to change lift and therefore the normal acceleration and flight path. This parameter was smallest for airplane B and had about the same value for airplanes A and C. The product of these parameters and the available elevator deflection (called the total elevator effectiveness) for airplanes B and C was about one-quarter and two-thirds, respectively, of that of airplane A. This indicates why the impractically large increase in up-elevator deflection, previously referred to, was required for airplane B.

The parameter $VC_{L_{\delta_e}}\Delta\delta_e/2\mu\bar{c}$ (Table 3), of course, indicates the change in normal acceleration due to control deflection. Considering the up-elevator deflections available, this parameter is about the same for airplanes A and B. The value for airplane C was about two and one-third times as great as for either of the other airplanes.

In general, the time it takes an airplane of a specific configuration to respond in height, for a given elevator deflection, depends on the rate at which it can change its flight-path angle. It has been shown that, for a short-period motion, the rate of changing the flight-path angle depends mainly on the magnitude of the weight, moment of inertia (I_y), $C_{m_{\delta_e}}$, C_{L_α}, $C_{L_{\delta_e}}$, and $\Delta\delta_e$. An increase in weight, I_y, or $C_{L_{\delta_e}}$, or a decrease in C_{L_α}, $C_{m_{\delta_e}}$, or $\Delta\delta_e$ will tend to decrease the airplane's abilitv to quickly respond in height.

CONCLUDING REMARKS

The investigation reported in this paper was undertaken to see whether there were inherent differences in the response of the flight-path angle to control movements between swept-wing airplanes having no horizontal tail and using trailing-edge flaps for longitudinal control and conventional airplanes that are known to have satisfactory response characteristics. Particular emphasis is placed on the final few seconds of the landing approach.

This study shows that the only difference in the short-time response of the flight path between the two types of airplanes is in a time lag in the flight-path angle response of the swept-wing airplanes. This time lag was found to result from two factors: first, a relatively small value of the parameter

$$(VC_{L_\alpha}/2\mu c)\ (V^2C_{m_{\delta_e}}/2\mu k_y^2)\Delta\delta_e$$

which is a measure of the effectiveness of the control in

changing the flight-path angle, and, second, a relatively large value of the parameter

$$(VC_{L_{\delta_e}}/2\mu\bar{c})\Delta\delta_e$$

which is a measure of the amount of undesirable change in lift accompanying the control deflection required to change the angle of attack. It had been suspected that the relatively large change in drag with angle of attack of low aspect ratio swept-wing airplanes having no horizontal tails would be an important factor in the flight-path angle response but this was found not to be the case for the short time intervals under consideration.

The importance of the differences found in the response characteristics between the two types of airplanes studied can only be evaluated by flight experience. Other factors such as range of vision, control feel, the pilot's reaction to the relatively large nose-up attitudes of the low aspect ratio swept-wing airplanes, and psychological influences associated with new type airplanes may be of equal or greater importance.

Reference

[1] McKinney, Marion O., and Drake, Hubert M., *Flight Characteristics at Low Speed of Delta-Wing Models*, NACA RM L7K07.

Fourth Plasticity Symposium

Brown University, Providence, R.I. **September 1–3, 1953**

This symposium will cover three principal topics: (1) stress-strain relations (perfectly plastic, workhardening, viscoelastic, and viscoplastic materials); (2) distribution of stress and strain in bodies exhibiting inelastic properties (static and dynamic problems, infinitesimal and finite deformations); and (3) structural analysis and design in the inelastic range (limit analysis, static and dynamic loading, shakedown, inelastic buckling). Papers will be presented by American and foreign experts.

Certain sessions will be sponsored by Brown University in cooperation with the American Society of Civil Engineers' Engineering Mechanics Division. The remaining sessions will be sponsored jointly by Brown University and the Office of Naval Research.

For further information, please contact: Prof. Harry J. Weiss, Graduate Division of Applied Mathematics, Brown University, Providence 12, R.I.

Supersonic Flow over Conical Bodies Without Axial Symmetry*

ANTONIO FERRI,† NATHAN NESS,‡ AND THADDEUS T. KAPLITA**

Polytechnic Institute of Brooklyn

SUMMARY

Conical flow around cones without axial symmetry is analyzed by the superposition of linear conical solutions to a nonlinear axially symmetric conical flow. The aerodynamic properties of cones with elliptical, drop-shape, and triangular cross sections are determined from these linearized solutions. It is shown that some gain on the shock drag can be obtained by using bodies having cross sections different from circular.

INTRODUCTION

THE PRACTICAL DESIGN of any fuselage for airplanes or missiles is obtained normally from an engineering compromise of aerodynamic, structural, and installation requirements that are peculiar to each particular design. One of the parameters obtained from such a compromise is the shape of the cross section of the fuselage. Since the aerodynamic properties—e.g. lift and drag—are affected by the cross-section contour, methods that permit the analysis of a supersonic flow as a function of this parameter are of practical interest.

The pressure distribution around slender bodies without axial symmetry can be obtained by the linearized characteristic method discussed in reference 1. However, this analysis can be performed only when the flow field near the apex of the slender body is known. This flow field, which is of the conical type, is analyzed by the method outlined in reference 1. The present paper is an extension of this method, with special emphasis placed on its practical application to conical bodies without axial symmetry.

This method consists of the superposition of linearized flow solutions upon the solution of the nonlinear flow around a circular cone. Because the same linearized flow solutions can be used regardless of the difference in cross-section shape between the circular cone and any of the other bodies considered, this procedure is especially effective for the analysis of the effect of cross section on aerodynamic properties. The equations that define the velocity components of the linearized flow fields are solved by a step-by-step numerical procedure (i.e., the hodograph method).

The present procedure permits the determination of the shock wave created by nonaxially symmetric bodies and, hence, gives solutions also at high Mach Numbers, where methods based on linearized theory (superposition of linearized solutions on a uniform flow field) cannot be used because in the latter case the Mach cone at high Mach Numbers falls inside the body.

In this paper, the flow fields around conical bodies of elliptical, drop-shape, and triangular cross section for a wide range of Mach Numbers are considered.

LIST OF SYMBOLS

r, ψ, ϑ	= spherical coordinates
v_r, v_n, w	= velocity components in spherical coordinates
a	= speed of sound
S	= entropy
R	= gas constant
γ	= ratio of specific heats
V_1	= undisturbed velocity, referred to limiting velocity
ρ_1	= free-stream density
β	= defined by Eq. (8)
ψ_{ns}, ψ_{ms}	= coefficients of the Fourier series defining nonaxially symmetric shock surface
ψ_{nb}, ψ_{mb}	= coefficients of the Fourier series defining nonaxially symmetric conical body surface
H	= radius of hodograph diagram
M_1	= free-stream Mach Number
c_p	= pressure coefficient
c_v	= specific heat at constant volume
V	= local resultant velocity, referred to limiting velocity
a/b	= ratio of semidiameters of ellipse
h	= distance along body axis from apex
πab	= cross-sectional area of ellipse
α	= angle of attack
c_L, c_D, c_t	= lift, drag, and horizontal force coefficients referred to cross-sectional area normal to body axis
c_N	= normal force coefficient referred to cross-sectional area in the meridian plane perpendicular to normal force component N
N	= normal force component
H	= horizontal force component
L/D	= lift-drag ratio
$dc_L/d\alpha$	= lift curve slope
$\varkappa$	= $\tan^{-1}(a/h)$
Subscripts	
a	= properties of the basic axially symmetric conical flow
n, m	= properties of the superposed linearized flow fields

Received February 27, 1953.

* This research was conducted under the sponsorship of the Office of Scientific Research, Air Research and Development Command under contract AF 18(600)-186. The authors hereby express their thanks to Prof. Fred Pohle for his valuable suggestions.

† Professor of Aerodynamics.

‡ Research Group Leader.

** Research Assistant

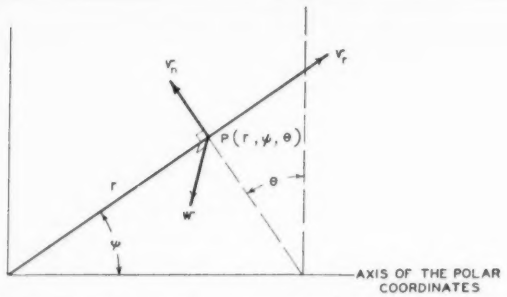

FIG. 1. The polar coordinate system and velocity components.

s = properties at the shock wave
b = properties at the body surface

DESCRIPTION OF THE METHOD

Consider a conical flow field. Assume a spherical coordinate system r, ψ, ϑ whose center is at the apex of the conical flow. Denote by v_r the velocity component along the radius r; v_n, the component normal to the radius in the meridian plane ϑ = constant; and w, the component normal to the meridian plane (Fig. 1). By combining the laws of conservation of mass, momentum, and energy, the following equations can be obtained for a nonviscous perfect gas without heat conduction:[2]

$$v_r\left(2 - \frac{v_n^2 + w^2}{a^2}\right) + v_n \cot\psi + \frac{\partial v_n}{\partial\psi}\left(1 - \frac{v_n^2}{a^2}\right) + \frac{\partial w}{\sin\psi\,\partial\vartheta}\left(1 - \frac{w^2}{a^2}\right) - \frac{wv_n}{a^2}\left(\frac{\partial v_n}{\sin\psi\,\partial\vartheta} + \frac{\partial w}{\partial\psi}\right) = 0 \quad (1)$$

$$\frac{a^2}{\gamma R}\frac{\partial S}{\partial\vartheta} = v_n \sin\psi \frac{\partial w}{\partial\psi} - v_r\frac{\partial v_r}{\partial\vartheta} - v_n\frac{\partial v_n}{\partial\vartheta} + wv_r \sin\psi + wv_n\cos\psi \quad (2)$$

$$\frac{a^2}{\gamma R}\frac{\partial S}{\partial\psi} = -v_r\frac{\partial v_r}{\partial\psi} - w\frac{\partial w}{\partial\psi} + \frac{w}{\sin\psi}\frac{\partial v_n}{\partial\vartheta} + v_rv_n - w^2\cot\psi \quad (3)$$

where a is the speed of sound, S is the entropy, R is the gas constant, and γ is the ratio of specific heats (assumed constant).

A conical body traveling at supersonic speed creates a shock front that is conical with apex at the apex of the conical body. This shock front separates the upstream undisturbed air from the downstream nonuniform flow field and may be expressed in spherical coordinates by

$$\psi_s = \psi_{as} + \sum_{n=0}^{\infty}\psi_{ns}\cos n\vartheta + \sum_{m=1}^{\infty}\psi_{ms}\sin m\vartheta \quad (4)$$

In the classical linearized theory the shock surface is coincident with the Mach cone and has a circular cross section; therefore, in the classical theory, the terms ψ_{ns} and ψ_{ms} are considered equal to zero, while the angle ψ_{as} is equal to the Mach angle. In this analysis the terms ψ_{ns} and ψ_{ms} are considered small but different from zero, and only first-order terms of ψ_{ns} and ψ_{ms} are retained in the differential equations and in the boundary condition. The term ψ_{as} is assumed different from the free-stream Mach angle.

From physical considerations across the shock, the velocity components immediately downstream of the shock front (i.e., at $\psi = \psi_s$) are obtained.[1]

$$(v_r)_{\psi_s} = V_1\cos\psi_s \quad (5)$$

$$(v_n)_{\psi_s} = -\frac{\gamma-1}{\gamma+1}\left(\frac{1 - V_1^2\cos^2\psi_s - V_1^2\sin^2\psi_s\sin^2\beta}{V_1\sin\psi_s}\right) - V_1\sin\psi_s\sin^2\beta \quad (6)$$

$$(w)_{\psi_s} = -V_1\sin\psi_s\sin\beta\cos\beta + \frac{\gamma-1}{\gamma+1}(1 - V_1^2\cos^2\psi_s - V_1^2\sin^2\psi_s\sin^2\beta)\times\frac{\tan\beta}{V_1\sin\psi_s} \quad (7)$$

where all the velocity components are nondimensionalized with respect to the limiting velocity, V_1 is the free-stream velocity (also referred to the limiting velocity), and β is defined by

$$\tan\beta = \partial\psi_s/\sin\psi_s\partial\vartheta \quad (8)$$

As only first-order terms of ψ_{ns} and ψ_{ms} are being considered, any velocity component behind the shock created by the nonaxially symmetric body (at $\psi = \psi_s$) may be expressed as a function of the same velocity component at the shock created by the axially symmetric body (at $\psi = \psi_{as}$) and of the derivative of the velocity component with respect to ψ multiplied by the difference between ψ_s and ψ_{as}. In this way, velocity components consistent with the shape of the shock [defined by Eq. (4)] and with the shock relations [defined by Eqs. (5) to (7)] are obtained in the form

$$v_r = v_{ra} + \sum_{n=0}^{\infty}\psi_{ns}v_{rn}\cos n\vartheta + \sum_{m=1}^{\infty}\psi_{ms}v_{rm}\sin m\vartheta \quad (9)$$

$$v_n = v_{na} + \sum_{n=0}^{\infty}\psi_{ns}v_{nn}\cos n\vartheta + \sum_{m=1}^{\infty}\psi_{ms}v_{nm}\sin m\vartheta \quad (10)$$

$$w = \sum_{n=1}^{\infty} n\psi_{ns}w_n\sin n\vartheta + \sum_{m=0}^{\infty} m\psi_{ms}w_m\cos m\vartheta \quad (11)$$

The quantities v_{ra}, v_{na}, v_{rn}, v_{rm}, v_{nn}, v_{nm}, w_n, and w_m are functions only of ψ and are independent of ϑ; v_{ra} and v_{na} are the radial and normal velocity components of a conical axially symmetric flow field and may be obtained from reference 3. At the angle $\psi = \psi_{as}$, the velocity components v_{rn}, v_{rm}, v_{nn}, v_{nm}, w_n, and w_m are independent of n and m and are given by the following expressions:

$$(v_{rn})_{\psi_{a_s}} = (v_{rm})_{\psi_{a_s}} = -[V_1\sin\psi + v_{na}]_{\psi_{a_s}} \quad (12)$$

$$(v_{s_n})_{\psi_{a_s}} = (v_{nm})_{\psi_{a_s}} =$$

$$-\left[\frac{\gamma-1}{\gamma+1}\cos\psi\left(2V_1 - \frac{1-V_1^2\cos^2\psi}{V_1\sin^2\psi}\right) + \frac{\partial v_{na}}{\partial\psi}\right]_{\psi_{a_s}} \quad (13)$$

$$(w_n)_{\psi_{a_s}} = (w_m)_{\psi_{a_s}} = V_1 + (v_{na}/\sin\psi)_{\psi_{a_s}} \quad (14)$$

where

$$(v_{ra})_{\psi_{a_s}} = V_1\cos\psi_{a_s} \quad (15)$$

$$(v_{na})_{\psi_{a_s}} = -\frac{\gamma-1}{\gamma+1}\left(\frac{1-V_1^2\cos^2\psi}{V_1\sin\psi}\right)_{\psi_{a_s}} \quad (16)$$

$$\left(\frac{\partial v_{na}}{\partial\psi}\right)_{\psi_{a_s}} = -\left[v_{ra} + \frac{v_{ra}+v_{na}\cot\psi}{1-(v_{na}/a_a)^2}\right]_{\psi_{a_s}} \quad (17)$$

When the velocity components, as defined by Eqs. (9) to (11), are substituted into Eq. (1) and only first-order terms of ψ_{ns} and ψ_{ms} are retained, the following three independent equations result:

$$v_{ra}\left(2 - \frac{v_{na}^2}{a_a^2}\right) + v_{na}\cot\psi + \frac{\partial v_{na}}{\partial\psi}\left(1 - \frac{v_{na}^2}{a_a^2}\right) = 0 \quad (18)$$

$$\left(v_{rn} + \frac{\partial v_{nn}}{\partial\psi}\right)\left(1 - \frac{v_{na}^2}{a_a^2}\right) = -A_a v_{nn} - B_a v_{rn} - \frac{n^2 w_n}{\sin\psi} \quad (19)$$

$$\left(v_{rm} + \frac{\partial v_{nm}}{\partial\psi}\right)\left(1 - \frac{v_{na}^2}{a_a^2}\right) = -A_a v_{nm} - B_a v_{rm} - \frac{m^2 w_m}{\sin\psi} \quad (20)$$

where

$$A_a = \cot\psi + \left(\frac{2v_{na}}{a_a^2} + \frac{\gamma-1}{a_a^4}v_{na}^3\right)\times\left[\frac{v_{ra}+v_{na}\cot\psi}{1-(v_{na}^2/a_a^2)}\right]$$

$$B_a = 1 + \frac{\gamma-1}{a_a^4}\left[\frac{v_{ra}+v_{na}\cot\psi}{1-(v_{na}^2/a_a^2)}\right]v_{ra}v_{na}^2$$

Eqs. (18), (19), and (20) are independent of ϑ. Eq. (18) is the ordinary nonlinear differential equation for conical axially symmetric flow whose numerical solutions are given in tabulated form in reference 3. Eq. (19) is an ordinary linear differential equation independent of ψ_{ns}, and Eq. (20) is an ordinary linear differential equation independent of ψ_{ms}. Therefore, the flow field considered is represented by a superposition of linearized disturbances proportional to $v_{r_{n,m}}$, $v_{n_{n,m}}$, $w_{n,m}$ [the proportionality coefficients are the shock-front coefficients $(\psi_{n,m})_s$] upon the nonlinear axially symmetric conical flow defined by Eq. (18).

By combining Eqs. (2) and (3) and the momentum equation in the radial direction, the relation

$$v_n\sin\psi(\partial S/\partial\psi) = -w(\partial S/\partial\vartheta) \quad (21)$$

can be obtained.[2] From Eq. (2), for the approximation accepted, $\partial S/\partial\vartheta$ is of the order ψ_{ns}; therefore, when v_n is at least of one order larger than ψ_{ns}, Eq. 21 indicates that $\partial S/\partial\psi$ is of the order of $(\psi_{ns})^2$ and can be neglected. (The identical reasoning applies when the subscript m is considered; henceforth, in this section, only the subscript n will be used.) Then Eq. 3 gives

$$v_{na} = \partial v_{ra}/\partial\psi, \quad v_{nn} = \partial v_{rn}/\partial\psi \quad (22)$$

while Eq. 2 results in

$$-\frac{a_a^2}{\gamma R}S' = v_{na}\sin\psi\frac{\partial w_n}{\partial\psi} + v_{ra}v_{rn} + v_{na}v_{nn} + v_{ra}w_n\sin\psi + v_{na}w_n\cos\psi \quad (23)$$

Eqs. (22) and (23) are independent of ϑ; S' is a constant obtained from the shock equation at the shock front ψ_{a_s}—i.e.,

$$S' = (dS/d\psi)_{\psi_{a_s}}$$

Eq. (23), with the use of Eq. (22), can be written as

$$-\frac{a_a^2}{\gamma R}S' = v_{ra}(v_{rn} + w_n\sin\psi) + v_{na}\frac{\partial}{\partial\psi}(v_{rn} + w_n\sin\psi) \quad (24)$$

When Eq. (24) is multiplied by the integrating factor

$$a_a^{-1/(\gamma-1)}/v_{na}(-v_{na}\sin\psi)^{1/2}$$

the following expression is obtained:

$$v_{rn} + w_n\sin\psi = -\left(\frac{S'}{\gamma R}\right)a_a^{1/(\gamma-1)}\times(-v_{na}\sin\psi)^{1/2}\int_{\psi_{a_s}}^{\psi}\frac{a_a^{(2\gamma-3)/(\gamma-1)}}{v_{na}(-v_{na}\sin\psi)^{1/2}}d\psi \quad (25)$$

where the constant of integration is zero because at $\psi = \psi_{as}$ [from Eqs. (12) and (14)]

$$w_n = -v_{rn}/\sin\psi \quad (26)$$

In Eq. (19) all the coefficients of the perturbation velocities and in Eq. (25) the right-hand side of the equation are known for any value of ψ; therefore, the quantity

$$[v_{rn} + (\partial v_{nn}/\partial\psi)]$$

which is the radius H_n of the hodograph diagram (for example, see reference 4), can be evaluated at any ψ. The quantities v_{rn}, v_{nn}, and w_n, for any value of n may then be determined between the shock front ψ_{as} and the surface of the circular body ψ_{ab} (which created the shock front ψ_{as}) with the use of Eqs. (19) and (25) and the following step-by-step process:

$$(v_{nn})_{\psi-\Delta\psi} = (v_{nn})_\psi\cos(-\Delta\psi) + (H_n - v_{rn})_\psi\times\sin(-\Delta\psi) \quad (27)$$

$$(v_{rn})_{\psi-\Delta\psi} = (v_{nn})_\psi\sin(-\Delta\psi) - (H_n - v_{rn})_\psi\times\cos(-\Delta\psi) + (H_n)_\psi \quad (28)$$

Boundary Conditions

The conical body that produces the shock front defined by Eq. (4) can be expressed in the form

$$\psi_b = \psi_{a_b} + \sum_{n=0}^{\infty} \psi_{nb} \cos n\vartheta + \sum_{m=1}^{\infty} \psi_{mb} \sin m\vartheta \tag{29}$$

The boundary condition requires that the body surface be a stream surface for the conical flow field. For conical bodies, this condition can be expressed as

$$\left(\frac{v_n}{w}\right)_{\psi_b} = \frac{1}{\sin \psi_b} \frac{\partial \psi_b}{\partial \vartheta} = \frac{1}{\sin \psi_b} \left[-\Sigma n\psi_{nb} \sin n\vartheta + \Sigma m\psi_{mb} \cos m\vartheta\right] \tag{30}$$

But at the body surface ψ_b, $(v_n)_{\psi_b}$ may be expressed in terms of a Taylor expansion about the basic circular cone ψ_{ab}—i.e.,

$$(v_n)_{\psi_b} = (v_{na})_{\psi_{a_b}} + \left(\frac{\partial v_{na}}{\partial \psi}\right)_{\psi_{a_b}} (\psi_b - \psi_{ab}) + \frac{1}{2}\left(\frac{\partial^2 v_{na}}{\partial \psi^2}\right)_{\psi_{a_b}} \frac{(\psi_b - \psi_{ab})^2}{2} + \Sigma\psi_{ns} (v_{nn})_{\psi_{a_b}} \cos n\vartheta + \Sigma\psi_{ms} (v_{nm})_{\psi_{a_b}} \times$$

$$\sin m\vartheta + \left[\Sigma\psi_{ns}\left(\frac{\partial v_{nn}}{\partial \psi}\right)_{\psi_{a_b}} \cos n\vartheta + \Sigma\psi_{ms}\left(\frac{\partial v_{nm}}{\partial \psi}\right)_{\psi_{a_b}} \sin m\vartheta\right] (\psi_b - \psi_{ab}) + \ldots \tag{31}$$

$$(w)_{\psi_b} = \Sigma\psi_{ns} (w_n)_{\psi_{a_b}} n \sin n\vartheta + \Sigma\psi_{ms} (w_m)_{\psi_{a_b}} m \cos m\vartheta +$$

$$\left[\Sigma\psi_{ns}\left(\frac{\partial w_n}{\partial \psi}\right)_{\psi_{a_b}} n \sin n\vartheta + \Sigma\psi_{ms}\left(\frac{\partial w_m}{\partial \psi}\right)_{\psi_{a_b}} m \cos m\vartheta\right] (\psi_b - \psi_{ab}) + \ldots \tag{32}$$

Therefore, when Eqs. (31) and (32) are substituted into the boundary condition [Eq. (30)], relations defining the coefficients ψ_{ns} and ψ_{ms} can be obtained. These relations will differ for different assumptions of the relative order of magnitude of the body surface coefficients ψ_{nb}, ψ_{mb} with respect to the shock surface coefficients ψ_{ns}, ψ_{ms}.

For high Mach Numbers or for large cone angles, the shape of the shock follows closely the shape of the body, and the coefficients ψ_{nb}, ψ_{mb}, ψ_{ns}, ψ_{ms} are of the same order; therefore, terms of the order of $\psi_{ms}\psi_{nb}$, $\psi_{ns}\psi_{mb}$, ψ_{nb}^2, ψ_{mb}^2 or higher can be neglected in the boundary conditions, as well as in the differential equations of motion, and linearized boundary conditions can be used. For these linearized boundary conditions, Eq. (30) simplifies to $(v_n)_{\psi_b} = 0$ or

$$(v_{na})_{\psi_{a_b}} + \left(\frac{\partial v_{na}}{\partial \psi}\right)_{\psi_{a_b}} (\Sigma\psi_{nb} \cos n\vartheta + \Sigma\psi_{mb} \sin m\vartheta) = -\Sigma\psi_{ns} (v_{nn})_{\psi_{ab}} \cos n\vartheta - \Sigma\psi_{ms} (v_{nm})_{\psi_{a_b}} \sin m\vartheta \tag{33}$$

If, at a given Mach Number, ψ_{as} is the shock angle produced by the circular cone ψ_{ab}, then $(v_{na})_{\psi_{a_b}} = 0$, and $(\partial v_{na}/\partial\psi)_{\psi_{a_b}}$ as defined by Eq. (18) is

$$(\partial v_{na}/\partial\psi)_{\psi_{a_b}} = -2(v_{ra})_{\psi_{a_b}}$$

Therefore, the boundary conditions as obtained from Eq. (33) are

$$\left.\begin{aligned} \psi_{ns} &= 2\psi_{nb} (v_{ra}/v_{nn})_{\psi_{a_b}} \\ \psi_{ms} &= 2\psi_{mb} (v_{ra}/v_{nm})_{\psi_{a_b}} \end{aligned}\right\} \tag{34}$$

These equations relate the shock coefficients ψ_{ns}, ψ_{ms} to the radial velocity of the conical axially symmetric flow v_{ra} (which can be obtained in tabulated form, for example, from reference 3), to the normal perturbation velocities v_{nn}, v_{nm} [which are obtained from a solution of Eqs. (19) and (20)], and to the body coefficients ψ_{nb}, ψ_{mb} which can be calculated once the body shape is prescribed. Therefore, the shock shape can be obtained from Eq. (4).

For small cone angles and small Mach Numbers, the values of ψ_{nb} and ψ_{mb} are larger than the values of ψ_{ns} and ψ_{ms}, and, therefore, higher order terms of ψ_{nb} and ψ_{mb} can be retained in Eq. (30). If higher order terms of ψ_{nb}, ψ_{mb} are retained in the boundary condition, a system of linear equations is obtained where each equation contains the unknowns ψ_{ns}, ψ_{ms}; therefore, in this case, the determination of the shock coefficients is much more involved. In this paper all the results are based on the linearized boundary conditions as given by Eq. (34).

If the flow field has a plane of symmetry and the axis of the conical flow is in this plane of symmetry, the shock equation (as well as the equations for the velocity components) may be expressed in terms of only one summation. If the plane of symmetry is the plane $\vartheta = 0$, $\vartheta = \pi$, the coefficients ψ_{ms} are zero. If the flow field has two planes of symmetry, then only the even coefficients ψ_{0s}, ψ_{2s}, . . . , ψ_{ns}, where n is an even integer, appear in the summation. Furthermore, if the value of ψ_{as} corresponds to the value of ψ_{ab} for axially symmetric flow, ψ_{0s} is zero.

The particular case of the flow around circular cones at small angles of attack, where the plane of symmetry is the plane $\vartheta = 0$, $\vartheta = \pi$, is given by $n = 1$, $m = 0$. This analysis was considered first in reference 6. The present method is a generalization of this analysis to cones without axial symmetry. The analysis of the nonaxially symmetric cones is obtained by means of numerically determined linearized solutions presented in tabulated form.[7]

Application of the Method

In order to obtain aerodynamic results from the preceding analysis, several linearized flow fields have been determined for different circular cone semiapex angles ψ_{ab} and free-stream Mach Numbers M_1. The linearized solutions have been determined for the basic flow solutions shown in Table 1. For each basic flow solution, ten linearized solutions have been determined corresponding to values of n or m equal to 1 to 10.* These values of the linearized flow field (which will be published shortly in tabulated form[7]) were used to obtain the flow field around bodies of different cross section and to determine the effect of cross-section contour on the shock shape, on the pressure distribution, and on other aerodynamic properties.

The pressure distribution is obtained from the expression

$$C_p = \frac{2}{\gamma M_1^2}\left[\left(\frac{1 - V^2}{1 - V_1^2}\right)^{\gamma/(\gamma-1)} \cdot e^{-\Delta S/\epsilon R(\gamma-1)} - 1\right]$$

where V^2 is given by

$$V^2 = [(v_{r_a})_{\psi_{ab}} + \Sigma\psi_{n_s}(v_{r_n})_{\psi_{ab}} \cos n\vartheta + \Sigma\psi_{m_s}(v_{r_m})_{\psi_{ab}} \sin m\vartheta]^2 + [\Sigma n\psi_{n_s}(w_n)_{\psi_{ab}} \sin n\vartheta + \Sigma m\psi_{m_s}(w_m)_{\psi_{ab}} \cos m\vartheta]^2$$

The values w_n (and w_m) are defined by Eq. (26), which is valid along a stream line. The increase in entropy ΔS between the shock front and the surface of the body is considered constant along the body surface between meridian planes where the w velocity component is equal to zero, and its value is that obtained in the meridian plane ϑ = constant where the stream lines diverge.

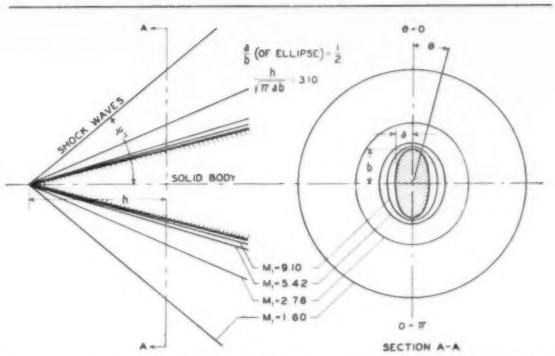

FIG. 2. Variation of shock wave with free-stream Mach Number for an elliptical cone at zero angle of attack.

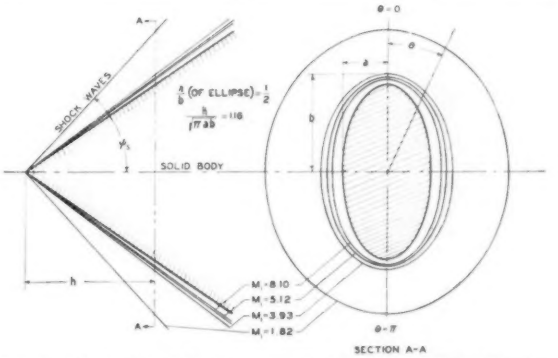

FIG. 3. Variation of shock wave with free-stream Mach Number for an elliptical cone at zero angle of attack.

Elliptical Bodies

At zero angle of attack only the even values of n ($n = 2, 4, \ldots, 10$) are necessary, while, because of the linearized boundary conditions, only $n = 1$ is required to express the effect of angle of attack and only $m = 1$ is required to express the effect of angle of yaw.

A preliminary investigation of the accuracy of the linearized procedure for purposes of comparison with the experimental results that were available for $M_1 = 1.81$ and $a/b = 1/3$ indicated very good agreement.[1] In the present paper, the investigation of elliptical bodies is extended to cover a wide range of Mach Numbers for ellipses with semidiameter ratio $a/b = 2/3$, $1/2$, and $1/3$ and for different values of $h/\sqrt{\pi ab}$ where h is the cone height and πab is the cross-sectional

TABLE 1

ψ_{ab} =	5°	7.5°	10°	12.5°	20°	25°
					1.467	
				1.455	1.871	
			1.596	1.881	2.443	1.825
M_1 =		2.685	2.779	2.891	3.369	3.926
	5.800	5.103	5.422	5.860	5.546	5.123
	8.492	8.059	9.100	11.091	9.593	8.096

* The linearized solution for $n = 1$, which gives the effect of a small angle of attack on a circular cone must correspond to the linearized flow field given in the M.I.T. tables[5] when both flow fields are referred to the same axis. The velocity components of the M.I.T. tables are proportional to the body parameter ψ_{1b} while these components are referred to the shock parameter ψ_{1s} in the present analysis, therefore the latter values must be multiplied by δ/ϵ of reference 5 in order to make a comparison.

A systematic error, however, has been found in the values of reference 5 due probably to an error in sign in the evaluation of the integral of Eq. (24) of that report [which corresponds to Eq. (25) of this report]. This error affects all the velocity components and is most pronounced for the w component, especially at high Mach Numbers and large cone angles. This error probably also affects all the values of reference 8 which are determined from the linear solution.

TABLE 2
Coefficients Defining Shock-Wave Cross Section [See Eq. (4)]

	Ellipse $a/b = 1/2$	Ellipse $a/b = 1/2$	Circle	Drop-Shape	Triangle
Shown in Fig(s).	2	2, 18	18	18	18
M_1	1.60	9.10	9.10	9.10	9.10
ψ_{a_a}	0.693	0.219	0.219	0.219	0.219
ψ_{1a}	0	0	0	−0.0134	−0.0100
ψ_{2a}	0.00162	0.0399	0	0.0196	−0.00560
ψ_{3a}	0	0	0	0.00600	0.0198
ψ_{4a}	0.00001	0.00487	0	0.00166	−0.000521
ψ_{5a}	0	0	0	0.000573	−0.000775
ψ_{6a}	0	0.00065	0	0.000322	0.00176
ψ_{7a}	0	0	0	0.000166	−0.00174
ψ_{8a}	0	0.00010	0	0.000059	−0.000119
ψ_{9a}	0	0	0	0.000021	0.000155
ψ_{10a}	0	0.00002	0	0.000012	0.0000002

TABLE 3
Coefficients Defining Conical-Body Cross Section [See Eq. (29)]

	Ellipse $a/b = 1/2$	Ellipse $a/b = 1/3$	Ellipse $a/b = 1/2$	Ellipse $a/b = 2/3$	Circle	Drop-Shape	Triangle
Shown in Figure	3		2		...	13	14
Semiapex Angle of Basic Circular Cone	25°	10°	10°	10°	10°	10°	10°
ψ_{a_b}	0.436	0.175	0.175	0.175	0.175	0.175	0.175
ψ_{1b}	0	0	0	0	0	−0.0150	−0.0112
ψ_{2b}	0.128	0.0879	0.0577	0.0344	0	0.0284	−0.00809
ψ_{3b}	0	0	0	0	0	0.0122	0.0401
ψ_{4b}	0.0281	0.0325	0.0142	0.00506	0	0.00485	−0.00158
ψ_{5b}	0	0	0	0	0	0.00239	−0.00324
ψ_{6b}	0.00687	0.0133	0.00387	0.000826	0	0.00190	0.0104
ψ_{7b}	0	0	0	0	0	0.00138	−0.00014
ψ_{8b}	0.00177	0.00565	0.00110	0.000141	0	0.00068	−0.00136
ψ_{9b}	0	0	0	0	0	0.00032	0.00241
ψ_{10b}	0.000470	0.00246	0.000323	0.000025	0	0.00025	−0.000004

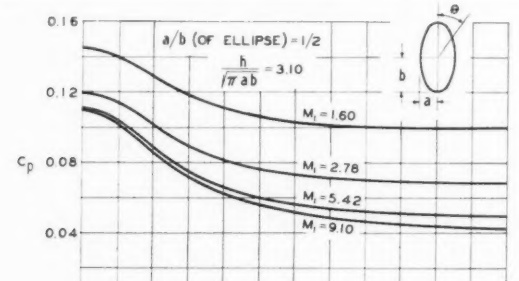

FIG. 4. Variation of pressure coefficients around an elliptical cone with free-stream Mach Numbers at zero angle of attack.

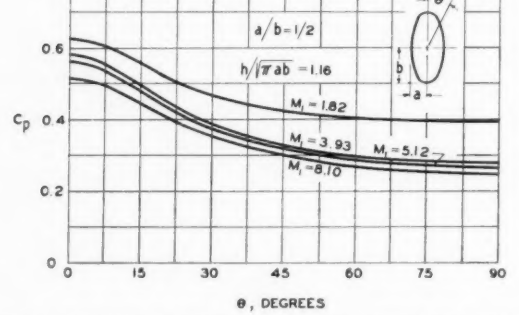

FIG. 5. Variation of pressure coefficients around an elliptical cone with free-stream Mach Numbers at zero angle of attack.

area. Some of the more interesting results are presented in the figures.

In Figs. 2 and 3 are shown the shock shapes for two cones with the same elliptic cross section ($a/b = 1/2$) both at zero angle of attack, but with different ratios of $h/\sqrt{\pi ab}$. The coefficients defining the cross sections of the various bodies considered and the coefficients of the cross sections of some of the resulting shock shapes are tabulated in Tables 2 and 3. It will be noted that, for small Mach Numbers and small cone angle, the shock is close to a Mach cone, but for high Mach Numbers or large cone angle the shock shape is far from circular. To realize the limitations of the linearized theory, consider, for example, the body in Fig. 2. For Mach Numbers of the order of 3, the Mach cone would intersect the ellipse; therefore, the linear theory or any other higher order methods that start from linear solutions cannot give results in this range of Mach Numbers.

In Figs. 4 and 5 the pressure distribution for different Mach Numbers around the two cones of Figs. 2 and 3 are presented.

In Fig. 6, the effect of the variation of the parameter a/b of the ellipse on the pressure coefficients at a constant Mach Number and with approximately constant $h/\sqrt{\pi ab}$ ratios is presented. (These conical flows were obtained from the same basic axially symmetric conical flow corresponding to a circular cone of 10° semiapex angle at $M_1 = 2.78$; the cross-sectional areas of the

elliptical cones are not exactly the same, but the variations are small.)

In order to determine the effect of the variation of the a/b ratio on the shock drag, the drag coefficient of each elliptical cone is divided by the drag coefficient of a circular cone of exactly the same cross-sectional area. The results are given in Fig. 7. As expected, the shock drag decreases as the ratio a/b approaches zero.

The effect of angle of attack (or angle of yaw), within the accuracy of the linearized boundary condition, is considered by superposing upon the linearized flow solution of the nonaxially symmetric cone at zero angle of attack (or yaw), the flow solution for a circular cone (from which the nonaxially symmetric body is perturbated) at the angle of attack (or yaw) at which the actual body is being analyzed.

In Figs. 8 and 9, the pressure distribution at an angle of attack or yaw of 6° and $M_1 = 2.78$ for the cones considered in Fig. 6 is presented. In Fig. 10, the lift, drag, horizontal, and normal force coefficients are shown; the lift, drag, and horizontal force coefficients are referred to the area of the cross section which is normal to the body axis; the normal force coefficient is referred to the cross-sectional area in the meridian plane which is perpendicular to the normal component N. Also given in Fig. 10 is the normal force coefficient c_N, as obtained from linearized theory, of a triangular flat plate of plan-form area equal to the respective ellipse. It can be seen that L/D of the body increases rapidly when a/b increases.

In Fig. 11 the drag coefficient as a function of Mach Number of elliptical cones with $a/b = 1/2$, but for different values of $h/\sqrt{\pi ab}$, is presented. The value of ψ_{ab} of the basic circular cone corresponding to each value of $h/\sqrt{\pi ab}$ is also given. In Fig. 12 the effect of Mach Number and $h/\sqrt{\pi ab}$ on the ratio between the drag of the elliptical body to a circular cone of equal cross-sectional area and height h is presented. The ratio is less than unity for all Mach Numbers and $h \div \sqrt{\pi ab}$ ratios and changes slightly when M_1 or $h/\sqrt{\pi ab}$ changes, indicating that some gain on the shock drag

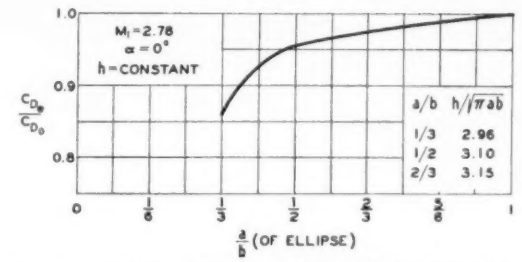

FIG. 7. Variation of drag coefficient of elliptical cone C_{D_0} as function of a/b ratio of ellipse. (Drag coefficient is referred to circular cone of same height and cross-sectional area as ellipse.)

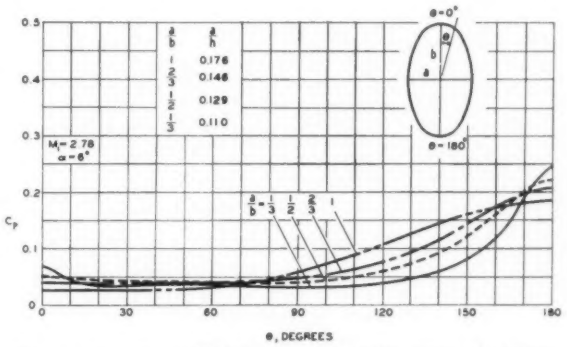

FIG. 8. Pressure coefficient around elliptical cones of different shape at 6° angle of attack.

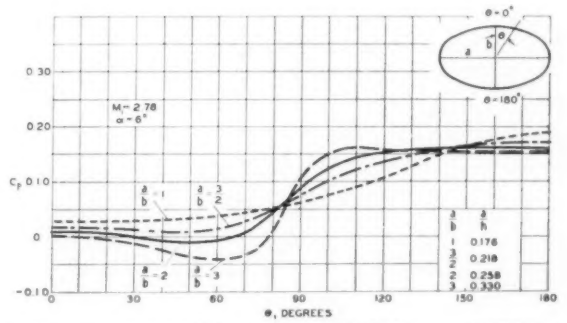

FIG. 9. Pressure coefficient around elliptical cones of different shape at 6° angle of yaw.

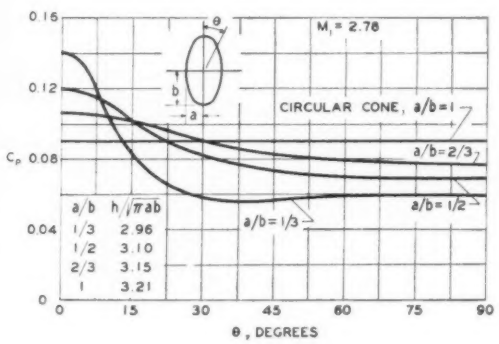

FIG. 6. Variation of pressure coefficients around different elliptical cones at the same free-stream Mach Number at zero angle of attack.

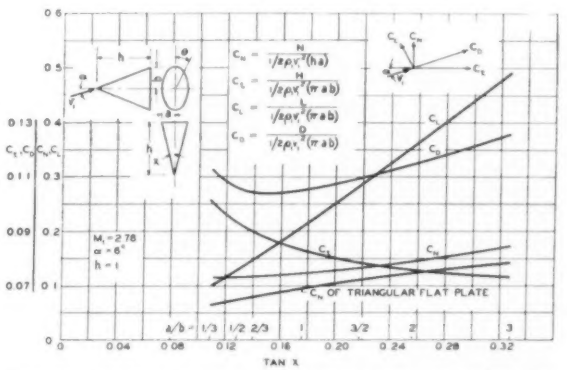

FIG. 10. Lift, drag, normal, and tangential coefficients for elliptical cones with different a/b ratios at $M_1 = 2.78$ and $\alpha = 6°$.

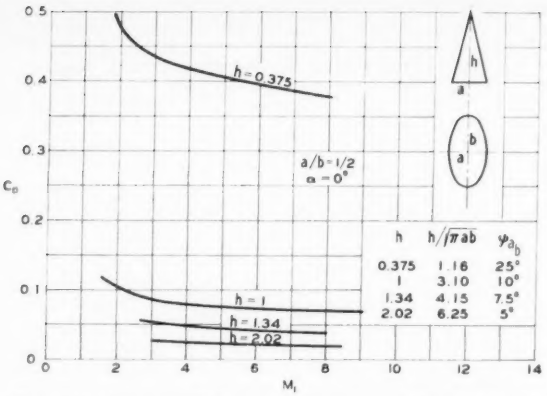

FIG. 11. Drag coefficient as a function of Mach Number for elliptical cones of equal cross-sectional areas for different values of $h/\sqrt{\pi ab}$.

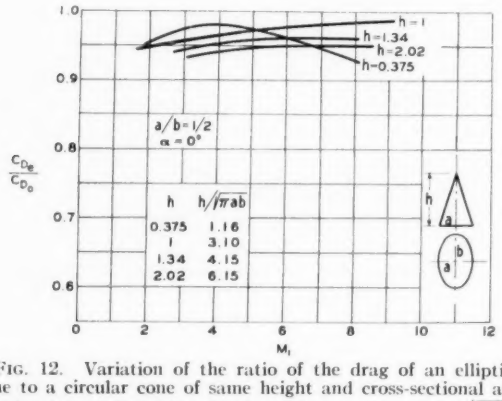

FIG. 12. Variation of the ratio of the drag of an elliptical cone to a circular cone of same height and cross-sectional area as a function of Mach Number for different values of $h/\sqrt{\pi ab}$.

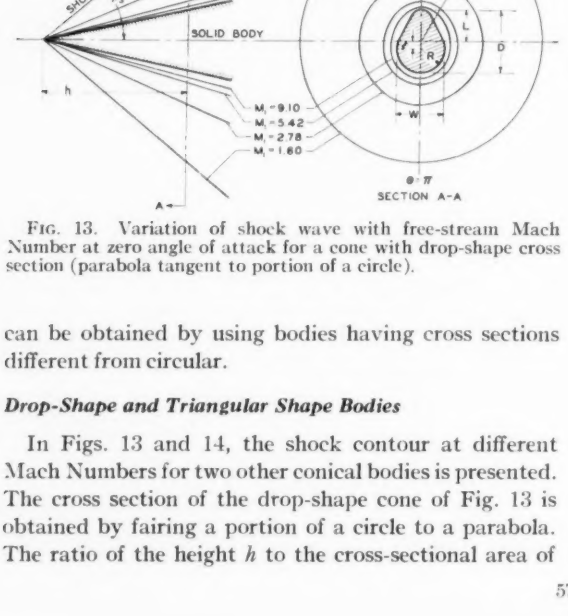

FIG. 13. Variation of shock wave with free-stream Mach Number at zero angle of attack for a cone with drop-shape cross section (parabola tangent to portion of a circle).

can be obtained by using bodies having cross sections different from circular.

Drop-Shape and Triangular Shape Bodies

In Figs. 13 and 14, the shock contour at different Mach Numbers for two other conical bodies is presented. The cross section of the drop-shape cone of Fig. 13 is obtained by fairing a portion of a circle to a parabola. The ratio of the height h to the cross-sectional area of this cone is about the same as the corresponding ratio of the elliptical body shown in Fig. 2. The value of $h/\sqrt{\text{area}}$ for this cone is 3.16; the corresponding ratio for the elliptical cone of Fig. 2 is 3.10, while this ratio for a circular cone of 10° semiapex angle is 3.21. The ratio between the maximum width to maximum height at any cross section is 1/1.34.

The cross section of the cone of Fig. 14 is a triangle whose corners are faired by circular arcs. The ratio of the height to the cross-sectional area of this body is 3.14, practically the same as the other bodies mentioned above. Its ratio of maximum width to height is 1.26. In Figs. 15 and 16 the pressure distribution around the two bodies is presented.

It has been found that the drop-shape body at $M_1 = 2.78$ has zero lift at $\alpha = -1°$, its minimum drag at $\alpha = -2°$, and a lift curve slope $(dc_L/d\alpha)_{\alpha=0} = 1.72$ rad.; similarly, it has been found that the triangular shaped body at the same Mach Number has both zero lift and minimum drag at about $\alpha = 0°$ and a lift curve slope $(dc_L/d\alpha)_{\alpha=0} = 2.41$ rad.

In Fig. 17, the drag coefficients of the circular, elliptical, drop-shape, and triangular bodies as a function of Mach Number are presented. Curves for the drop-shape body at $\alpha = 0$ and $\alpha = -2°$ are shown, while the other bodies are at zero angle of attack.

The value of the drag coefficient has been divided by the drag coefficient of a circular cone of the same area and height in order to eliminate the effects of small differences due to the ratio $h/\sqrt{\text{area}}$. It will be noted that the drag ratio remains practically constant for a wide range of Mach Numbers and is less than unity for all bodies other than circular. Therefore, as in the case of elliptical bodies, some gain in shock drag may also be obtained from the drop-shape and triangular bodies. Furthermore, the drag ratio for the drop-shape body is less at $\alpha = -2°$ than at zero angle of attack for the range of Mach Numbers considered. In Fig. 18, the shock shapes for the various bodies are shown for $M_1 = 9.10$, $\alpha = 0°$.

It is important to mention that the linearized approximation in this analysis is not the same for all bodies considered because the intensity of the linearized flow

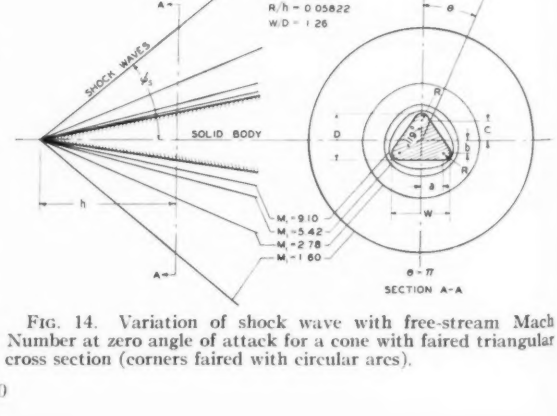

FIG. 14. Variation of shock wave with free-stream Mach Number at zero angle of attack for a cone with faired triangular cross section (corners faired with circular arcs).

fields varies with different boundary conditions. These simplified boundary conditions introduce different approximations for the various body shapes. However, the linearized flow fields are all small, and it is expected that the trend of the variations given in this report is correct.

Conclusions

The method of superposing linear solutions to a nonlinear nonuniform flow field has been applied to the analysis of conical flows without axial symmetry.

For elliptical cones, the results indicate that, at a constant free-stream Mach Number, the shock drag ratio (i.e., the ratio of the drag coefficient of the elliptical cone to the drag coefficient of a circular cone of the same cross-sectional area and height) decreases as the ratio of the minor to major axis of the ellipse decreases.

Furthermore, for a given elliptical body at zero angle of attack, the drag ratio remains practically constant and less than unity for the range of Mach Numbers considered.

The effect of angle of attack is also analyzed, and the lift coefficient is determined. The lift coefficient is not far from the lift coefficient of a triangular flat plate of the same plan form.

Cones having drop-shape and triangular cross sections are also analyzed. The drag ratio of these bodies also remains practically constant and less than unity for a wide range of Mach Numbers. Therefore, the results indicate that some gain on the shock drag can be obtained by using bodies having cross sections different from circular.

References

[1] Ferri, Antonio, *The Linearized Characteristics Method and Its Application to Practical Nonlinear Supersonic Problems*, NACA TN No. 2515, 1951.

[2] Ferri, Antonio, *Supersonic Flow around Circular Cones at Angles of Attack*, NACA TN No. 2236, 1950.

[3] Staff of the Computing Section, Center of Analysis (under direction of Zdenek Kopal), *Tables of Supersonic Flow Around Cones*, Tech. Rep. No. 1, M.I.T., 1947.

[4] Ferri, Antonio, *Elements of Aerodynamics of Supersonic Flows*, p. 236 and following: The Macmillan Company, New York, 1949.

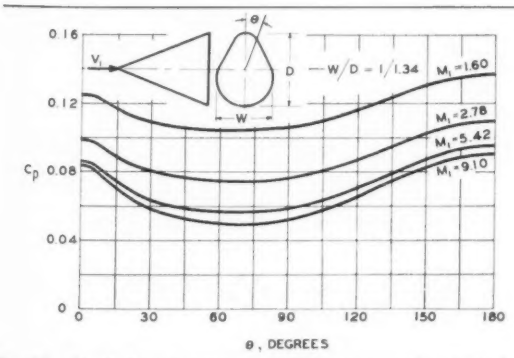

FIG. 15. Variation of pressure coefficients around a drop-shape cone with free-stream Mach Number at zero angle of attack.

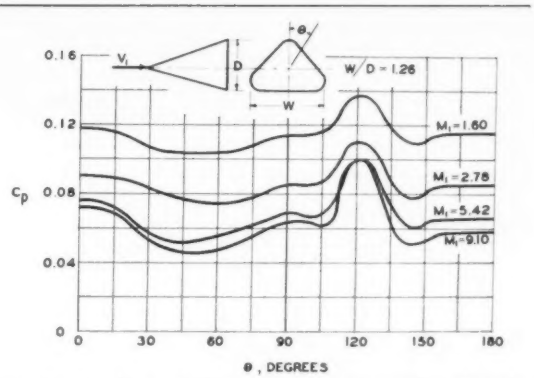

FIG. 16. Variation of pressure coefficients around a triangular shaped cone with free-stream Mach Number at zero angle of attack.

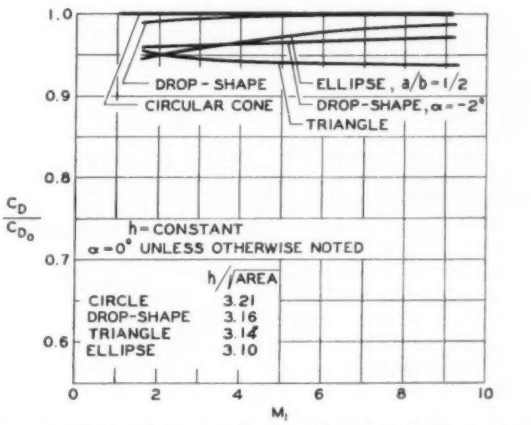

FIG. 17. Ratio of drag coefficients of conical bodies to the circular body of same height and cross-sectional area as a function of Mach Number.

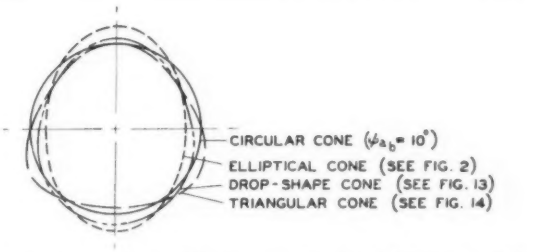

FIG. 18. Comparison of shock-wave shapes for different conical bodies at $M_1 = 9.10$ and $\alpha = 0°$.

[5] Staff of the Computing Section, Center of Analysis (under direction of Zdenek Kopal), *Tables of Supersonic Flow Around Yawing Cones*, Tech. Rep. No. 3, M.I.T., 1947.

[6] Sauer, Robert, *Supersonic Flow About Projectile Heads of Arbitrary Shape at Small Incidence*, R.T.P. Translation No. 1573, British Ministry of Aircraft Production. (From Luftfahrtforschung, Vol. 19, No. 4, pp. 148–152, May, 1942.)

[7] PIBAL Report No. 220, *Tabulated Values of Linearized Conical Flow Solutions for Solution of Supersonic Conical Flows Without Axial Symmetry* (to be published).

[8] Staff of the Computing Section, Center of Analysis (under direction of Zdenek Kopal), *Tables of Supersonic Flow Around Cones of Large Yaw*, Tech. Rep. No. 5, M.I.T., 1949.

Readers' Forum

BRIEF REPORTS of investigations in the aeronautical sciences and discussions of papers published in the JOURNAL are presented in this special department. Publication will be completed as soon as possible after receipt of the material. The Editorial Committee does not hold itself responsible for the opinions expressed by the correspondents. Contributions should not exceed 800 words in length

On the Nonexistence of a Finite Critical Time for Linear Viscoelastic Columns

Joseph Kempner and Frederick V. Pohle
Assistant Professors, Department of Aeronautical Engineering and Applied Mechanics, Polytechnic Institute of Brooklyn, Brooklyn, N. Y.
May 7, 1953

Symbols

- E = Young's modulus
- I = moment of inertia of the cross section with respect to a principal axis
- L = length of column
- M = bending moment
- P = axial compressive end load
- P_E = $\pi^2 EI/L^2$
- c_0 = eccentricity
- n = $(P_E/P) > 1$
- t = time
- u = x/L
- x = axial coordinate measured from one end of column
- y = deflection due to loading
- ξ = t/τ
- τ = relaxation time

Introduction

In a paper presented in 1946, Freudenthal[1] concluded, for columns fabricated from a linear viscoelastic material, that a finite critical time existed. Since that time, the same conclusion has been repeated by Freudenthal in his book[2] and apparently has been accepted by Rosenthal and Baer.[3] Libove[4] stated that no finite critical time existed for such columns and referred to an unpublished letter by the present authors. Hilton[5] referred both to the letter and to Freudenthal's work. The purpose of this note is to show briefly that Freudenthal's conclusion is incorrect and at the same time to make available the contents of the communication referred to above.

Discussion

Freudenthal analyzed a simply supported column fabricated from a Maxwell material and with a constant eccentricity c_0. The basic differential equation that governs the deflection is

$$EI\partial(d^2y/dx^2)/\partial t = -(\partial M/\partial t) - (M/\tau) \tag{1}$$

The method used by Freudenthal to solve Eq. (1) was that of successive approximations. The first approximation to M was assumed to be Pc_0. The differential equation for the first approximation y_1 to the deflection y is

$$EI\partial(d^2y_1/dx^2)/\partial t = -Pc_0/\tau \tag{2}$$

The solution of Eq. (2) for a simply supported column undergoing purely elastic deformation at zero time is

$$y_1 = c_0(\pi^2/n)\,(1/2!)\,(u - u^2)\,(1 + \xi) \tag{3}$$

where $u = x/L$ and $\xi = t/\tau$.

A correction to the assumed moment is thus $\Delta M = Py_1$. Since Eq. (1) is linear, the increment in moment when substituted into the right-hand side of Eq. (1) yields the following differential equation for y_2, the correction to y_1:

$$\partial(d^2y_2/dx^2)\partial t = -c_0(\pi^2/n)^2\,(1/2!)\,(u - u^2)\,(\xi)\,(2 + \xi) \tag{4}$$

The procedure used to obtain y_2 can be applied repeatedly to obtain the deflection in the form $y = y_1 + y_2 + y_3 + \ldots$. The result is

$$y = c_0 \sum_{m=1}^{\infty} (\pi^2/n)^m [1/(2m)!]g_m(u)f_m(\xi) \tag{5}$$

where

$$\left.\begin{aligned} g_1(u) &= u - u^2 \\ g_2(u) &= u - 2u^3 + u^4 \\ g_3(u) &= 3u - 5u^3 + 3u^5 - u^6 \\ g_4(u) &= 17u - 28u^3 + 14u^5 - 4u^7 + u^8 \\ &\ldots \qquad\quad \ldots \qquad\quad \ldots \end{aligned}\right\} \tag{6}$$

and

$$\left.\begin{aligned} f_1(\xi) &= 1 + \xi \\ f_2(\xi) &= 1 + 2\xi + (1/2)\xi^2 \\ f_3(\xi) &= 1 + 3\xi + (3/2)\xi^2 + (1/6)\xi^3 \\ f_4(\xi) &= 1 + 4\xi + 3\xi^2 + (2/3)\xi^3 + (1/24)\xi^4 \\ &\ldots \qquad\quad \ldots \qquad\quad \ldots \end{aligned}\right\} \tag{7}$$

The recursion formula for $f_m(\xi)$ is

$$f_m(\xi) = \int_0^\xi f_{m-1}(\xi)\,d\xi + f_{m-1}(\xi) \qquad [m \geq 1;\ f_0(\xi) = 1] \tag{8}$$

The relation (8) was not stated by Freudenthal, but it will be essential for the determination of the general term of Eq. (5).

The maximum bending moment occurs at $x = L/2$ and is

$$M_{max.} = Pc_0[1 + 1.2337(1/n)f_1(\xi) + 1.2683(1/n)^2f_2(\xi) + 1.2727(1/n)^3f_3(\xi) + 1.2728(1/n)^4f_4(\xi) + \ldots] \tag{9}$$

A Fourier analysis of the polynomials in $u = x/L$ which occur in Eq. (6) shows that the numerical coefficients of $(1/n)^m f_m(\xi)$ in Eq. (9) are given by

$$(4/\pi)\,[1 - (1/3)^{2m+1} + (1/5)^{2m+1} - \ldots] \tag{10}$$

Thus the numerical coefficients have $4/\pi = 1.27324$ as an upper bound. The corresponding coefficients stated by Freudenthal were 1, 1.22, 1.26, 1.26, 1.26, . . . ; these coefficients were not computed accurately, nor was any proof given that the sequence of coefficients possessed an upper bound.

Clearly, the convergence or divergence of the infinite series in Eq. (9) depends entirely upon the properties of

$$\varphi(\xi) = \sum_{m=1}^{\infty} (1/n)^m f_m(\xi) \tag{11}$$

The function $\varphi(\xi)$ can be evaluated in closed form in the following way: If both sides of Eq. (8) are multiplied by $(1/n)^m$ and summations are carried out over m from 1 to ∞, the left side of the result will be $\varphi(\xi)$, but the right side will contain an integral of $\varphi(\xi)$. Differentiation of the result with respect to ξ yields the differential equation

$$d\varphi/d\xi - [1/(n-1)]\varphi = 1/(n-1) \tag{12}$$

The solution of Eq. (12), with $\varphi(0) = 1/(n-1)$ is

$$\varphi(\xi) = [n/(n-1)]e^{\xi/(n-1)} - 1 \tag{13}$$

It is easily verified that Eqs. (13) and (11) are identical if the exponential in Eq. (13) is replaced by its infinite series expansion and like powers of $(1/n)$ are collected.

Since Eq. (13) is a closed expression for $\varphi(\xi)$, the convergence question is decided at once: $\varphi(\xi)$ converges for all finite $\xi = t/\tau$, provided that $n = P_E/P > 1$. Thus no finite critical time exists.

References

[1] Freudenthal, A. M., *Some Time Effects in Structural Analysis*, Report 6th International Congress for Applied Mechanics, Paris, 1946.

[2] Freudenthal, A. M., *The Inelastic Behavior of Engineering Materials and Structures*, p. 518; John Wiley & Sons, Inc., New York, 1950.

[3] Rosenthal, D., and Baer, H. W., *An Elementary Theory of Creep Buckling of Columns*, Proceedings of the First U.S. National Congress of Applied Mechanics, Chicago, June 11–16, 1951; Edwards Bros. Inc., Ann Arbor, Mich., 1952.

[4] Libove, Charles, *Creep Buckling of Columns*, Journal of the Aeronautical Sciences, Vol. 19, No. 7, p. 459, July, 1952.

[5] Hilton, Harry H., *Creep Collapse of Viscoelastic Columns with Initial Curvature*, Journal of the Aeronautical Sciences, Vol. 19, No. 12, p. 844, December, 1952.

The Minimum Weight Design of Wings for Flutter Conditions

E. P. MacDonough

Chief of Structures, Chance Vought Aircraft Division, United Aircraft Corporation, Dallas, Tex.

April 22, 1953

Summary

A method is presented for defining the best distribution of material in a wing to obtain maximum values of primary bending and torsional frequencies for a given amount of structural weight. With this method, the essential information for a preliminary flutter analysis can be provided early in the design. This information includes mass distribution, primary bending, and torsional mode shapes and the relation between primary bending and torsional frequencies. It is necessary to determine what frequencies are needed to ensure freedom from flutter. The material requirements can then be determined directly. The procedure as presented is applicable only to the primary bending and torsional modes.

Discussion

The design of the primary structure of a wing is the result of compromises between the requirements for bending and torsional strength and bending and torsional stiffness. The methods for determining the optimum spanwise distribution of material to meet strength requirements are well known. It has generally been the practice to calculate the flutter speed that resulted when material was distributed according to the strength and aileron effectiveness requirements. With the increased speeds and lower thickness ratios that are being encountered, flutter requirements are becoming more critical and must therefore be given more consideration in establishing the wing design.

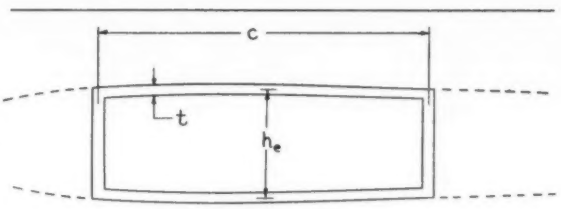

Fig. 1.

For a given wing plan form and weight distribution, the flutter speed is a function of the bending and torsional frequencies. It is, therefore, desirable to have a procedure by which the maximum frequencies can be obtained for a given amount of structural weight. The procedure presented below is applicable only to the primary bending and torsional modes of the wing.

The minimum strain energy for a given loading condition is obtained when the structural material is distributed in such a way that the energy per unit volume is constant throughout the structure. For vibrating systems it can also be shown that the minimum weight of structure to attain a given frequency is approached when the energy per unit volume is constant under the loading associated with the primary mode. The condition of constant energy per unit volume exists when a constant stress is used. With a constant stress, the deflection shape of the primary bending and torsional modes is a function of the effective depth of the wing primary structure. The acceleration at any point along the span can then be expressed as a function of the displacement. The spanwise distributions of acceleration and wing weight may be used to determine moment curves corresponding to the assumed primary mode shapes. The flange area and skin thickness can then be determined to resist the moments at any point along the span and provide the natural frequency that is necessary for the required flutter speed. The calculations for this work can be set up in a simple tabular form by dividing the wing into several chordwise strips. A detailed description of the procedures is presented below.

(*a*) *Torsional Frequency*

Consider a box beam, as shown in Fig. 1, where spanwise stations, y, are measured along the structural axis.

Flange area, $A_{fl.} = tc$.

Torsional shear stress, $f_s = T/2At = T/2A_{fl.}h_e$.

Angle of twist, $\theta = Tl/GJ = \gamma l[(1/h_e) + (1/c)]$, where γ = shearing strain.

At any station y,

$$\frac{\theta}{\gamma} = \int_0^y \left(\frac{1}{h_e} + \frac{1}{c}\right) dy$$

The torsional moment resulting from the inertia of a chordwise strip, where the inertia is I_p, is

$$\Delta T = I_p \omega^2 \theta$$

where ω is the *desired torsional frequency* in radians per second.

The torsional moment at any station is then

$$T = \sum_{i=y}^{l} \Delta T_i$$

(Note that the torsional moment will be expressed as a function of shearing strain, γ.)

The required flange area at any station can then be determined directly from the expression

$$A_{fl.} = T/2Gh_e\gamma$$

(*b*) *Bending Frequency*

The bending stress, $f_b = M/h_eA_{fl.}$

The radius of curvature of the deflected beam is $R = h_e/2\epsilon$ and the deflection at any station y is

$$\delta = \int_0^y \left[\int_0^y (2\epsilon/h_\epsilon) dy \right] dy = 2\epsilon \int_0^y \left[\int_0^y \left(\frac{1}{h_\epsilon} \right) dy \right] dy$$

The load resulting from the inertia of a chordwise strip, where the mass of the strip $m = w/g$, is

$$\Delta p = m\omega^2\delta$$

where ω is the *desired bending frequency* in radians per second.

The shear at any station is

$$S = \sum_{i=y}^{l} \Delta P_i$$

and the moment at any station is

$$M = \int_y^l S\, dy$$

(Note that the bending moment will be expressed as a function of bending strain, ϵ.)

The required flange area at any station can then be determined directly from the expression

$$A_{fl} = M/Eh_\epsilon\epsilon$$

In order to make effective use of this procedure, methods must be available to estimate the primary bending and torsional frequencies necessary to prevent flutter. The procedure then provides a systematic method for studying the influence of various parameters on the primary frequencies of a wing and provides the information needed to attain the required frequencies most efficiently.

Gap Effect on Slender Wing-Body Interference

H. Mirels
Cornell University, Ithaca, N.Y.
April 9, 1953

THE LIFT EFFECTIVENESS of wings that are hinged, rather than solidly connected, to a cylindrical body was discussed in a previous note.[1] This arrangement introduces a gap, between the body and wing root, which becomes more pronounced as the wing is differentially reflected in respect to the body. The presence of the gap reduces the lift of the wing-body combination. An estimate of this loss in lift has been published by Bleviss and Struble,[2] who replace the body by a reflecting wall and thus reduce the problem to one involving a wing and its mirror image. When the wing and body are at the same angle of attack, however, the loss of lift can be found exactly within the limitations of slender-body theory. The solution is presented herein. Unless otherwise specified, the notation is the same as that used in reference 1.

Consider the wing-body combination of Fig. 1. Both wing and body are at angle of attack α with respect to a free stream of velocity U. The body is cylindrical of radius a and the gap is of constant width $(y_1 - a)$. According to slender-body theory, the cross flow in each yz plane may be considered as a two-dimensional problem. The complex velocity in the yz plane can then be shown to equal

$$v - i(w + \alpha U) = -i\alpha U \times \left\{ \frac{\left(1 + \frac{a^2}{\zeta^2}\right)\left[\left(\zeta + \frac{a^2}{\zeta}\right)^2 - 4a^2 - \left(y_2 - \frac{a^2}{y_2}\right)^2 (E'/K')\right]}{\sqrt{\left[\left(\zeta + \frac{a^2}{\zeta}\right)^2 - \left(y_1 + \frac{a^2}{y_1}\right)^2\right]\left[\left(\zeta + \frac{a^2}{\zeta}\right)^2 - \left(y_2 + \frac{a^2}{y_2}\right)^2\right]}} \right\} \quad (1)$$

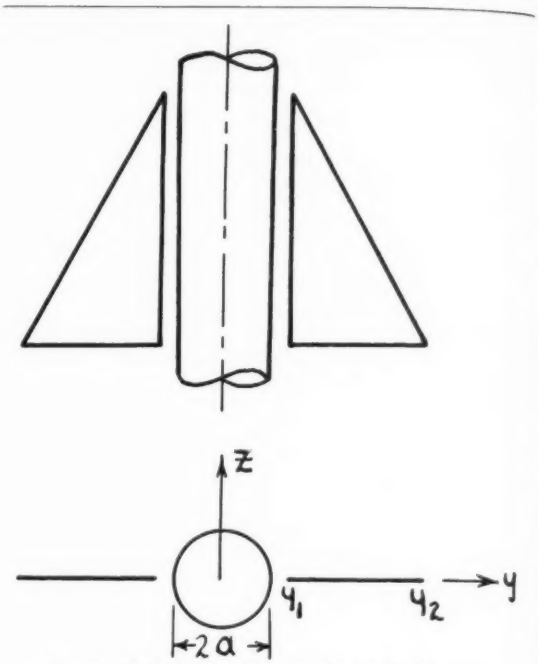

FIG. 1. Slender wing-body combination with gap.

Eq. (1) satisfies the following required boundary conditions:

(a) The velocity normal to the wing and body surface is $w = -\alpha U$ and $v_r = -\alpha U \sin\theta$, respectively.

(b) The perturbation velocity potential is zero in the plane of the wing for $a^2 \le \delta^2 \equiv y^2 \le y_1^2$.

(c) The complex velocity behaves like $1/\zeta^2$ for large ζ. In Eq. (1), K' and E' are complete elliptic integrals of the first and second kind with modulus

$$k' = \sqrt{\frac{(y_2^2 - y_1^2)(y_2^2 y_1^2 - a^4)}{y_1^2(y_2^2 - a^2)^2}}$$

The other symbols are defined in either Fig. 1 or reference 1.

The lift of the portion of the wing-body combination shown in Fig. 1 (i.e., excluding forebody lift) is then

$$\frac{L_{\alpha\alpha,\,g}}{2\pi q\alpha} = (y_2^2 + y_1^2)\left(1 + \frac{a^4}{y_1^2 y_2^2}\right) - 2\left(y_2 - \frac{a^2}{y_2}\right)^2 \left(\frac{E'}{K'}\right) - 4a^2 \quad (2)$$

Designating by $L_{\alpha\alpha}$ the lift for the no-gap case ($y_1 = a$ but y_2 unchanged),

$$L_{\alpha\alpha}/2\pi q\alpha = [y_2 - (a^2/y_2)]^2 \quad (3)$$

The loss of lift due to the presence of the gap is

$$L_{\alpha\alpha,\,g}/L_{\alpha\alpha} = 1 - 2(E'/K') + k^2 \quad (4)$$

where

$$\left.\begin{aligned} k &= \sqrt{1 - (k')^2} \\ &= \frac{y_2(y_1 + a)}{y_1(y_2 + a)}\left(\frac{y_1 - a}{y_2 - a}\right) \end{aligned}\right\} \quad (5)$$

From Eqs. (4) and (5) it is seen that the lift is a function of k only. For $k^2 \ll 1$, Eq. (4) becomes

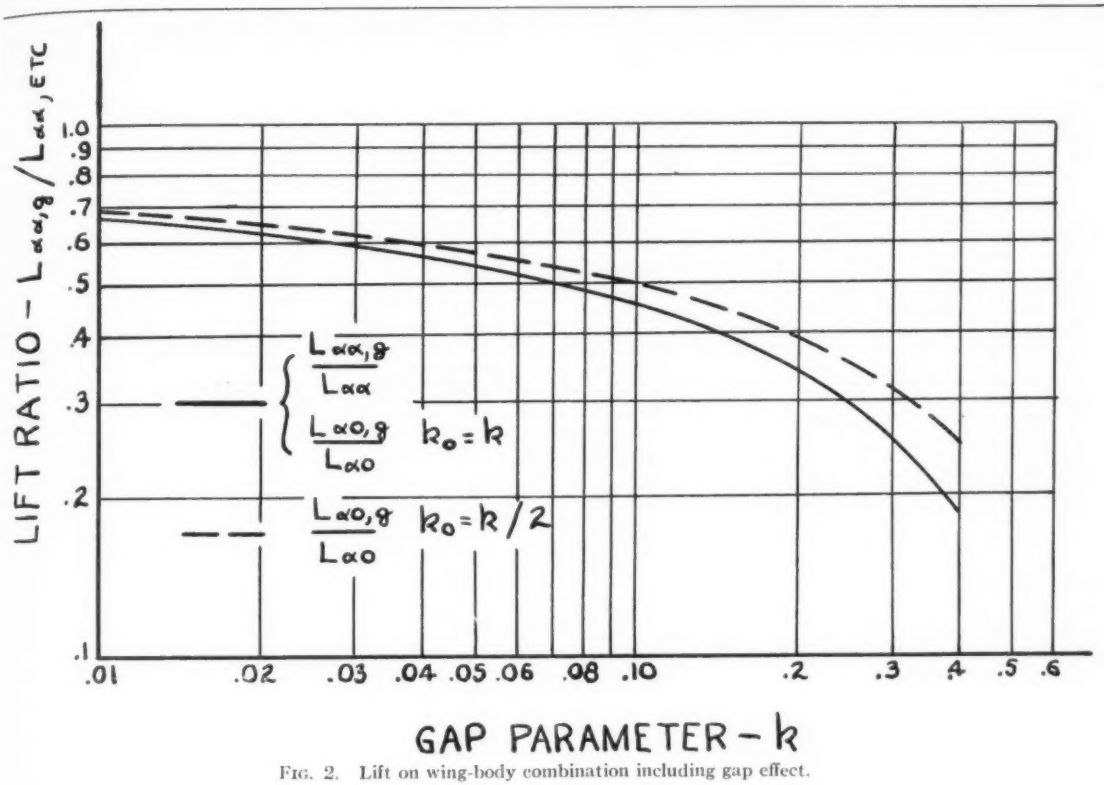

FIG. 2. Lift on wing-body combination including gap effect.

$$\frac{L_{\alpha\alpha,\,g}}{L_{\alpha\alpha}} = 1 - \frac{2}{\ln(4/k)}\left[1 - \frac{k^2}{2} + \frac{k^2}{4\ln(4/k)} + \cdots\right] \tag{6}$$

Eq. (4) is plotted as the solid line in Fig. 2. A logarithmic scale is used. Because of the logarithmic nature of K' for small k, the initial loss of lift, for even the most minute gap sizes, is relatively large. Thus, for $k = 10^{-6}$, the lift is 87 per cent of the no-gap value.

If the body is considered to act as a reflecting surface, carrying no lift and inducing no upwash, Eqs. (4) and (6) become

$$\left.\begin{aligned}\frac{L_{\alpha,\,g}}{L_\alpha} &= 1 - 2\left(\frac{E_0'}{K_0'}\right) + k_0^2 \\ &= 1 - \frac{2}{\ln(4/k_0)}\left[1 - \frac{k_0^2}{2} + \frac{k_0^2}{4\ln(4/k_0)} + \cdots\right]\end{aligned}\right\} \tag{7}$$

where the elliptic integrals are of modulus k_0' and

$$\left.\begin{aligned}k_0' &= \sqrt{1 - k_0^2} \\ k_0 &= (y_1 - a)/(y_2 - a)\end{aligned}\right\} \tag{8}$$

Eq. (7) corresponds to the case of an isolated slender wing at angle of attack α with a central semigap width of $y_1 - a$ and is a result presented in reference 2. It is noted that Eq. (7) has the same functional dependence on k_0 that Eqs. (4) and (6) have on k. These parameters differ, at most by a factor of 2. Namely,

$$k/2 \leq k_0 \leq k \tag{9}$$

If the effectiveness of the wing as a control surface is desired, it is necessary to solve for the case where the wing is at angle of attack α and the body is at zero angle of attack. The flow about such a configuration was presented in reference 1 for the no-gap case. When the gap effect is included, the solution appears to involve untabulated functions, even for the slender-body case, and recourse to numerical methods is required. It was shown in reference 1, for the no-gap case, that the lift of this configuration, $L_{\alpha 0}$, is equal (within 4 per cent) to the geometric mean of L_α and $L_{\alpha\alpha}$. If the same relationship is assumed to apply when a gap is present, then

$$\frac{L_{\alpha 0,\,g}}{L_{\alpha 0}} \cong \sqrt{\left(\frac{L_{\alpha,\,g}}{L_\alpha}\right)\left(\frac{L_{\alpha\alpha,\,g}}{L_{\alpha\alpha}}\right)} \tag{10}$$

Eq. (10) depends on both k_0 and k and is plotted in Fig. 2 for the limiting cases $k_0 = k/2$ and $k_0 = k$.

If there is no afterbody and the flight Mach Number is sufficiently above 1, slender-body theory tends to overestimate the lift on the body. In this case it may be more fruitful to follow the approach used in reference 2. The results of reference 2 become identical with those presented herein for $k_0 = k$.

The presence of a boundary layer will tend to modify the results for the case of very small gaps. Viscous effects might possibly be incorporated into Eqs. (4), (7), and (10) by multiplying k and k_0 by the ratio of the estimated mass flow through the gap (based on viscous considerations) divided by the theoretical value of mass flow based on potential theory. At any rate, with increasing gap size, the equations become more realistic and a large loss of lift is indicated.

REFERENCES

[1] Mirels, H., *Lift Effectiveness of Slender Wings on Cylindrical Bodies*, Readers' Forum, Journal of the Aeronautical Sciences, Vol. 20, No. 7, p. 504, July, 1953.

[2] Bleviss, Z. O., and Struble, R. A., *Some Aerodynamic Effects of Streamwise Gaps in Low-Aspect Ratio Lifting Surfaces at Supersonic Speeds*, IAS Preprint No. 396, 1953.

The Propulsive Efficiency and Best Division of Power in an Augmented Jet Engine

John Mitchell Stephenson
Research Associate, Division of Engineering, Brown University, Providence, R.I.
May 4, 1953

(1) Introduction

A HEAT ENGINE USED FOR PROPULSION consists of two basic elements: (a) a gas generator, which converts the chemical energy of the fuel burnt into the mechanical energy of a hot stream of gas; and (b) a propulsive device, which converts this energy into axial kinetic energy and, thence, into work done by forward thrust. The device consists of a jet nozzle, with or without the augmenting effect of a power turbine driving a screw propeller or fan.

Controversy over the best type of thrust conversion for a particular aircraft duty has touched most people connected with aeronautics in the past decade, and the subject is still unsettled. Even 5 years ago it was widely accepted that pure jet engines were only suitable for short-range military aircraft; that the turboprop gave a better range; but that, for extremely long routes, the old-style piston engine held the field. Today, exactly the opposite arrangement is often recommended. It is even less clear (except to their proponents) where the supersonic propeller and the by-pass engine fit in the economic scheme of aircraft operation.

The extra weight, complexity, and cost of an engine with augmentation of the jet is only justified by its higher propulsive efficiency in the required region of operation. Therefore, one step toward a solution of the problem is an analysis of the propulsive efficiency of engines with two separate sources of thrust.

An excellent discussion of the ideal propulsive ("Froude") efficiency of propellers and jets was given by A. V. Cleaver and D. H. Mallinson in *Aircraft Engineering* for June and September, 1945. But neither author considered the friction losses involved in the conversion process.

Then, in the issue of *Aviation Week* for November 15, 1948, there appeared an article on turboprops by Ivan H. Driggs which took the conversion efficiency into account. It was shown that there is an optimum division of power between propeller and jet, which depends not just on the forward speed but on a new "number"—the ratio of the ram power to the available engine power. Thus it is not possible to say, for instance, that "pure jets are the best above 500 m.p.h." It depends on the altitude and the engine top temperature, as well as the propeller efficiency. The analysis was based on the assumption that the *propulsive* efficiency of a propeller is constant.

In the present note it is only assumed that the *conversion* efficiencies of propellers, fans, and jet nozzles are constant—that is, that the friction coefficients of all the components are independent of scale. It then appears that for any value of Mr. Driggs' number ϕ, the optimum division of power between the two jet streams depends on the division of mass flow or "by-pass ratio." If this ratio is extremely large, as for a turboprop, the result is similar to that of Mr. Driggs. Curves of propulsive efficiency against ϕ are shown in Fig. 1 for by-pass ratios of 0, 1, 10, and ∞, assuming a jet efficiency of 0.95 and a fan efficiency (including the power turbine) of 0.80.

Many results of interest can be calculated from these curves. For example, the least efficiency of a supersonic propeller—below which the by-pass engine is better—is about 0.60 in the usual range of ϕ. Another result is that for an aircraft flying at 500 knots at the tropopause, a reduction of jet-engine top temperature from 1,150° to 900°K. gives approximately the same improvement in propulsive efficiency as augmenting with a by-pass ratio of 1.

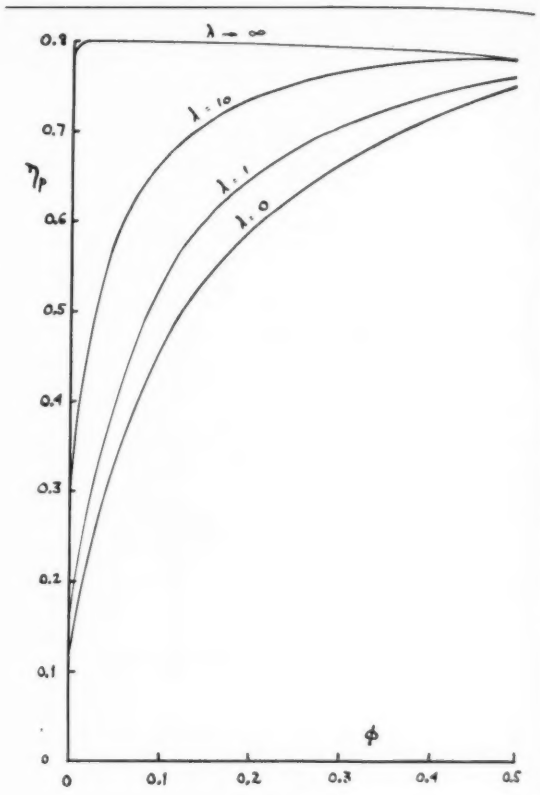

FIG. 1.

(2) The Propulsive Efficiency

Let G_t be the power generated, per unit mass flow, in an isentropic expansion from the pressure and temperature at the gas generator exit to atmospheric pressure. Let G_x be the net thrust power per unit air-mass flow. If the forward speed is v, the ram power of the entering air is $(1/2)v^2$. Then the propulsive efficiency is defined as the ratio of the thrust power to the power added to the air stream by the engine

$$\eta_p = G_x/[G_t - (1/2)v^2] \tag{1}$$

For comparison between engine types, it is sometimes better to write the numerator as $[G_x - C_D(1/2)v^2]$, where C_D is the external drag coefficient of the engine installation, based on the upstream entry cross-sectional area of the flow stream tube. But the drag will not be considered here.

Consider a system where the gas from the generator is exhausted through a propulsive jet, at a velocity v_j, but a fraction α of the available power is tapped off to drive a fan or propeller. The final exit velocity from the fan is v_f. Then, if the ratio of the mass flows through the fan and gas generator is λ—the "by-pass ratio"—we have

$$G_x = v(v_j - v) + \lambda v(v_f - v)$$

Hence, writing $(1/2)v^2/G_t$ as ϕ, Eq. (1) becomes

$$\eta_p = [2\phi/(1 - \phi)]\,[(v_j/v) + (\lambda v_f/v) - (1 + \lambda)] \tag{2}$$

Now we define the conversion efficiencies of the jet nozzle (η_j) and of the fan or propeller (η_f) as the ratio of the axial kinetic energy produced to the energy input. Thus,

$$\eta_j = (1/2)v_j^2/(1 - \alpha)G_t = \phi(v_j/v)^2/(1 - \alpha)$$

$$\eta_f = (1/2)\lambda(v_f^2 - v^2)/\alpha G_t = \lambda\phi[(v_f/v)^2 - 1]/\alpha$$

Substituting in Eq. (2), we find the propulsive efficiency to be

$$\eta_p = \frac{2\phi}{1-\phi}\left[\sqrt{\frac{(1-\alpha)\eta_j}{\phi}} + \sqrt{\lambda^2 + \frac{\lambda\alpha\eta_f}{\phi}} - (1+\lambda)\right] \quad (3)$$

There are two extreme cases of this propulsive system: firstly, the pure jet engine, when $\alpha = \lambda = 0$, and

$$\eta_p = [2\phi/(1-\phi)]\left(\sqrt{\eta_j/\phi} - 1\right) \quad (4)$$

Secondly, the turboprop, where λ is extremely large, and

$$\eta_p = \frac{2\phi}{1-\phi}\left[\sqrt{\frac{(1-\alpha)\eta_j}{\phi}} + \frac{\alpha\eta_f}{2\phi} - 1\right] \quad (5)$$

(3) The Best Division of Power

We can now find, for any value of ϕ, the value of α which gives the highest propulsive efficiency. For $\partial\eta_p/\partial\alpha = 0$ when

$$\alpha = \frac{1 - (\phi\eta_j/\eta_f^2)}{1 + (\eta_j/\lambda\eta_f)} \quad (6)$$

This shows that there is no gain in propulsive efficiency at all by augmenting when $\phi > \eta_f^2/\eta_j$.

For the turboprop, λ is extremely large, and Eq. (6) becomes

$$(1-\alpha) = \phi\eta_j/\eta_f^2 \quad (7)$$

and substituting in Eq. (5), the best efficiency of a turboprop is

$$\eta_p = \frac{2\phi}{1-\phi}\left(\frac{\eta_f}{2\phi} + \frac{\eta_j}{2\eta_f} - 1\right) \quad (8)$$

(4) Propeller Efficiency

The efficiency of a screw propeller is usually quoted in the form of thrust power divided by the torque—i.e., in such a way as to include the propulsive efficiency, as well as the friction and eddy losses. Thus, including the gear and power turbine losses as well, we define

$$\eta = \lambda v(v_f - v)/\alpha\, G_t$$

and Eq. (3) becomes

$$\eta_p = \frac{2\phi}{1-\phi}\left[\sqrt{\frac{(1-\alpha)\eta_j}{\phi}} + \frac{\alpha\eta}{2\phi} - 1\right] \quad (3a)$$

Then if we assume that η is constant, differentiation of Eq. (3a) yields the best division of power as

$$(1-\alpha) = \phi\eta_j/\eta^2 \quad (7a)$$

Substituting in Eq. (3a), we have the best efficiency of a turboprop as

$$\eta_p = \frac{2\phi}{1-\phi}\left(\frac{\eta}{2\phi} + \frac{\eta_j}{2\eta} - 1\right) \quad (8a)$$

However the assumption on which this latter analysis rests is certainly not true for a set of fans and may be doubted for a wide range of propellers.

I have recently learned that P. C. Gupta, of Bristol, England, has arrived at a more complete result. In particular, he takes into account the intake efficiency η_i and the outlet efficiency η_0 of the fan duct, so that the fan efficiency is written

$$\eta_f = (\lambda\phi/\alpha)\cdot[(v_f/v)^2/\eta_0 - \eta_i]$$

The expressions for the propulsive efficiencies of the pure jet and the turboprop are, of course, unaltered, but the best division of power in the by-pass engine takes a form slightly different from Eq. 6,

$$\alpha = \frac{1 - (\phi\eta_j\eta_i/\eta_f^2\eta_0)}{1 + (\eta_j/\lambda\eta_f\eta_0)}$$

This refinement of the analysis is valuable, for it shows that the by-pass engine is extremely sensitive to the quality of the fan duct

On the Role of Three-Dimensional Disturbances in the Stability of Supersonic Boundary Layers*

D. W. Dunn and C. C. Lin
Department of Mathematics, Massachusetts Institute of Technology, Cambridge, Mass.

May 4, 1953

In a previous note,[1] it has been pointed out that, although the equations for three-dimensional disturbances in a compressible fluid transform formally to two-dimensional ones, it cannot be concluded from the properties of the transformation that three-dimensional disturbances necessarily have a higher critical Reynolds Number of instability (as in the case of an incompressible fluid[2]). Calculations have now been carried out to demonstrate this point with numerical results and to show the exact nature of this effect of three-dimensional disturbances.

The case considered is a boundary layer in a gas with a free-stream Mach Number $M = 1.6$. For convenience of calculation, the viscosity coefficient is taken as proportional to the absolute temperature. Estimation of errors involved shows that this approximation would not influence the main results to any appreciable extent.

Present calculations show that two-dimensional disturbances will be completely stabilized[3] at a wall-to-free-stream temperature ratio of 1.073. The critical Reynolds Number of wavy three-dimensional disturbances is obtained as a function of the angle θ, which the direction of propagation of a given wave makes with the free stream. For convenience of application, the Reynolds Number is represented in terms of the downstream distance in Fig. 1.

It is seen that the oblique disturbances have a critical Reynolds Number of the order of 10^6, leading to the conjecture that the transition Reynolds Number would be of the order of 10^7–10^8, with turbulence level prevailing under ordinary experimental conditions. Thus, by such cooling processes, one can materially

* Work done under Contract N5ori-07872 of the Office of Naval Research.

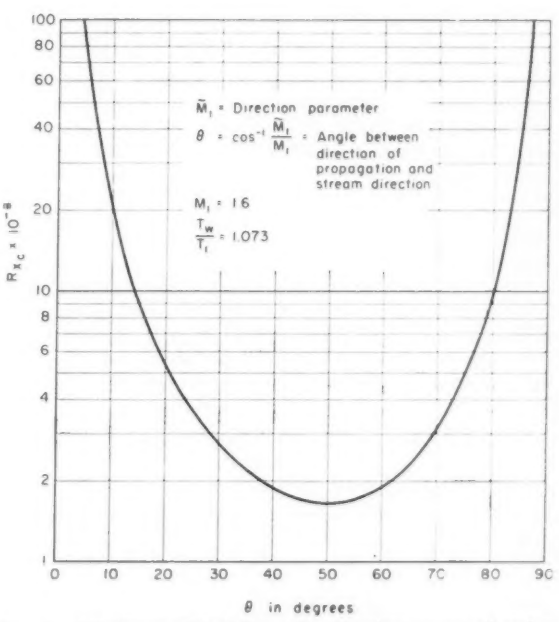

Fig. 1. Minimum critical Reynolds Number versus direction of propagation of oblique waves.

delay the transition process but *cannot achieve complete stabilization*.

Studies of small disturbances also lead to the conjecture that surface roughness is not always so effective in producing transition in the boundary layer in the supersonic case as in the subsonic case. The disturbance produced by a stationary roughness (including surface roughness and other stationary obstacles) is a supersonic disturbance[4] and has the nature of a Mach wave outside the boundary layer. The energy of such disturbances is easily carried away from the boundary layer in the nature of sound waves.

References

[1] Dunn, D. W., and Lin, C. C., *The Stability of the Laminar Boundary Layer in a Compressible Fluid for the Case of Three-Dimensional Disturbances*, Journal of the Aeronautical Sciences, Vol. 19, No. 7, p. 491, July, 1952.

[2] Squire, H. B., *On the Stability for Three-Dimensional Disturbances of Viscous Fluid Flow Between Parallel Walls*, Proc. Roy. Soc. London, A142, pp. 621–628, 1933.

[3] Lees, L., *The Stability of the Laminar Boundary Layer in a Compressible Fluid*, NACA TR No. 876, 1947 (formerly NACA TN No. 1360).

[4] Lees, L., and Lin, C. C., *Investigation of the Stability of the Laminar Boundary Layer in a Compressible Fluid*, NACA TN No. 1115, 1946.

Apparent Recovery Factors on the Leading Edge of a Flat Plate in Supersonic Laminar Flow

Irving Korobkin

U.S. Naval Ordnance Laboratory, White Oak, Silver Spring, Md.

April 16, 1953

WIND-TUNNEL MEASUREMENTS on a flat plate with a supersonic laminar boundary layer consistently result in the determination of recovery factors higher than the theoretically predicted value, $Pr^{0.5}$, and the experimental values obtained on cones.[1–5] The leading edge of the flat plate model is usually beveled away from the measuring surface forming a wedge, and it will be shown that the high recovery temperature measurements are the result of steady-state heat conduction in the wedge.

An approximate calculation of recovery temperature can be made for a thin flat plate with its measuring surface oriented parallel to the flow and with a solid metallic wedge of small angle which is insulated from the rest of the model as the upstream section. In Fig. 1 the origin of the orthogonal coordinate system used in the calculation is located at the tip of the model with the x-axis lying along the wedge-angle bisector.

The measuring surface of the plate (Surface 2) has a local free-stream Mach Number equal to the Mach Number upstream from the model, but the other surface (Surface 1) has a lower free-stream Mach Number because of the presence of a shock wave produced by the flow deflection. It will be assumed that each surface has a different constant recovery factor equal to $Pr^{0.5}$ based on conditions outside the boundary layer adjacent to each surface, with the corresponding recovery temperatures being T_1 and T_2.

The contour of the wedge can be specified by

$$y = Kx \tag{1}$$

The expression for the local heat-transfer coefficient on an isothermal flat plate with laminar boundary layer is given in reference 6 as

$$Nu = 0.29 Pr^{1/3} Re^{0.5} \tag{2}$$

where Nu is Nusselt Number, Pr is Prandtl Number, and Re is Reynolds Number. Therefore on each surface

$$h_1 = A/x^{0.5}, \qquad h_2 = B/x^{0.5} \tag{3}$$

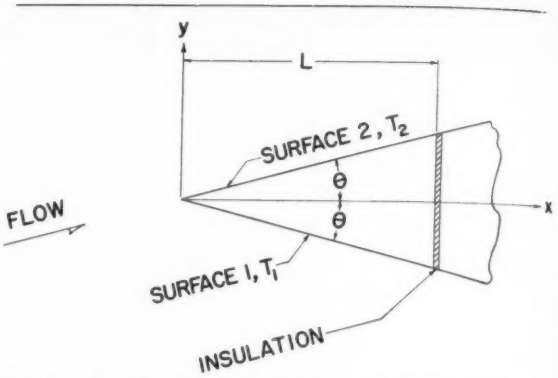

FIG. 1. Beveled leading edge of flat plate with supersonic laminar boundary layer.

where A and B are constants of proportionality and h is the local heat-transfer coefficient. Assuming the plate to be thin and the wedge angle small, the variation in plate temperature in the y-direction may be neglected. The following differential equation then describes the steady-state heat-transfer process in the wedge:

$$\frac{d}{dx}\left(2y\, k_w \frac{dT_w}{dx}\right) = h_1(T_w - T_1) + h_2(T_w - T_2) \tag{4}$$

where k_w is the thermal conductivity of the wedge and T_w is the wedge temperature.

After substituting y, h_1, and h_2, the following expression is obtained:

$$\frac{d}{dx}\left(x \frac{dT_w}{dx}\right) - cx^{-0.5}(T_w - \tau) = 0 \tag{5}$$

where $c = (A + B)/2k_wK$ and $\tau = (AT_1 + BT_2)/(A + B)$.

Eq. (5) is now reduced to the same form as used in reference 7 for heat transfer to a wedge-shaped fin in natural convection, the resulting solution being

$$T_w - \tau = EJ_0(4x^{1/4} i\sqrt{c}) + FY_0(4x^{1/4} i\sqrt{c}) \tag{6}$$

where E and F are integration constants and J_0 and Y_0 are Bessel functions of first and second kinds of order zero. When x equals zero, then

$$Y_0(4x^{1/4} i\sqrt{c}) = \infty \tag{7}$$

Since the temperature is finite along the wedge, F must be zero and, therefore,

$$T_w - \tau = EJ_0(4x^{1/4} i\sqrt{c}) \tag{8}$$

The insulation at $x = L$ means that

$$dT_w/dx|_{x=L} = 0 \tag{9}$$

Since

$$dT_w/dx|_{x=L} = 0 = -Ei\sqrt{c}L^{-3/4} J_1(4L^{1/4} i\sqrt{c}) \tag{10}$$

then

$$E = 0, \qquad T_w = \tau \tag{11}$$

The above analysis indicates that the entire wedge, under the assumed conditions, is at a constant temperature that justifies the use of Eq. (2) for the local heat-transfer coefficient on an isothermal flat plate.

The apparent recovery factor measured on the wedge is given by

$$r = (\tau - T_{\infty 2})/(T_0 - T_{\infty 2}) \tag{12}$$

where T_0 is stagnation temperature and $T_{\infty 2}$ is local free-stream temperature along the measuring surface.

TABLE 1

Wedge Angle (2θ of Fig. 1)	Apparent Recovery Factor
0°	0.869
5°	0.874
10°	0.880
15°	0.887
20°	0.897

Table 1 is based on the foregoing analysis and is computed at a Mach Number of 2.4 for a supersonic wind tunnel with a 1-atmosphere supply pressure and a 300°K. supply temperature, where the theoretical value of recovery factor based on free-stream conditions is 0.869.

It can be seen from Table 1 that the wedge is at a temperature higher than the value obtained from $Pr^{0.5}$ when calculated for the measuring surface of the flat plate. Consequently, the boundary layer in contact with the wedge is warmer than under zero heat-transfer conditions. The effects of this high temperature are felt downstream along the main part of the model, since the plate now attains thermal equilibrium with a boundary layer of higher temperature resulting in the measurement of erroneous recovery factors. This phenomenon must be considered when dealing with all flat-plate wind-tunnel models with laminar boundary layers. Though the above analysis assumes a thin plate with a solid metallic wedge of small angle which is insulated from the rest of the model, the same effects will be present in flat plates with different details of construction.

REFERENCES

[1] Johnson, H. A., and Rubesin, M. W., *Aerodynamic Heating and Convective Heat Transfer*, Summary of Literature Survey, Trans. ASME, Vol. 71, p. 447, 1949.

[2] Blue, R. E., *Interferometer Corrections and Measurements of Laminar Boundary Layer in Supersonic Stream*, NACA TN No. 2110, 1950.

[3] Stalder, J. R., Rubesin, M. W., and Tendeland, T., *A Determination of the Laminar, Transitional, and Turbulent Boundary Layer Recovery Factors on a Flat Plate in Supersonic Flow*, NACA TN No. 2077, 1950.

[4] Slack, E. G., *Experimental Investigation of Heat Transfer through Laminar and Turbulent Boundary Layers on a Cooled Flat Plate at a Mach Number of 2.4*, NACA TN No. 2686, 1952.

[5] Eber, G. R., *Recent Investigation of Temperature Recovery and Heat Transmission on Cones and Cylinders in Axial Flow in the NOL Aeroballistics Wind Tunnel*, Journal of the Aeronautical Sciences, Vol. 19, No. 1, p. 1, January, 1952.

[6] Crocco, L., *Laminar Boundary Layer in Gases*, Translation, North American Aviation, Inc., Report CF-1038, 1948.

[7] Boelter, L. M. K., Cherry, V. H., Johnson, H. A., and Martinelli, R. C., *Heat Transfer Notes*, p. 11 b-16, University of California Press, 1948.

Effect of Gas Radiation in the Boundary Layer on Aerodynamic Heat Transfer

John W. Smith
Aerodynamicist, Bell Aircraft Corporation, Buffalo, N.Y.

May 7, 1953

THE USUAL CALCULATION of skin temperatures in very-high-speed supersonic flight involves the balancing of two major terms: heat conducted into the skin from the boundary layer, and heat radiated by the skin into outer space. The latter keeps skin temperatures at values less than adiabatic wall temperature and also lowers temperatures in the interior of the boundary layer. Nevertheless, at critical flight conditions, temperatures many times higher than skin temperature can occur in the boundary layer. This raises the question whether radiant emission and absorption by the gas molecules in the boundary layer, hitherto neglected, can appreciably influence the aerodynamic heating. Skin temperatures could be affected in two ways: (1) radiant heating or cooling of gas elements in the boundary layer can alter the temperature profile, causing a change in the conduction heat-transfer coefficient; and (2) radiant emission from gas molecules causes an additional quantity of heat to be transmitted to the skin. These effects will be briefly considered here.

The chief constituents of atmospheric air are nitrogen and oxygen molecules, which are practically inert in the infrared frequency range. The greatest contribution to radiative heat transfer in atmospheric air is due to relatively minor constituents, such as water vapor and carbon dioxide. The chemical composition of the boundary layer, on the other hand, may differ appreciably from atmospheric air because of the high temperatures, with the result that such gases as nitric oxide may contribute appreciably to the radiative heat transfer. For the present it will be assumed that there exists a certain density concentration n of radiating gases in the boundary layer and that the emissivities of these gases are comparable to that of water vapor. Let the emissivity ϵ of a thin slab of gas be defined as the total energy emitted across a unit area of one face in unit time divided by the black body intensity σT^4 (σ = Stefan-Boltzmann constant; T = gas temperature). For slabs of small optical thickness $n\rho y$ (ρ = total density; y = thickness), the emissivity is expressible in the differential form,

$$d\epsilon = \phi(T) n \rho \, dy \tag{1}$$

where $\phi(T)$ is independent of y—i.e., reabsorption can be neglected. Consider now the radiative energy balance for an infinitesimal slab of gas in the boundary layer with faces parallel to the solid surface. The incident radiant intensity transmitted across the lower surface of the slab is approximately σT_w^4 (T_w = skin temperature). Since absorptivity and emissivity are related by Kirchhoff's law, one obtains

$$\frac{de}{dt} = \sigma \frac{d\epsilon}{dy} (T_w^4 - \beta T^4) = \sigma \phi(T) n \rho (T_w^4 - \beta T^4) \tag{2}$$

where de/dt is the rate of change of energy in the slab per unit volume and the geometrical factor $\beta \cong 2$. The instantaneous radiative cooling is therefore given by

$$\frac{dT}{dt} = \frac{1}{\rho c_p} \frac{de}{dt} = \frac{\sigma \phi(T) n}{c_p} (T_w^4 - \beta T^4) \tag{3}$$

For the numerical example cited below, this can assume negative values of about 10^{4}°R. per sec.

In order to calculate the effect of radiative cooling on the temperature profile, it is necessary to solve the boundary-layer energy equation subject to an additional term expressed by Eq. (2). The modified energy equation (in the ordinary notation) is

$$\rho u \frac{\partial}{\partial x}(c_p T) + \rho v \frac{\partial}{\partial y}(c_p T) = u \frac{\partial p}{\partial x} + \frac{\partial}{\partial y}\left(k \frac{\partial T}{\partial y}\right) + \mu \left(\frac{\partial u}{\partial y}\right)^2 + \frac{de}{dt} \tag{4}$$

Let $T = T_0 + \theta$, where T_0 satisfies the energy equation neglecting the radiation term. Then θ satisfies the equation

$$\rho u \frac{\partial}{\partial x}(c_p \theta) + \rho v \frac{\partial}{\partial y}(c_p \theta) = \frac{\partial}{\partial y}\left(k \frac{\partial \theta}{\partial y}\right) + \frac{de}{dt} \tag{5}$$

Suppose, for the moment, that ρ, u, and T depend only on the "similarity variable" $\eta = y/\sqrt{x}$, and let Eq. (5) be transformed from the (x, y) plane to the (x, η) plane. One can eliminate ρv by use of the continuity equation

$$\rho v = -\frac{\partial}{\partial x}\int_0^y \rho u \, dy = -\frac{1}{2\sqrt{x}}\left(\int_0^\eta \rho u \, d\eta - \eta \rho u\right) \tag{6}$$

Eq. (5) then becomes

$$\left(-\frac{1}{2x}\int_0^\eta \rho u\, d\eta\right)\frac{d\theta}{d\eta} = \frac{1}{x}\frac{d}{d\eta}\left(k\frac{d\theta}{d\eta}\right) + \frac{de}{dt} \qquad (7)$$

Because of the radiation term, x does not drop out, and the assumption of similar profiles cannot be maintained.

This result greatly complicates the general solution of Eq. (5). The approach adopted here assumes that the convection terms are small in comparison to the conduction term for points sufficiently far downstream. This leads to a simple solution for θ, which in turn is used to justify the given assumption *a posteriori*. Neglecting convection terms, Eq. (5) becomes an ordinary differential equation,

$$(d/dy)\,[k(d\theta/dy)] + (de/dt) = 0 \qquad (8)$$

As a first approximation, one can set $T = T_0$ in the radiation term to obtain the integral,

$$\theta = \sigma n \int_0^y dy' \, k^{-1}(T_0)\int_0^{y'} dy''\phi(T_0)\rho(\beta T_0^4 - T_w^4) + K_1\int_0^y k^{-1}(T_0)\,dy + K_2 \qquad (9)$$

The integration constants K_1 and K_2 are determined by the condition that θ vanish at the boundaries $y = 0$ and $y = \delta$ (δ = boundary-layer thickness).

We are now in a position to calculate the change in heat conduction—viz.,

$$\Delta q = \left[k\left(\frac{\partial T}{\partial y} - \frac{\partial T_0}{\partial y}\right)\right]_{y=0} = K_1 \qquad (10)$$

as well as the radiative heat transfer from the boundary layer to the skin, the latter being expressible as an effective reduction in the emissivity of the skin by an amount $\Delta\epsilon$. According to Eq. (1), this becomes

$$\Delta\epsilon = -n\int_0^\delta \phi(T)\rho\left(\frac{T}{T_w}\right)^4 dy \qquad (11)$$

A numerical calculation was carried out for the following condition: flight Mach Number = 20; altitude = 150,000 ft., ratio of wall to free-stream temperature = 4; n (active gas concentration) = 1/10; and x (distance from the leading edge) = 10 ft. Laminar T_0-profiles were taken from Van Driest,[1] and $\phi(T)$ was taken from the data of Hottel and Egbert[2] for water-vapor emissivities. The results are, summarily,

$$\begin{aligned}(\theta/T)_{max.} &= -2.2\times10^{-3}\\ (\Delta q/q) &= -1.7\times10^{-3}\\ \Delta\epsilon &= -5.3\times10^{-4}\end{aligned}$$

indicating effectively no change in any of the given quantities. It should be noted that the net effect, though small, tends to lower the equilibrium skin temperature.

References

[1] Van Driest, E. R., *Investigation of the Laminar Boundary Layer in Compressible Fluids Using the Crocco Method*, NACA TN No. 2597, January, 1951.

[2] Hottel, H. C., and Egbert, R. B., *Radiant Heat Transmission from Water Vapor*, Trans. Am. Inst. Chem. Eng., Vol. 38, No. 3, June, 1941.

On the Flow at the Rear of a Two-Dimensional Supersonic Airfoil with Thickness*

Ronald F. Probstein
Assistant Professor, Aeronautical Engineering Department, Princeton University, Princeton, N.J.

May 4, 1953

A TREATMENT OF THE PROBLEM of the flow deflection immediately rearward of a two-dimensional supersonic airfoil was given by Kahane and Lees[1] in 1948. Their analysis was carried out on the basis of oblique shock and Prandtl-Meyer wave theory, utilizing the fact that the dynamic and static pressure change through isentropic and shock waves can be expressed as a power series in the flow deflection angle. Since, to the writer's knowledge, this is the only place where the dynamic pressure coefficients have been published, it was thought worth while to point out that one of the coefficients in the expansion for an isentropic wave (also appearing in the shock expansion) appears to be incorrect.

The authors expressed the change in dynamic pressure through an isentropic wave as

$$\Delta q = q_1(\pm G_1\theta + G_2\theta^2 \pm G_3\theta^3 + \dots)$$

and through a shock wave as

$$\Delta q = q_1(\pm G_1\theta + G_2\theta^2 \pm (G_3 - H)\theta^3 + \dots)$$

where $q = \rho w^2/2$ (ρ = density, w = flow velocity); θ is the angle of deflection, positive in a counterclockwise sense; and q_1 is the dynamic pressure ahead of the wave. The corrected value for G_3 should be

$$G_3 = \frac{\frac{(3-\gamma)(2-\gamma)}{12}M^{10} + \frac{(-3\gamma^2+17\gamma-36)}{12}M^8 + \frac{(21-4\gamma)}{3}M^6 - 8M^4 + \frac{14}{3}M^2 - \frac{4}{3}}{(M^2-1)^{7/2}}$$

where M is the flow Mach Number ahead of the wave.

Determination of the flow angle immediately rearward of a flat-plate airfoil at angle of attack and for a thick airfoil at angle of attack, where it was assumed that the configuration was such that four oblique shock waves were attached to the nose and tail of the airfoil (see Fig. 1), was carried out. Fortunately, the calculations did not involve the use of the incorrect coefficient G_3 directly. In spite of this, however, for the thick airfoil shown in Fig. 1, the analytic formulation of the flow deflection angle β to first order appears to be incorrect.

* This note is an outgrowth of work supported by the Office of Naval Research and Office of Scientific Research, ARDC, U.S. Air Force, under Contract No. N6-onr-270.

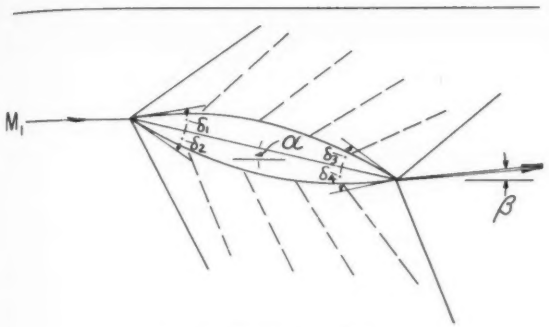

FIG. 1. The thick airfoil.

Recalculation of β gives

$$\beta = \frac{D}{2C_1}\left[(\delta_2+\alpha)^3 + (\delta_1-\alpha)^3 - (\delta_4-\alpha)^3 - (\delta_2+\alpha)^3\right] +$$

$$\frac{E}{2C_1}\left[(\delta_2+\alpha)^4 + (\delta_1-\alpha)^4 - (\delta_4-\alpha)^4 - (\delta_2+\alpha)^4\right] +$$

$$H/2\left[(\delta_2+\alpha)^4 - (\delta_1-\alpha)^4\right] -$$

$$\frac{[(dD/d\theta) + DG_1]}{2C_1}\left[(\delta_3+\alpha)^4 - (\delta_4-\alpha)^4\right]$$

where D, C_1, and E are the coefficients of θ in the following expansion for the static pressure change through an oblique shock wave:

$$\Delta p = q_1\left[\pm C_1\theta + C_2\theta^2 \pm (C_3 - D)\theta^3 + (C_4 - E)\theta^4 \pm \ldots\right]$$

The required coefficients for the determination of β are functions only of the free-stream Mach Number, M_1, and the ratio of specific heats, γ. Their values (other than E) are given in reference 1, while $(C_4 - E)$ may be found in reference 2. The computation of C_4 and, hence, E is easily carried out by use of the results of Miles.[3]

REFERENCES

[1] Kahane, A., and Lees, L., *The Flow at the Rear of a Two-Dimensional Supersonic Airfoil*, Journal of the Aeronautical Sciences, Vol. 15, No. 3, pp. 167–170, March, 1948.

[2] Hilton, W. F., *High-Speed Aerodynamics*, p. 226; Longmans, Green & Company, New York, 1951.

[3] Miles, E. R. C., *Supersonic Aerodynamics*, pp. 245–246; McGraw-Hill Book Company, Inc., New York, 1950.

Interaction of a Plane Flame Front with a Plane Sinusoidal Shear Wave*

George H. Markstein
Head, Combustion Section, Cornell Aeronautical Laboratory, Inc., Buffalo, N. Y.

May 6, 1953

THE INTERACTION OF A WEAK PLANE DISTURBANCE with a plane shock wave has been studied recently by several investigators.[1–3] These linearized treatments were carried out as a first step toward the solution of problems of interaction between turbulent flow and shock waves. An analogous approach to the problem of interaction between turbulent flow and flame fronts appears to be of interest, particularly in connection with observations and analyses of "flame-generated turbulence."[4, 5]

Following the procedure of references 1 and 3, the general case of interaction between a combustion wave with an oblique sinusoidal shear wave can be transformed into a steady-flow problem by superposing a velocity V tangential to the flame front that makes the resultant flow velocities parallel to the shear waves. This is shown in Fig. 1, which is analogous to Fig. 2 of reference 1. The case of the combustion wave differs from that of the shock wave, however, in the following respects:

(1) Since the burning velocity S_u is extremely small compared to the speed of sound (the Mach Number is of the order of 10^{-3} for hydrocarbon-air mixtures), compressibility effects can be neglected, except for almost glancing intersection of the waves (φ and ψ nearly 90°), where the fictitious sweep velocity V and the resultant velocities W_u and W_b may approach and surpass sonic values.

(2) For subsonic resultant velocity W_u, a perturbation potential flow must be considered upstream, as well as downstream, of the combustion wave.

(3) While plane shock waves are always stable, combustion waves may be unstable,[6] at least for wave lengths of the disturbance larger than a critical wave length λ_s. This circumstance obviously reduces the range of validity of linearized analysis.

In the present note, only the case of normal intersection of shear wave and combustion wave, $\varphi = \psi = 0$, will be discussed in detail. For this case, the linearized equations of incompressible and nonviscous flow are satisfied by the perturbations

$$\left.\begin{aligned} u_u/S_u &= (A_0 + A_1 e^{kx})e^{iky} \\ iv_u/S_u &= p_u/\rho_u S_u^2 = -A_1 e^{k(x+iy)} \end{aligned}\right\} \qquad (1)$$

upstream ($x < 0$), and

$$\left.\begin{aligned} u_b/S_u &= (A_2 e^{-kx} + A_3)e^{iky} \\ -i\,v_b/S_u &= p_b/\rho_u S_u^2 = -A_2 e^{k(-x+iy)} \end{aligned}\right\} \qquad (2)$$

downstream ($x > 0$) of the flame front. Here A_0, A_3 are the amplitudes of the respective shear flows and A_1, A_2 those of the potential flows, all referred to the burning velocity S_u, and $k = 2\pi/\lambda$ is the wave number.

The problem consists of determining A_1, A_2, A_3 for given $A1$ from the boundary conditions at the flame front. The sinusoidal displacement x_F of the latter, which is caused by the flow disturbance, can be written

$$kx_F = A_4 e^{iky} \qquad (3)$$

with a further unknown amplitude factor A_4. The simplest boundary conditions would be obtained by assuming constant density ratio $\rho_u/\rho_b = \epsilon$ and constant burning velocity S_u. However, these assumptions imply instability of the flame front for *all* wave numbers[6] and would thus invalidate the linearized analysis completely. While it seems reasonable to retain the as-

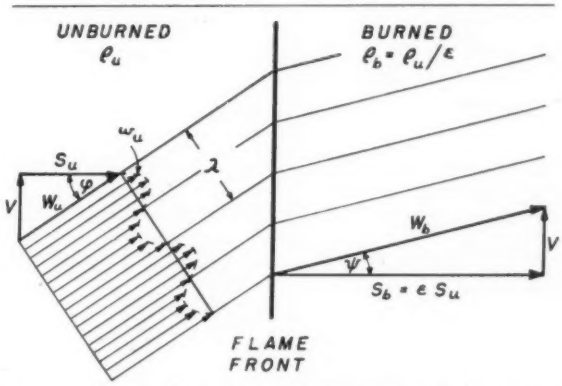

FIG. 1. Oblique interaction of flame front and shear wave treated as steady-flow problem.

* This work was conducted under the auspices of Project SQUID, jointly sponsored by ONR, ARDC, and OOR under Contract N6-ori-105, T.O.III, Subcontract 1.

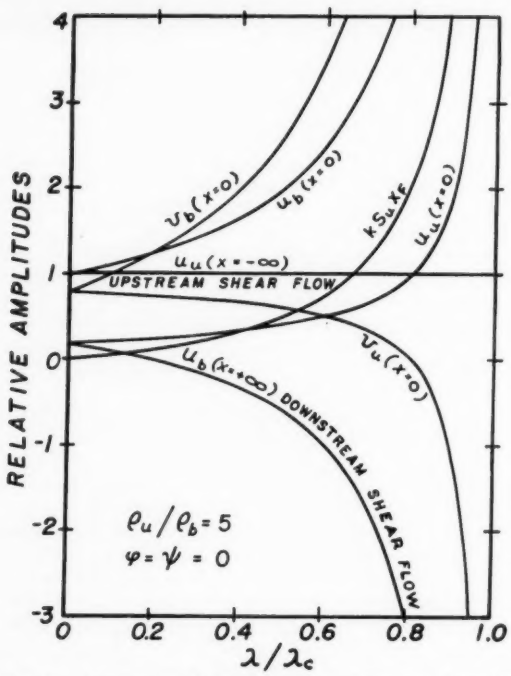

FIG. 2. Amplitudes of velocity perturbations and flame front deflection relative to that of upstream shear flow. Signs are based on u_u, u_b, and $x_F \propto \cos ky$, v_u and $v_b \propto \sin ky$.

sumption ρ_u/ρ_b = constant, the influence of transport processes and chemical kinetics will normally cause perturbations of the burning velocity. Because of our present ignorance about the details of these effects, they are lumped into a phenomenological parameter μ. The first-order perturbation of burning velocity is thus introduced, as in previous work, in the form

$$s_u/S_u = \mu L/R = -\mu L(d^2x_F/dy^2) = \sigma A_4 e^{iky} \tag{4}$$

with

$$\sigma = k\mu L = 2\pi\mu L/\lambda \tag{5}$$

where R is the local radius of curvature of the distorted flame front and L is a length of the order of the thickness of the combustion zone.

With these assumptions, the boundary conditions for velocity components and pressure lead to the equations

$$\left.\begin{aligned} A_1 &\qquad\qquad -\sigma A_4 = -A_0 \\ A_2 + A_3 &\qquad\quad -\epsilon\sigma A_4 = 0 \\ A_1 + A_2 &\qquad -(\epsilon-1)A_4 = 0 \\ A_1 - A_2 &\qquad +2\sigma(\epsilon-1)A_4 = 0 \end{aligned}\right\} \tag{6}$$

The determinant of the coefficients of this system vanishes for $\sigma = (\epsilon - 1)/2\epsilon$, a value corresponding to the wave length of neutral stability

$$\lambda_c = 4\pi\mu L\epsilon/(\epsilon - 1) \tag{7}$$

The linearized analysis breaks down for $\lambda > \lambda_c$, since for these wave lengths the flame front is unstable.[6] A lower limit is obviously also imposed on λ by the finite width of the combustion zone.

Substituting Eqs. (5) and (7), one arrives at the following solutions of Eqs. (6):

$$\left.\begin{aligned} A_1 &= A_0(\lambda/\lambda_c + \epsilon^{-1} - 1)/(1 - \lambda/\lambda_c) \\ A_2 &= A_0(\lambda/\lambda_c - \epsilon^{-1} + 1)/(1 - \lambda/\lambda_c) \\ A_3 &= A_0(\epsilon^{-1} - \lambda/\lambda_c)/(1 - \lambda/\lambda_c) \\ A_4 &= 2A_0(\lambda/\lambda_c)/[(\epsilon - 1)(1 - \lambda/\lambda_c)] \end{aligned}\right\} \tag{8}$$

These results are plotted in Fig. 2 in the form of amplitudes of the various perturbations relative to that of the upstream shear flow.

Even though no detailed conclusions regarding the much more complicated case of flame-generated turbulence can be drawn from this specialized result, certain features would seem to be of general significance. Thus, amplification of shear flow by the flame occurs only for

$$\lambda/\lambda_c > (1/2)(\epsilon^{-1} + 1)$$

although the flow perturbations immediately downstream of the flame front always exceed the upstream shear flow in amplitude. This distinction between shear flow and local potential flow that decays to extremely small amplitude within a few wave lengths up- and downstream of the flame would appear to be of equal importance in the case of actual turbulence.

Another prominent feature of the Eqs. (8) is the "resonance" that occurs when λ approaches λ_c. This effect will, in reality, be suppressed to some extent by the leveling influence of nonlinearity on amplitude. Moreover, the amplitudes tend toward infinity only for normal intersection; in the oblique case one finds that the coefficient determinant vanishes only for a complex value of σ, and thus no true resonance occurs for real values of λ. In spite of these factors, one would still expect a different response of flames to turbulent approach flow, depending on whether λ_c is large compared with the scale of turbulence or not. This expectation seems indeed to be borne out by observations on lean and rich turbulent butane flames.[7]

A fuller account of this work will be published later.

REFERENCES

[1] Ribner, H. S., *Convection of a Pattern of Vorticity Through a Shock Wave* NACA TN No. 2864, January, 1953.

[2] Moore, F. K., *Unsteady Oblique Interaction of a Shock Wave with a Plane Disturbance*, NACA TN No. 2879, January, 1953.

[3] Kovasznay, L. S. G., and Morkovin, M. V., Unpublished Work; cf Project SQUID Semi-Annual Report, 1 October, 1952, p. 22.

[4] Williams, G. C., Hottel, H. C., and Scurlock, A. C., *Flame Stabilization and Propagation in High Velocity Gas Streams*, Third Symposium on Combustion, Flame and Explosion Phenomena, p. 21; Williams & Wilkins, Baltimore, 1949. Scurlock, A. C., and Grover, J. H., *Propagation of Turbulent Flames*, Fourth Combustion Symposium; Williams & Wilkins, Baltimore (in press).

[5] Karlovitz, B., Denniston, D. W., Jr., and Wells, F. E., *Investigation of Turbulent Flames*, J. Chem. Phys., Vol. 19, p. 541, 1951. Karlovitz, B., *Open Turbulent Flames*. Fourth Combustion Symposium; Williams & Wilkins, Baltimore (in press).

[6] Markstein, G. H., *Experimental and Theoretical Studies of Flame Front Stability*, Journal of the Aeronautical Sciences, Vol. 18, p. 199, 1951. *Instability Phenomena in Combustion Waves*, Fourth Combustion Symposium; Williams & Wilkins, Baltimore (in press).

[7] Wohl, K., Shore, L., von Rosenberg, H., and Weil, C. W., *The Burning Velocity of Turbulent Flames*, Fourth Combustion Symposium; Williams & Wilkins, Baltimore (in press).

Errata—"An Experimental Study of Natural Vibrations of Cantilevered Triangular Plates"

P. N. Gustafson, W. F. Stokey, and C. F. Zorowski
Carnegie Institute of Technology, Pittsburgh

May 20, 1953

TWO OMISSIONS OF SYMBOLS appeared in a paper by P. N Gustafson, W. F. Stokey, and C. F. Zorowski.[1] These are corrected as follows:

(1) The last term on the right-hand side of Eq. (18), page 336, should read

$$\frac{1}{\alpha^4}\frac{E'\rho h'^2(1-\mu^2)}{E\rho' h^2(1-\mu'^2)}\lambda$$

(2) Eq. (20) on page 336 should read

$$f' = \frac{1}{\alpha^2}\frac{h'}{h}\left[\frac{E'}{E}\frac{\rho}{\rho'}\frac{(1-\mu^2)}{(1-\mu'^2)}\right]^{1/2} f$$

REFERENCE

[1] Gustafson, P. N., Stokey, W. F., and Zorowski, C. F., *An Experimental Study of Natural Vibrations of Cantilevered Triangular Plates*, Journal of the Aeronautical Sciences, Vol. 20, No. 5, pp. 331–337, May, 1953.

Transformation Between Compressible and Incompressible Boundary-Layer Equations

Nguyen Van Le
AiResearch Manufacturing Company, Los Angeles

April 10, 1953

IT IS PROPOSED TO SHOW that the boundary-layer equation of compressible flow can be reduced to that of incompressible flow. Such work was initiated by Stewartson[1] and by Rott and Crabtree.[2] In the following some of the restrictions imposed by references 1 and 2 will be removed, and it will be shown that the transformation from compressible boundary layer to incompressible boundary layer can be applied to the laminar, as well as turbulent, case. A direct method will be used for this purpose.

DERIVATION OF THE COMPRESSIBLE BOUNDARY-LAYER EQUATION

The following assumptions are made (see Fig. 1): (1) two-dimensional flow; (2) Prandtl Number is taken equal to 1 ($Pr = 1$); (3) in the case of turbulent boundary layer, the time average value of the density, velocity, . . . etc., are considered; (4) the usual boundary layer assumption of $\partial p/\partial y = 0$; and (5) no heat is transferred across the boundary-layer wall.

In the control volume ABCD, application of the momentum theorem gives

$$\frac{d}{dx}\int_0^\delta \rho u^2\,dy - U_1\frac{d}{dx}\int_0^\delta \rho u\,dy = -\frac{dp}{dx} - \tau_0 \quad (1)$$

Outside the boundary layer there is isentropic flow

$$T\,ds = 0 = dh - (1/d\rho_1)d\rho_1 \therefore dh = (1/\rho_1)dp_1 \quad (2)$$

From the energy equation we have

$$dh_1 + U_1\,dU_1 = 0 \quad (3)$$

Combining Eqs. (2) and (3) yields

$$(1/\rho_1)\,(dp_1/dx) = -U_1\,dU_1 \quad (4)$$

Since $\partial p/\partial y = 0$, $p = p_1$, and $dp_1/dx = dp/dx$, relation (4) gives, then,

$$(1/\rho_1)\,dp_1 = -U_1\,dU_1/dx$$

which can be written

$$\delta\frac{dp_1}{dx} = -\frac{d}{dx}\rho_1 U_1^2 + U_1\frac{d}{dx}\rho_1 U_1$$
$$= -\frac{d}{dx}\int_0^\delta \rho_1 U_1^2\,dy + U_1\frac{d}{dx}\int_0^\delta \rho_1 U_1\,dy \quad (5)$$

With the Eq. (5), the momentum balance from Eq. (1) yields

$$\frac{d}{dx}\int_0^\delta (\rho_1 U_1^2 - \rho u^2)\,dy - U_1\frac{d}{dx}\int_0^\delta (\rho_1 U_1 - \rho u)\,dy = \tau_0 \quad (6)$$

The momentum and displacement thicknesses are now defined so that the energy equation can be taken into consideration in the boundary layer

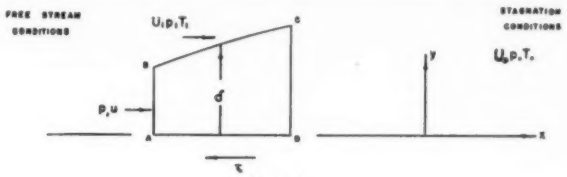

FIG. 1.

$$\left.\begin{aligned}\delta_1 &= \int_0^\delta \left(1 - \frac{u}{U_1}\right)\frac{\rho}{\rho_1}\,dy \\ \theta_1 &= \int_0^\delta \left(1 - \frac{u}{U_1}\right)\frac{u}{U_1}\frac{\rho}{\rho_1}\,dy\end{aligned}\right\} \quad (7)$$

With $Pr = 1$, satisfying the energy equation in the boundary layer has, as consequence,

$$\frac{T}{T_1} = 1 + \frac{K-1}{2}M_1^2\left(1 - \frac{u^2}{U_1^2}\right) \quad (8)$$

Upon introducing the stagnation temperature T_0 as a reference, Eq. (8) becomes

$$\frac{T}{T_1} = 1 + \left(\frac{T_0}{T} - 1\right)\left(1 - \frac{u^2}{U_1^2}\right) \quad (9)$$

In addition the assumption $\partial p/\partial y = 0$ shows that in the boundary layer the density and temperature are related by

$$\rho T = \rho_1 T_1 \quad (10)$$

With relations (9) and (10), one can evaluate the different terms of Eq. (6)

$$\int_0^\delta (\rho_1 U_1 - \rho u)\,dy = \rho_1 U_1\frac{T_0}{T_1}\int_0^\delta \left(1 - \frac{u}{U_1}\right)\frac{\rho}{\rho_1}\,dy +$$
$$\rho_1 U_1\left(\frac{T_0}{T_1} - 1\right)\int_0^\delta \left(1 - \frac{u}{U_1}\right)\frac{u}{U_1}\frac{\rho}{\rho_1}\,dy = \rho_1 U_1 \times$$
$$\left(1 + \frac{K-1}{2}M_1^2\right)\delta_1 + \rho_1 U_1\left(\frac{K-1}{2}\right)M_1^2\theta_1 \quad (11)$$

$$\int_0^\delta (\rho_1 U_1^2 - \rho u^2)\,dy = \int_0^\delta U_1(\rho_1 U_1 - \rho u)\,dy +$$
$$\rho_1 U_1^2\int_0^\delta \frac{\rho}{\rho_1}\left(\frac{u}{U_1} - \frac{u^2}{U_1^2}\right)dy = \int_0^\delta U_1 \times$$
$$(\rho_1 U_1 - \rho u)\,dy + \rho_1 U_1^2\theta_1 \quad (12)$$

The momentum equation (6) then becomes

$$\frac{d}{dx}\rho_1 U_1^2\theta_1 + \frac{d}{dx}\int_0^\delta (\rho_1 U_1 - \rho u)\,dy -$$
$$U_1\frac{d}{dx}\int_0^\delta (\rho_1 U_1 - \rho u)\,dy = \tau_0$$

or after integration by parts

$$\frac{d}{dx}\rho_1 U_1^2\theta_1 + \frac{dU_1}{dx}\int_0^\delta (\rho_1 U_1 - \rho u)\,dy = \tau_0$$

and, with Eq. (11), we obtain the compressible boundary-layer equation,

$$\frac{d}{dx}\rho_1 U_1^2\theta_1 + \rho_1 U_1\frac{dU_1}{dx}\times$$
$$\left[\frac{K-1}{2}M_1^2\theta_1 + \delta_1\left(1 + \frac{K-1}{2}M_1^2\right)\right] = \tau_0$$

or

$$U_1^2 \frac{dU_1}{dx} + U_1^2\theta_1 \frac{1}{\rho_1}\frac{d\rho_1}{dx} + U_1 \frac{dU_1}{dx} \times$$

$$\left[\left(2 + \frac{K-1}{2} M_1^2\right)\theta_1 + \left(1 + \frac{K-1}{2} M_1^2\right)\delta_1\right] = \frac{\tau_0}{\rho_1} \quad (13)$$

But for isentropic flow outside the boundary layer, combination of the isentropic relation and the energy equation gives

$$U_1^2 \frac{1}{\rho_1}\frac{d\rho_1}{dx} = -\, U_1 \frac{dU_1}{dx} M_1^2 \quad (14)$$

Putting Eq. (14) in Eq. (13) we obtain the final equation for compressible boundary layer,

$$\frac{d\theta_1}{dx} + \left[\left(2 + \frac{K-3}{2} M_1^2\right) + \left(1 + \frac{K-1}{2} M_1^2\right)\frac{\delta_1}{\theta_1}\right] \times \frac{\theta_1}{U_1}\frac{dU_1}{dx} = \frac{\tau_0}{\rho_1 U_1^2} \quad (15)$$

As derived, the equation does not make any assumption on the viscosity in the boundary layer. The time average values of the velocity and density are considered for the case of turbulent boundary layer, although there may be possibility of treating their time components as in reference 3. Until measurements show the large contribution of the time components, the previous equation can be applied to laminar, as well as turbulent, boundary layer because of the nature of its derivation. For $M_1 = 0$, it reduces to the well-known incompressible case,

$$\frac{d\theta_1}{dx} + \left(2 + \frac{\delta_1}{\theta_1}\right)\frac{\theta_1}{U_1}\frac{dU_1}{dx} = \frac{\tau_0}{\rho_1 U_1^2} \quad (16)$$

Transformation Formulas

A set of transformation formulas modified from reference 1 is now adopted as follows:

$$\left.\begin{aligned} Y &= \frac{a_1}{a_0}\int_0^y \frac{\rho}{\rho_0}\, dy \\ z &= \int_0^x \left(\frac{a_1}{a_0}\right)^{(3K-1)/(K-1)} dx \\ V_1 &= a_0 M_1 = (a_0/a_1)\, U_1 \\ v &= (a_0/a_1)u \end{aligned}\right\} \quad (17)$$

where

a_0 = sound velocity T_0
a_1 = sound velocity T_1
$K = c_p/c_v$

Define further the following integrals:

$$\left.\begin{aligned} \delta_2 &= \int_0^{\delta'}\left(1 - \frac{v}{V_1}\right) dY \\ \theta_2 &= \int_0^{\delta'}\left(1 - \frac{v}{V_1}\right)\frac{v}{V_1}\, dY \end{aligned}\right\} \quad (18)$$

which can be interpreted as the displacement and momentum thicknesses of an incompressible flow where the characteristics are as shown in Fig. 2. Using the transformation formulas, one can show that

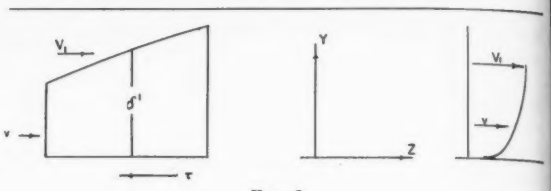

Fig. 2.

$$(\rho_1/\rho_0)\,(a_1/a_0)\,(\delta_1) = \delta_2$$

which gives, further,

$$\left(\frac{a_1}{a_0}\right)^4 \frac{d}{dz}(V_1^2\theta_2) = U_1^2 \frac{d\theta_1}{dx} + \theta_1 U_1 \frac{dU_1}{dx}\left(2 + \frac{K-3}{2} M_1^2\right) \quad (19)$$

$$\left(\frac{a_1}{a_0}\right)^4 \delta_2 V_1 \frac{dV_1}{dz} = \delta_1 U_1 \frac{dU_1}{dx}\left(1 + \frac{K-1}{2} M_1^2\right) \quad (20)$$

Upon introducing Eqs. (19) and (20) in the Eq. (15) for compressible flow, one obtains

$$\left(\frac{a_1}{a_0}\right)^4 \frac{d}{dz} V_1^2\theta_2 + \left(\frac{a_1}{a_0}\right)^4 \delta_2 V_1 \frac{dV_1}{dz} = \frac{\tau_0}{\rho_1}$$

or

$$\frac{d\theta_2}{dz} + \left(2 + \frac{\delta_2}{\theta_2}\right)\frac{\theta_2}{V_1}\frac{dV_1}{dz} = \frac{\tau_0}{\rho_0 V_1^2}(a_0/a_1)^{(4K-2)/(K-1)} \quad (21)$$

If a modified wall shear stress is now defined

$$\tau = \tau_0\,(a_0/a_1)^{(4K-2)/(K-1)} \quad (22)$$

the value of τ_0 being obtained from reference 4, for instance, Eq. (21) is reduced to

$$\frac{d\theta_2}{dz} + \left(2 + \frac{\delta_2}{\theta_2}\right)\frac{\theta_2}{V_1}\frac{dV_1}{dz} = \frac{\tau}{\rho_0 V_1^2} \quad (23)$$

which is exactly the equation of an incompressible boundary layer. Thus, in order to obtain the solution for a compressible boundary layer, turbulent as well as laminar, one chooses a temperature profile from experimental data just in the same way as for the velocity profiles. Then one carries out the transformation prescribed in Eqs. (17) and (22) and solves the incompressible boundary-layer equation (23), which is more familiar.

For comparative purpose it is reminded that the Polhausen method generalized to the compressible boundary layer required a solution for a system of two nonlinear differential equations.

References

[1] Stewartson, *Correlation Between Incompressible and Compressible Boundary Layer*, Proceedings, The Royal Society of London, Vol. 200, December, 1949.

[2] Rott and Crabtree, *Simplified Laminar Boundary-Layer Calculations for Bodies of Revolution and Yaw Wings*, Journal of the Aeronautical Sciences, Vol. 19, No. 8, p. 553, August, 1952.

[3] Van Le, N., *The von Kármán Integral Method as Applied to a Turbulent Boundary Layer*, Readers' Forum, Journal of the Aeronautical Sciences, Vol. 19, No. 9, p. 647, September, 1952.

[4] Donaldson, Coleman du P., *On the Form of the Turbulent Skin-Friction Law and Its Extension to Compressible Flow*, NACA TN No. 2692, May, 1952.